3D Strut-and-Tie Modeling for Design of Drilled Shaft Footings under Biaxial Eccentric Loading

Yousun Yi
Hyunsu Kim
Hwa-Ching Wang
Zachary D. Webb
Oguzhan Bayrak

Technical Report Documentation Page

1. Report No. FHWA/TX-22/0-6953-01-1	2. Government Accession No.	3. Recipient's Catalog No.
4. Title and Subtitle 3D Strut-and-Tie Modeling for Design of Drilled Shaft Footings under Biaxial Eccentric Loading		5. Report Date Submitted: May 2022 Published: August 2022
		6. Performing Organization Code
7. Author(s) Yousun Yi, Hyunsu Kim, Hwa-Ching Wang, Zachary D. Webb, Oguzhan Bayrak		8. Performing Organization Report No. 0-6953-01-1
9. Performing Organization Name and Address Center for Transportation Research The University of Texas at Austin 3925 W. Braker Lane, 4th Floor Austin, TX 78759		10. Work Unit No. (TRAIS)
		11. Contract or Grant No. 0-6953-01
12. Sponsoring Agency Name and Address Texas Department of Transportation Research and Technology Implementation Division 125 E. 11th Street Austin, TX 78701		13. Type of Report and Period Covered Technical Report October 2021 – June 2022
		14. Sponsoring Agency Code

15. Supplementary Notes
Project performed in cooperation with the Texas Department of Transportation and the Federal Highway Administration.

16. Abstract

This project establishes a series of design guidelines for drilled shaft footings subjected to biaxial eccentric loading by refining the design recommendations of TxDOT Project 0-6953. The refined guidelines include the single strut– and single tie–based equivalent force system, development of 3D strut-and-tie models for biaxial eccentric loading scenarios, and definitions of the 3D nodal geometry of the CCC node. The refinements were carried out from a conservative perspective. Nevertheless, they maintained most of the approaches of the previous design recommendations for a consistent design of drilled shaft footings under different loading conditions. The design of the drilled shaft footing developed in TxDOT Project 0-6953 was further updated with two additional biaxial eccentric load cases, applied to footings in use by TxDOT...

- Load Case VI: Axial compression combined with moderate biaxial flexure. The load combination induces tension at one corner of the column and non-uniform compression in drilled shafts

- Load Case VII: Axial compression combined with large biaxial flexure. The load combination induces tension at one corner of the column and one of four drilled shafts.

The updated drilled shaft footing design example was also confirmed to be safe for the selected biaxial eccentric design load cases through the refined design recommendations of this research. The design example from this research, which was safe even for extreme biaxial load cases, validates the conservativeness of the proposed refinements.

17. Key Words Biaxial Eccentric Load, Drilled Shaft Footings, Strut-and-Tie Modeling, Strength	18. Distribution Statement No restrictions. This document is available to the public through the National Technical Information Service, Alexandria, Virginia 22312; www.ntis.gov.

19. Security Classif. (of report) Unclassified	20. Security Classif. (of this page) Unclassified	21. No. of pages 134	22. Price

Form DOT F 1700.7 (8-72)   Reproduction of completed page authorized

THE UNIVERSITY OF TEXAS AT AUSTIN
CENTER FOR TRANSPORTATION RESEARCH

3D Strut-and-Tie Model Design Example for Drilled Shaft Footings under Biaxial Eccentric Loading

Yousun Yi
Hyunsu Kim
Hwa-Ching Wang
Zachary D. Webb
Oguzhan Bayrak

Disclaimers

Author's Disclaimer: The contents of this report reflect the views of the authors, who are responsible for the facts and the accuracy of the data presented herein. The contents do not necessarily reflect the official view or policies of the Federal Highway Administration or the Texas Department of Transportation (TxDOT). This report does not constitute a standard, specification, or regulation.

Patent Disclaimer: There was no invention or discovery conceived or first actually reduced to practice in the course of or under this contract, including any art, method, process, machine manufacture, design or composition of matter, or any new useful improvement thereof, or any variety of plant, which is or may be patentable under the patent laws of the United States of America or any foreign country.

Engineering Disclaimer

NOT INTENDED FOR CONSTRUCTION, BIDDING, OR PERMIT PURPOSES.

Project Engineer: Oguzhan Bayrak
Professional Engineer License State and Number: Texas No. 106598
P.E. Designation: Research Supervisor

Acknowledgments

Table of Contents

List of Tables

List of Figures

Chapter 1. Introduction

1.1. Background

Strut-and-tie method (STM) is a practical design tool for deep structural members that simplifies their internal force flow into idealized struts and ties. Typically, the configuration of the strut-and-tie models developed in drilled shaft footings forms three-dimensional (3D) shapes. *TxDOT Project 0-6953: 3D Strut-and-Tie Modeling for Design of Drilled Shaft Footings* (Yi et al., 2022) established a series of design recommendations for drilled shaft footings using the 3D STM based on large-scale tests and numerical analyses. However, the comprehensive research was limited to uniaxial loading scenarios, and the design example proposed by the research was also primarily based on the recommendations for drilled shaft footings subjected to uniaxial loads. The design example also includes one biaxial eccentric loading case: axial compression combined with mild biaxial flexure resulting in non-uniform compression in drilled shafts. The configuration of the 3D strut-and-tie model developed for the biaxial load case is the same as that developed from the simplest load scenario (uniaxial compression-only loading); therefore, the proposed recommendations could be applicable to the biaxial load case.

On the other hand, in-practice drilled shaft footings are also designed with biaxial eccentric loading cases inducing tension at one corner of the column or one of four drilled shafts. Due to the lack of research on the 3D strut-and-tie models of drilled shaft footings under these complex loading conditions, the recommendations proposed by Yi et al. (2022) cannot be directly applied when designing the footings under biaxial eccentric loading. These limitations hinder the application of the 3D STM to a consistent design of drilled shaft footings that can be subjected to various loading conditions. Therefore, refined recommendations for the 3D STM design for drilled shaft footings that cover biaxial loading scenarios are needed.

1.2. Project Objective and Scope

The research team expanded and refined the guidelines proposed by Yi et al. (2022) for using the 3D STM in drilled shaft footings under biaxial eccentric loading which is the more common loading scenario in practice. The refinements were conducted theoretically; therefore, all proposed recommendations in this research are established based on a conservative standpoint. The drilled shaft footing design example of Yi et al. (2022) was updated for two additional biaxial eccentric load cases using the refined recommendations.

1.3. Organization

The literature regarding design recommendations for drilled shaft footings subjected to biaxial eccentric loading is reviewed in Chapter 2. Chapter 3 categorizes the load cases used in the in-practice drilled shaft footings constructed by TxDOT in Texas to clarify the proportion of biaxial eccentric load cases in the total load cases. Chapter 4 contains a summary of the 3D STM design recommendations for drilled shaft footings proposed by Yi et al. (2022). The recommendations are refined in Chapter 5 to apply the 3D STM when designing drilled shaft footings subjected to biaxial eccentric loading. Chapter 6 provides the design example for a drilled shaft footing under biaxial eccentric load cases using the refined design recommendations to supplement the design example proposed by Yi et al. (2022). Lastly, the outcomes of this research and conclusions are summarized in Chapter 7.

Chapter 2. Literature Review

To the authors' knowledge, the research on drilled shaft footing subjected to biaxial loading conditions is limited despite the fact that this is a common loading scenario in current practice. Current specifications addressing strut-and-tie modeling were formulated based on research of 2D deep beams and thus those are conservative for 3D structures like four drilled shaft footings, so previous researchers mitigate some over-conservatism by updating and adapting their stress limits for 3D structures. In addition, most studies investigated the behavior of footings under pure axial compression, and a few studies tested specimens under uniaxial eccentric loading conditions due to the limited knowledge. Regarding the design examples for drilled shaft footings under biaxial eccentric loading, the only study found was conducted by Ballestrino et al. (2011) in *fib* bulletin 61, in which there are examples of strut-and-tie models for a variety of structural components.

| (a) Plan view | (b) Elevation view |
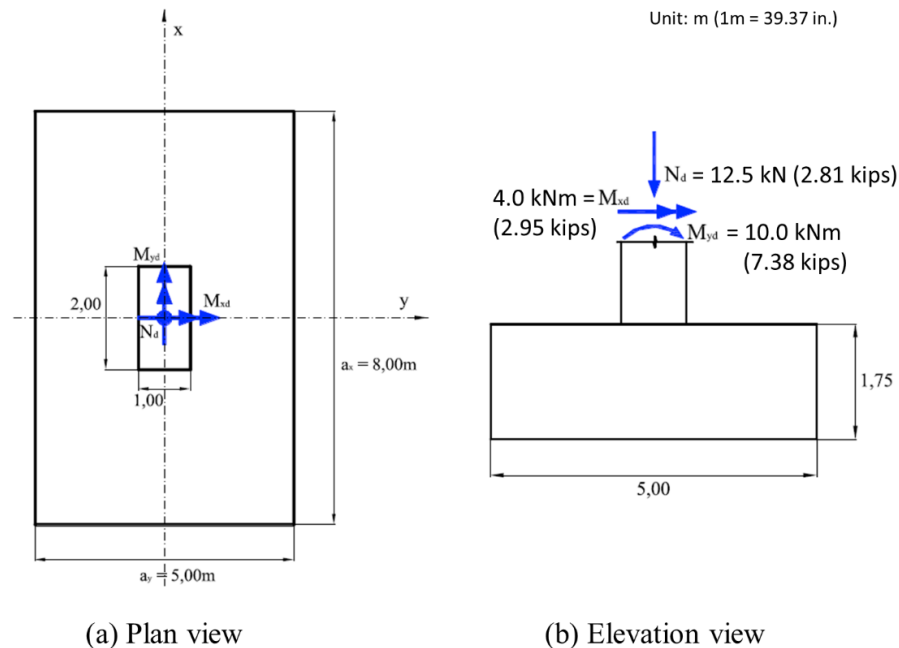
Figure 2.1 Dimension and load condition (Ballestrino et al., 2011)

In the example, a rectangular footing with a center-located rectangular column was supported on the ground, not on a group of drilled shafts, as shown in Figure 2.1. The biaxial bending resulted in a non-uniform distribution of the compression over the soil underneath, and tensile reaction would not be developed. Ballestrino et al. (2011) assumed that the reactions of the soil were calculated in four each quadrant and were located at the center of the corresponding quadrant. A sectional analysis of the column was used to determine the forces and the locations of the equivalent

forces. Based on their assumptions, they developed a strut-and-tie model in order to represent the internal force flow, as illustrated in Figure 2.2.

(a) Isometric view

(b) Elevation view

(c) Plan view
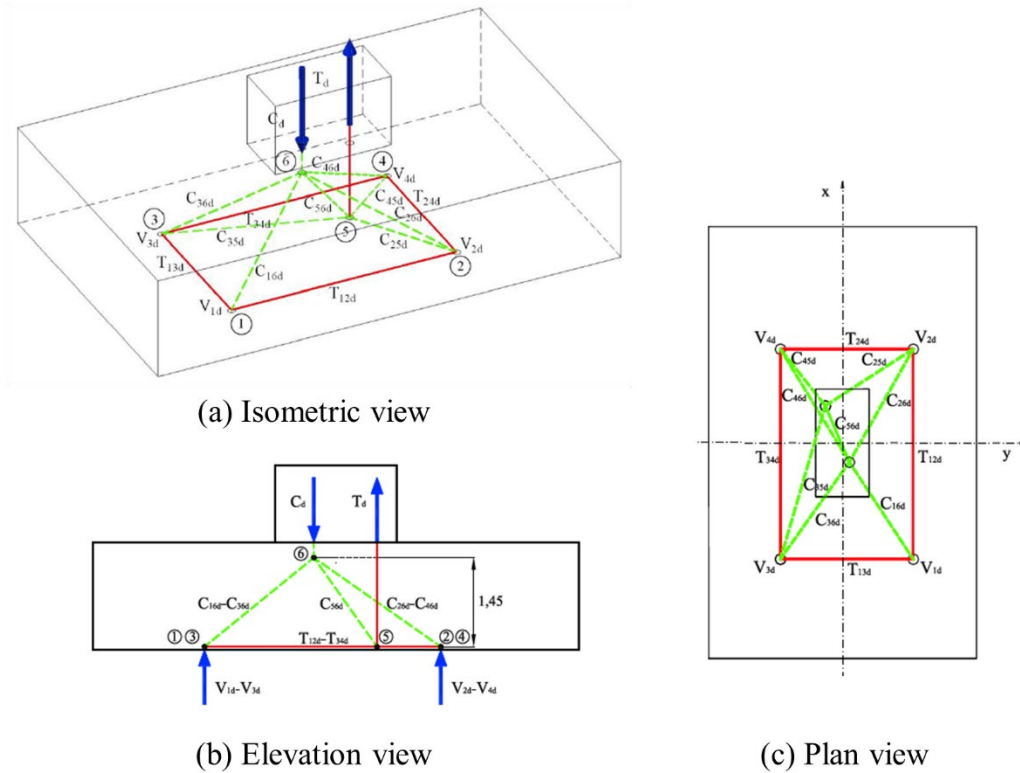
Figure 2.2 Strut-and-tie model of footing under biaxial loading (Ballestrino et al., 2011)

When proportioning ties, the authors assumed that the bottom mat reinforcement was distributed uniformly (i.e., a grid layout), and all reinforcement in the half of the cross-section was considered to contribute to the corresponding tie capacities since the ground supported the footing. The authors recommended that the column bars be bent inward for sufficient development.

The triaxial hydrostatic compressive strength of the concrete was employed for checking the nodal capacity of the CCC node, Node 6. The required area was calculated from that the factored force in the strut was divided by the triaxial concrete strength. The nodal strength was acceptable because the required area was much smaller than the column dimension.

The anchorage length of the vertical column bars at Node 5 started from the end of the bend with the assumption of 90-degree hooked bars. The anchorage length was calculated in accordance with CEB–FIP recommendations (1999).

In summary, there are several limitations to directly comparing this study and Ballestrino et al. (2011). The four drilled shafts support the footing in this study,

4

while the footings were supported by the ground. If tension develops on the bottom face due to large flexure, some part of the bottom face cannot resist the tension due to the characteristics of the soil. Additionally, it was not necessary to check stresses at bottom nodes because the extremely large bearing area of bottom nodes resulting from the ground supporting condition, not supporting by shafts. Moreover, anchorage length of column reinforcement was checked from the end of the bend to the end of steel while available development length usually defines from the critical section to the end of steel or the start of the bend. Notably, the research team found that Ballestrino et al. (2011) employed triaxial compressive strength.

Chapter 3. Design Load Case Review

The research team at the University of Texas at Austin, with support from the TxDOT project team, reviewed load cases of several constructed drilled shaft footings in bridge projects that TxDOT and their consultants have designed.

The load cases in drilled shaft footings can be divided into seven categories depending on the stress state over the column section and shaft, as illustrated in Figure 3.1. Load Case I (LC1) is pure axial compressive loading, resulting in a uniform compression over the column section and uniform compressive reactions in the shafts. Load Cases II (LC2), III (LC3), and IV (LC4) represent axial compression with uniaxial bending. Two groups of shafts react with non-uniform compression in LC2 and LC3, while severe uniaxial flexure in LC4 results in two shafts in tension. Mild flexure in LC2 leads to the compressive distribution over the entire column section, whereas moderate and severe uniaxial flexure in LC3 and LC4, respectively, result in tension on one side of the column section and compression on the other side. Biaxial load scenarios from Load Case V (LC5), VI (LC6), and VII (LC7) have a stress state in the column section similar to load cases with uniaxial flexure (LC2 through LC4). Non-uniform compressive reaction develops in LC5 and LC6. The moderate biaxial flexure in LC6 causes tensile stress at one corner of the column section. Severe biaxial flexure in LC7 results in tension in one shaft and tension on one side of the column section. Note that the design examples for LC1 through LC5 were provided in the previous research, Yi et al. (2022).
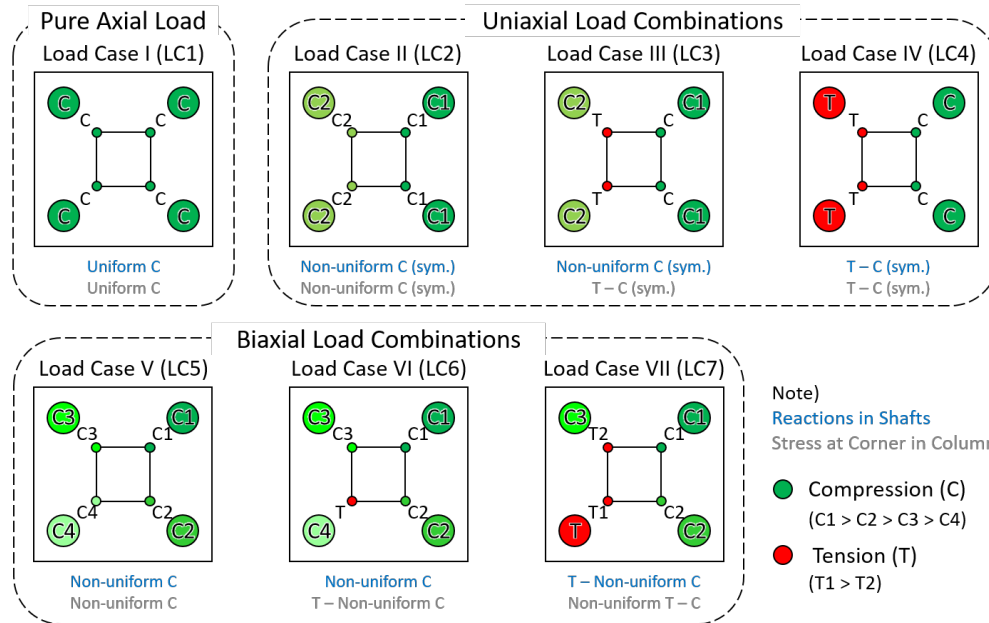
Figure 3.1 Load case classification depending on the stress over the column section and in shafts. The darker the circle, the higher the stress level.

From three constructed drilled shaft footings provided by TxDOT, total 354 load cases were compiled and reviewed. Cases where the ratio of minimum-to-maximum bending moments was less than 0.2 were categorized as under a uniaxial load rather than a biaxial load, since the flexural stresses induced from one of the bending moments about the certain axis would dominate the behavior of the footings. Table 3.1 summarizes the number of each load case for each constructed footing after calculating reactions in the drilled shafts and stresses at the corner of the columns. Figure 3.2 shows the distribution of the load cases. The most common load case was LC3, axial compression with moderate uniaxial flexure. LC6, axial compression with moderate biaxial flexure, is the next most common. Load cases with moderate uniaxial or biaxial flexure, resulting in a non-uniform compression in the shafts and tensile stress in at least one corner of the column section, occurred the most frequently (85.6%) in the design of the drilled shaft footing. Biaxial load combinations (LC6 and LC7), the focus of this research, made up 17.8% of the load cases.

7

Table 3.1 Summary of reviewed load cases

Footing Examples	Total	LC I	LC II	LC III	LC IV	LC V	LC VI	LC VII	Ratio (LC VI + LC VII)
Footing A	288	0	1	251	8	0	10	18	9.7%
Footing B	22	0	1	1	0	10	10	0	45.5%
Footing C	44	0	2	6	0	11	25	0	56.8%
Total	354	0	4	258	8	21	45	18	17.8%
Percentage of all load cases		0.0%	1.1%	72.9%	2.3%	5.9%	12.7%	5.1%	
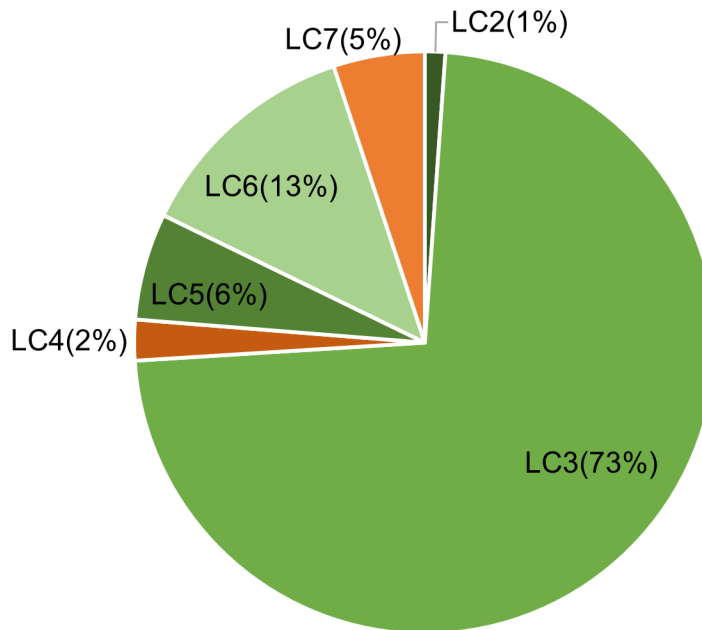
Figure 3.2 Distribution of reviewed load cases

Chapter 4. Design Recommendations: TxDOT Project 0-6953

TxDOT Project 0-6953 (Yi et al., 2022) proposed designs for drilled shaft footings using the 3D STM based on the data and insights obtained from large-scale tests and numerical analyses for drilled shaft footings under uniaxial loading scenarios. In accordance with the recommendations, Yi et al. (2022) also provided a drilled shaft footing design example under various uniaxial and biaxial loading scenarios.

The 3D STM-based design procedure for drilled shaft footings recommended by Yi et al. (2022) is summarized below and detailed in the following subsections:

1)   Developing a 3D strut-and-tie model

2)   Proportioning ties

3)   Performing nodal strength checks

4)   Proportioning shrinkage and temperature reinforcement

5)   Providing necessary anchorage for ties

4.1. Developing a 3D Strut-and-Tie Model

The configuration of a 3D strut-and-tie model for a drilled shaft footing was determined by the force flow according to the considered load combination. The internal stress field of the footing was expressed with struts and ties comprising an idealized truss. To do so, the applied load on the column was transformed into an equivalent force system over the column-to-footing interface. Assuming the column section remained plane during loading, the stress distribution over the column section was subdivided into four components, and struts were positioned at the centroids of the subdivided regions to describe the internal force flow of the footing flowing down to four drilled shafts. When the applied uniaxial flexural stresses induced tension at one face of the column, a simplified rectangular stress block was used for concrete in compression based on the factors proposed by Collins and Mitchell (1991). The equivalent stress block factors made it possible to model the linear and nonlinear behavior of the concrete. Further, the tensile capacity of the concrete was neglected, and the column reinforcement at the tensile face of the column was only considered to resist the tie force in the column. Figure

4.1 illustrates the 3D strut-and-tie models and their equivalent force systems at the interface depending on the applied loading scenarios.
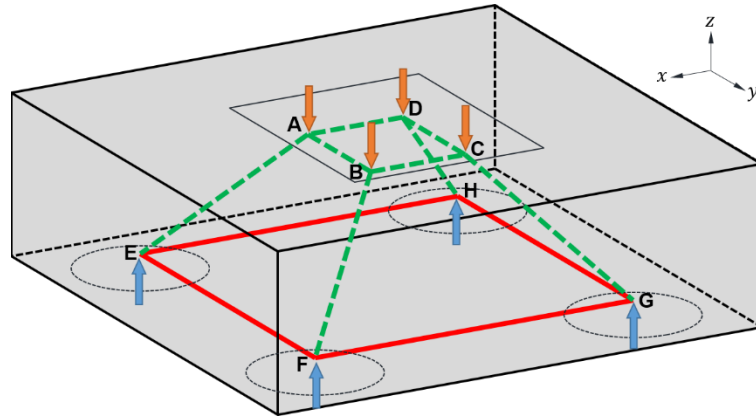
(a) Load Case I, II, and V
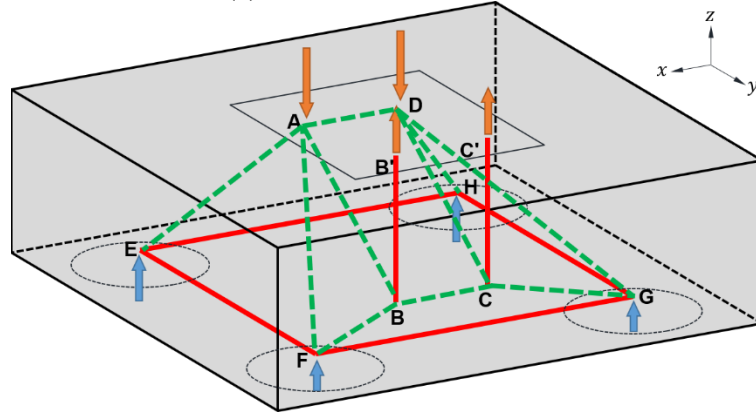
(b) Load Case III
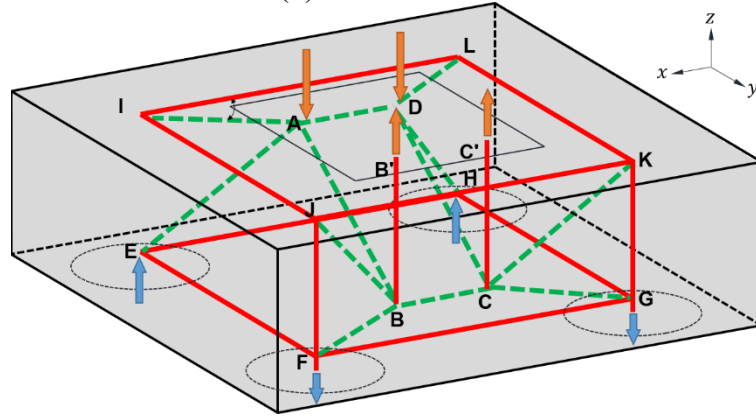
(c) Load Case IV

Figure 4.1 3D strut-and-tie models under various loading scenarios

The basic assumptions employed to determine 3D strut-and-tie models are as follows:

- The equivalent force system determined the nodal positions beneath the column, and the nodes were located 0.1 times the height along the z-axis if there was no top tie ring in the 3D STM. (Figure 4.1a and b).

- The position of the four nodes for the top tie ring (Figure 4.1c) was the projection of the center of the drilled shafts at the elevation of top mat reinforcement, and the nodes beneath the column were positioned on the same horizontal plane of the top tie ring.

- The position of the four nodes above the drilled shafts was the projection of the center of the drilled shafts at the elevation of bottom mat reinforcement.

- Ties on the plane of the bottom/top tie ring were placed along the axis of bottom/top mat reinforcement.

- Column ties stretched down to the plane of the bottom tie ring were positioned at the axis of the tensile column reinforcement array.

- A strut was placed to meet the equilibrium condition with applied forces and reaction forces in each axis at each node. The angle between a diagonal strut and the plane of bottom mat reinforcement and the angle between a strut and a tie on the same plane were limited to 25–65 degrees.

- Tie and strut forces could be computed using statics (method of joints or method of sections).

4.2. Proportioning Ties

The bottom and top mat reinforcement, which are placed the entire span of the footing, can be engaged to take the tie forces if the reinforcement is sufficiently anchored. This recommendation was established based on the experimental test results conducted for the grid and banded layouts, and the ultimate capacities of the specimens were comparable regardless of the layouts (Yi et al., 2022). Therefore, the capacity of a tie element can be estimated, as shown in Eq. (4.1).

$$P_{n,tie} = f_y A_{st} \hspace{6cm} \text{Eq. (4.1)}$$

where:
$P_{n,tie}$ = nominal resistance of a tie [kip]
f_y = yield strength of non-prestressed longitudinal reinforcement [ksi]
A_{st} = area of non-prestressed longitudinal reinforcement engaged in taking the tie force [in.^{2}]

Generally, two horizontal ties in each direction are provided to a 3D strut-and-tie model for drilled shaft footings supported by four drilled shafts. Therefore, half the amount of the top or bottom mat reinforcement is used to estimate the tie force. Further, all drilled shaft reinforcing bars in the drilled shaft under tension are also engaged to take the drilled shaft tie force. Like determining the equivalent force system, only the column reinforcement at the tensile face of the column is considered to calculate the capacity of the column tie element.

4.3. Nodal Strength Checks

A simple but straightforward 3D nodal geometry was proposed to take into account the triaxial confinement effect and the strut-to-node interface of the node (Figure 4.2). The sections of the nodes performing the nodal strength checks are illustrated in Figure 4.3. The assumptions for defining the 3D nodal geometry are described as follows:

- Non-hydrostatic nodes and prismatic struts with a rectangular cross-section were used.

- The circular bearing face at the drilled shafts was assumed to be an equivalent square-shaped bearing face to define the nodal geometry. Hence, the strut width at the node was used as the width of the equivalent square bearing face.

- The back face height of the CCC node was assumed to be twice the distance from the top surface.

- The back face height of the CTT nodes above the drilled shafts was assumed to be twice the distance from the bottom surface

- If multiple struts were connected to a node forming multiple strut-to-node interfaces, the strut forces were resolved into a single force applied perpendicularly to a single strut-to-node interface.

- The equivalent square bearing face was rotated towards the direction of the resolved strut, and the length of the strut-to-node interface was derived from the inclination of the resolved strut and the specified dimensions.

(a) CCC node   (b) CTT node
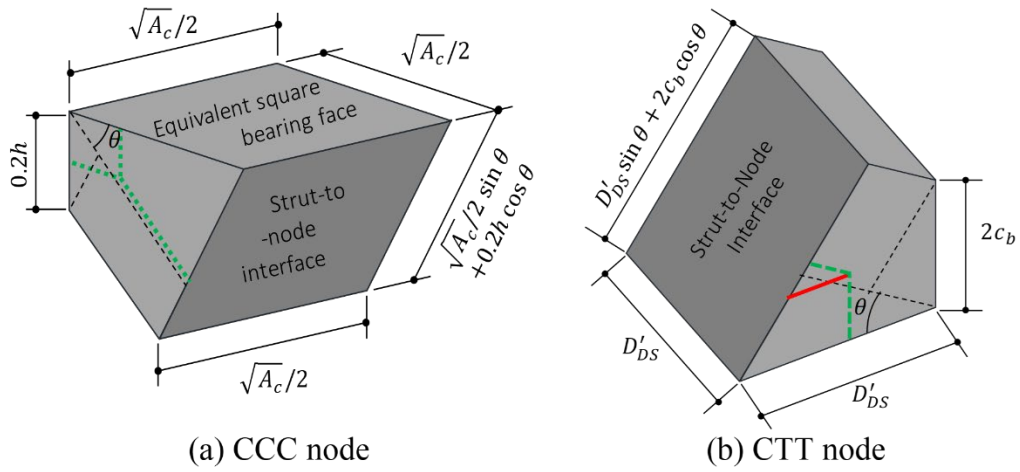
Figure 4.2 Detail of 3D nodal geometry in drilled shaft footing
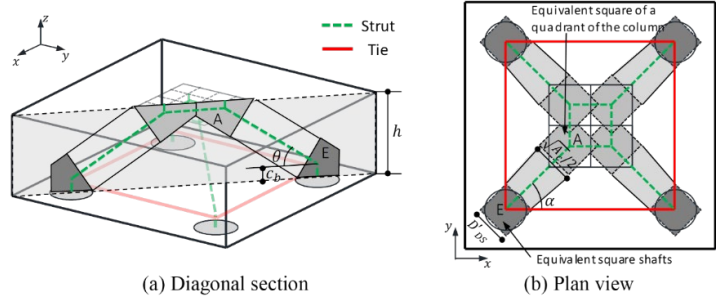
(a) Diagonal section (b) Plan view

Note α: Angle between x-axis and projected strut AB to the plane of the bottom mat reinforcement
θ: Angle between strut AE and the plane of bottom mat reinforcement
A_c: Area of the column
D_{DS}: Shaft diameter
D'_{DS}: Length of the equivalent square shaft ($= D_{DS}\sqrt{\pi/4}$)
c_b: Distance from bottom surface to the centroid of bottom mat reinforcement
h: Height of the footing

(a) Load Case I, II, and V
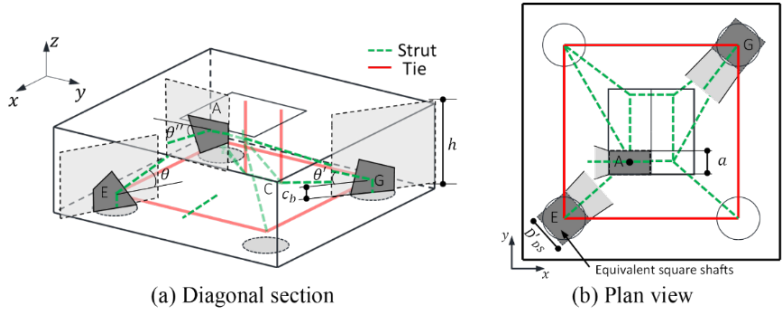
(a) Diagonal section (b) Plan view

Note θ: Angle between strut AE and the plane of bottom mat reinforcement
θ', θ'': Angle between the resolved strut and the plane of the bearing face
D_{DS}: Shaft diameter
D'_{DS}: Length of the equivalent square shaft ($= D_{DS}\sqrt{\pi/4}$)
a: Equivalent stress block depth
c_b: Distance from bottom surface to the centroid of bottom mat reinforcement
h: Height of the footing

(b) Load Case III
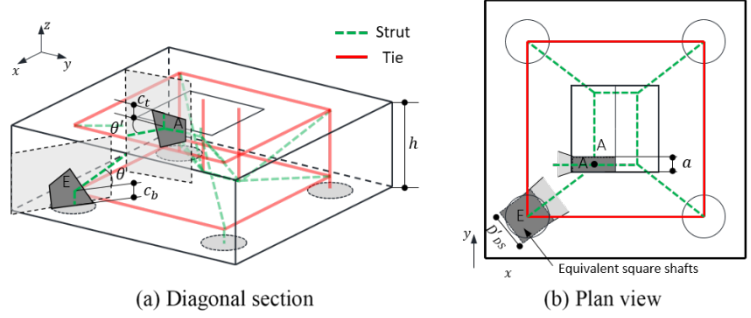
(a) Diagonal section (b) Plan view

Note θ: Angle between strut AE and the plane of bottom mat reinforcement
θ': Angle between the resolved strut and the plane of the bearing face
D_{DS}: Shaft diameter
D'_{DS}: Length of the equivalent square shaft ($= D_{DS}\sqrt{\pi/4}$)
a: Equivalent stress block depth
c_b: Distance from bottom surface to the centroid of bottom mat reinforcement
c_t: Distance from top surface to the centroid of top mat reinforcement
h: Height of the footing

(c) Load Case IV

Figure 4.3 Sectional views that demonstrates 3D nodal geometry for 3D strut-and-tie models under various loading scenarios

14

4.3.1. Confinement Modification Factor

Nodal strength enhancement due to the massive concrete surrounding a node can be considered by employing the confinement modification factor. The factor is determined by a bearing frustum and allowed up to 2.0 for CCT and CTT nodes, which is the same as the limit for all node types of 2D structures (AASHTO LRFD Bridge Design Specifications, 2019; ACI318-19, 2019; CSA A23.3-14, 2014). Yi et al. (2022) found that for drilled shaft footing specimens under flexural stresses, the nodal region of the CCC node, whose bearing area is smaller than that of the CTT node, remained largely undamaged until the ultimate state of the footing. Nevertheless, the ultimate state was governed by the failure in the vicinity of the CTT node. Therefore, the recommendations proposed using a maximum confinement of 3.0 for CCC nodes under triaxial compression, the same as specified in Eurocode 2 (2004) and fib Model Code 2010 (2013).
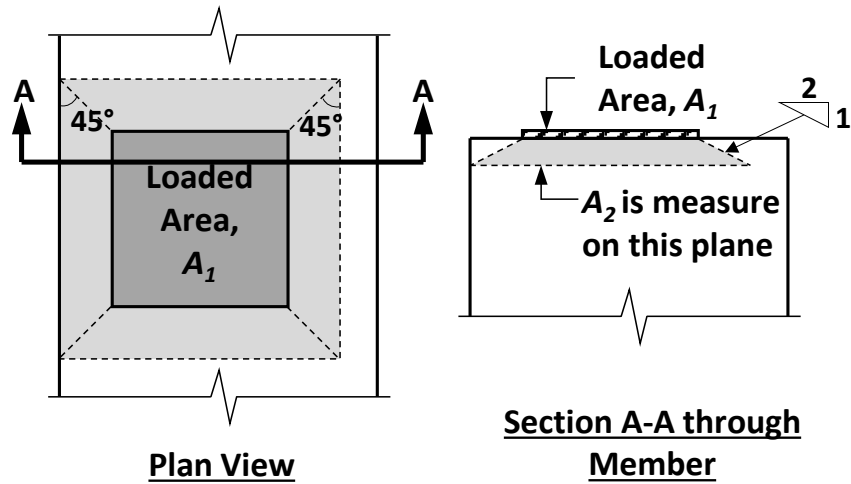
Figure 4.4 Determination of notional area (adapted from AASHTO LRFD, 2020)

$$m = \sqrt{A_2/A_1} \leq \begin{array}{l} 3.0 \ \ (\text{CCC nodes}) \\ 2.0 \ (\text{Other nodes}) \end{array} \qquad \text{Eq. (4.2)}$$

where:

m	= confinement modification factor
A_1	= area under bearing device [in.^{2}]
A_2	= notional area defined as shown in Figure 4.4 [in.^{2}]

4.3.2. Concrete Efficiency Factor

Providing crack control reinforcement at the plane of the strut is challenging for the 3D strut-and-tie model of drilled shaft footings. Further, Yi et al. (2022) identified the contribution of side face reinforcement to the ultimate capacity from large-scale drilled shaft footing tests. Therefore, the recommendations proposed providing at

least 0.18% side reinforcement orthogonally at all side surfaces of the footing, in accordance with the shrinkage and temperature reinforcement requirement specified in AASHTO LRFD (2020) (Article 5.10.6), instead of the crack control reinforcement requirement specified in current provisions for 2D structures. If the side reinforcement requirement was satisfied, the current 2D STM provision of the efficiency factor could be maintained, whereas the minimum strut efficiency factor (0.45) was recommended when the provided side reinforcement ratio is smaller than 0.18%.

4.3.3. Summary

The nodal strength at all faces of the nodes with defined nodal geometry in drilled shaft footings can be estimated based on Eq. (4.3).

$$P_{n,n} = f_{cu}A_{cn}$$ Eq. (4.3)

where:

$P_{n,n}$ = nominal resistance of a node face [kip]

f_{cu} = effective compressive stress at the node face, taken as $m\nu f_c'$ [ksi]

m = confinement modification factor, taken as $\sqrt{A_2/A_1} \leq 3.0$ for CCC nodes and 2.0 for other node types (CCT and CTT), as defined in Article 5.6.5

ν = the minimum concrete efficiency factor (0.45) if the side face reinforcement requirement (0.18%) is not satisfied OR the concrete efficiency factor as shown in Table 5.8.2.5.3a-1 if the side face reinforcement requirement (0.18%) is satisfied, in accordance with Article 5.10.6

Table 5.8.2.5.3a-1—Efficiency Factors for Nodes with Crack Control Reinforcement (AASHTO LRFD, 2020)

Face	Node Type		
	CCC	CCT	CTT
Bearing Face	0.85	0.70	$0.85 - \dfrac{f_c'}{20\ ksi}$ $0.45 \leq \nu \leq 0.65$
Back Face			
Strut-to-Node Interface		$0.85 - \dfrac{f_c'}{20\ ksi}$, $0.45 \leq \nu \leq 0.65$	

f_c' = compressive strength of concrete for use in design [ksi]

A_{cn} = effective cross-sectional area of the node faces as specified in Article 5.8.2.5.2; and in Figure 4.3 [in.^{2}]

4.4. Anchorage for Ties

4.4.1. Horizontal Ties (Top and Bottom Mat Reinforcement)

4.4.1.1. At Singular Nodes

Based on the determined 3D nodal geometry at singular nodes, the recommendations employed a similar approach using the extended nodal zone to define the critical section. Figure 4.5 illustrates the extended nodal zone in a 3D strut-and-tie model projected on the plane parallel to the tie. The critical section for the development of a tie is at the point where the centroid of the tie intersects the edge of the diagonal strut. Therefore, the available development length can be computed based on the geometry. The reinforcing bars can be sufficiently developed by satisfying the anchorage requirement, providing an available development length greater than the required development length.
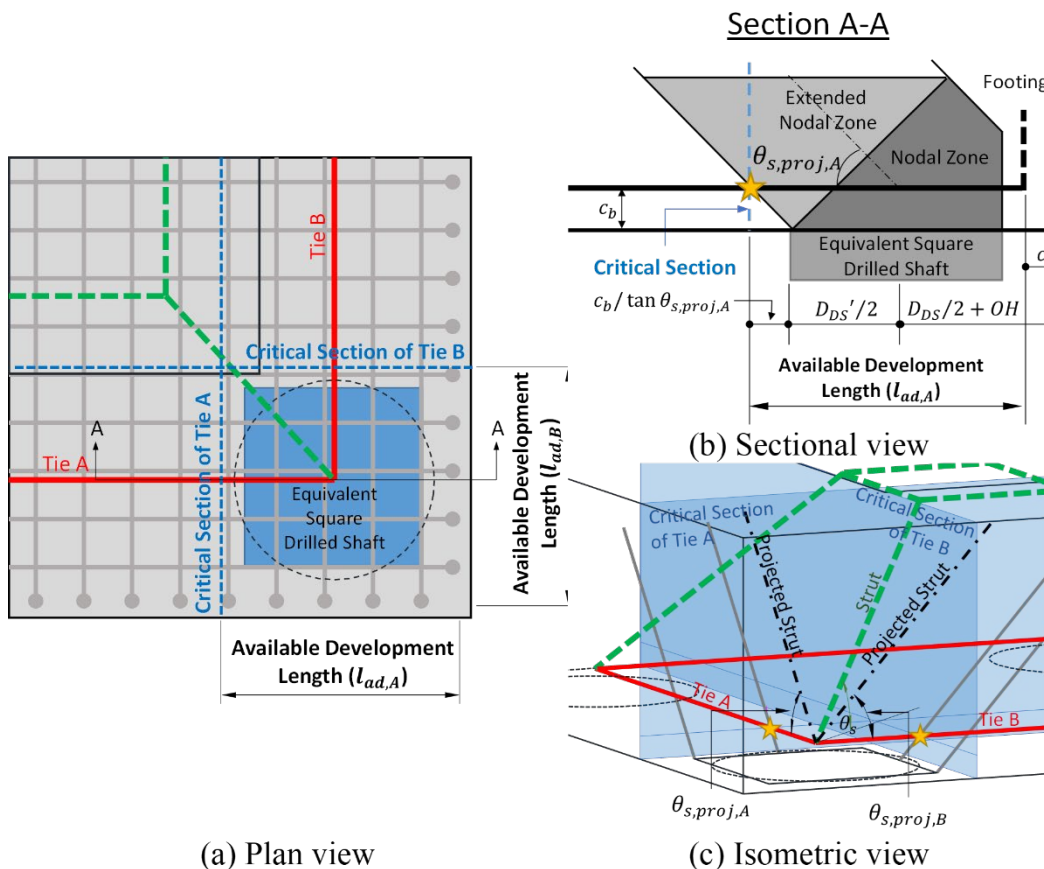
Figure 4.5 Critical section for bottom mat reinforcement in drilled shaft footings (at singular nodes)

4.4.1.2. At Smeared Nodes

The recommended extended nodal zone approach cannot be used at smeared nodes, for which the nodal geometry cannot be clearly defined. Therefore, the critical section of the tie at a smeared node is determined conservatively at the point directly above the interior edge of the equivalent square drilled shaft, as Williams et al. (2012) proposed.
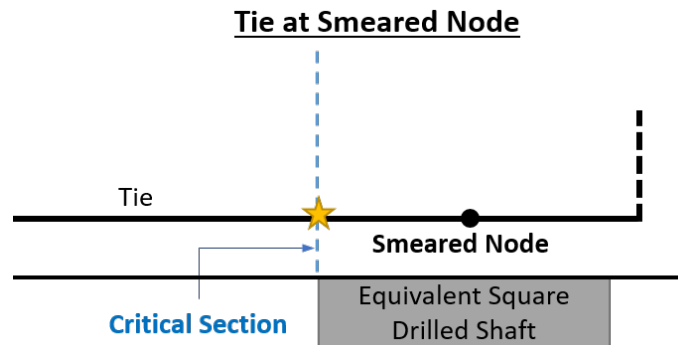
Figure 4.6 Critical section for bottom mat reinforcement in drilled shaft footings (at smeared nodes)

4.4.2. Vertical Ties (Column and Drilled Shaft Reinforcement)

4.4.2.1. Axial Compression Combined with Moderate Uniaxial Flexure

The 3D strut-and-tie model resulting from axial compression combined with moderate uniaxial flexure has vertical column tie elements connected to smeared nodes in the footing. Therefore, the critical section for the column ties cannot also be determined using the corresponding nodal geometry. Instead, a large compression field bounded by diagonal struts flowing down to the drilled shafts is considered to perform the same role as an extended nodal zone for establishing the critical section of the column tie elements, as shown in Figure 4.7. The available length of the column reinforcement can be determined based on the defined critical section. When hooked anchorage is employed for the column reinforcement, the hook needs to be oriented inwards to react against the diagonal strut flowing down from the compression face of the column to activate its bearing action.

(a) Isometric view   (b) Side view
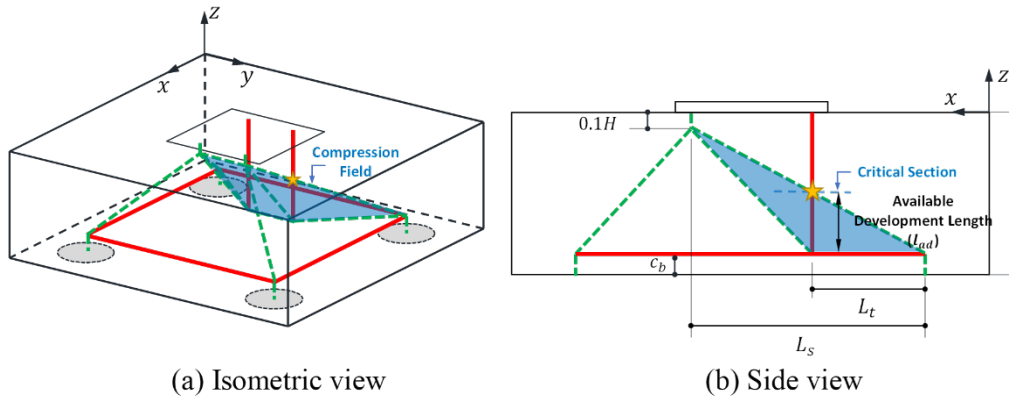
Figure 4.7 Critical section for column reinforcement in drilled shaft footings under Load Case III

4.4.2.2. *Axial Compression Combined with Large Uniaxial Flexure*

Due to the large flexure inducing tension at one face of the column and two of four drilled shafts, the anchorage checks for the vertical column tie elements, connected with smeared nodes, also need to be performed. Therefore, a large compression field between the column and drilled shaft tie elements was proposed to represent the force transfer mechanism between the tie elements, which resembles a non-contact lap splice behavior. The field is determined by the minimum strut angle specified in AASHTO LRFD (2020), 25 degrees, as illustrated in Figure 4.8. Hence, the critical sections for the column and drilled shaft reinforcement can be defined based on the compression field. In determining the available lengths for the column and drilled shaft reinforcement, the column reinforcement is assumed to be placed above the bottom mat reinforcement to facilitate constructability. Similarly, the drilled shaft reinforcement is assumed to extend up to the bottom layer of the top mat reinforcement.

(a) Isometric view   (b) Sectional view
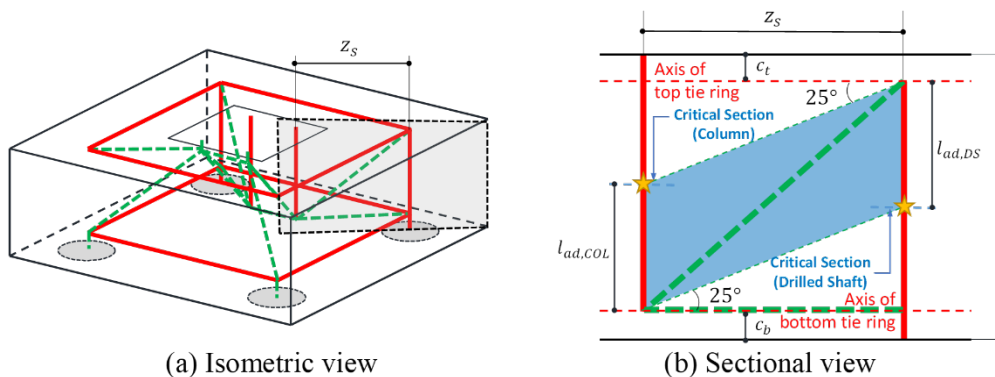
Figure 4.8 Critical section for column and drilled shaft reinforcement in drilled shaft footings under Load Case IV

Chapter 5. Refined Design Recommendations: Biaxial Load Scenarios

The 3D-STM recommendations for drilled shaft footings proposed by Yi et al. (2022) were used for the design examples of footings subjected to specific load scenarios. Those load scenarios were verified experimentally (Load Cases I, III, and IV in Figure 3.1) or resulted in simple strut-and-tie configurations (Load Cases II and V in Figure 3.1). However, the load cases involving biaxial flexural loading, which this research is interested in, have not been studied in detail, as summarized in Chapter 2. In particular, the 3D strut-and-tie model for drilled shaft footings under extremely complicated loading conditions inducing tension at one of four drilled shafts (axial compression combined with considerable biaxial flexure) has not been investigated.

Therefore, this section presents the modifications to the design recommendations proposed by Yi et al. (2022) for applying the 3D-STM to the design of drilled shaft footings under axial compression combined with moderate and large biaxial flexural loading.

5.1. Develop 3D Strut-and-Tie Model

5.1.1. Equivalent Force System

Yi et al. (2022) recommended that the equivalent force system of the column section partially under tension due to flexural loading be established by the actual stress distribution based on the applied loading to maintain the consistency of force flow between a B-region and a D-region. In the cases with uniaxial flexural loading (Load Case III and IV in Figure 3.1), the stress block factors proposed by Collins and Mitchell (1991) can be used to cover both linear and nonlinear behavior of the concrete. Further, the neutral axis becomes inclined owing to biaxial flexure. The inclined neutral axis determines a group of column reinforcement carrying column tie forces (reinforcing bars placed within the white-colored region in Figure 5.1). Therefore, a sectional analysis based on the linear strain distribution and constitutive relationships needs to be performed to clarify resultant forces at the column-footing interface. Three unknowns—neutral axis inclination (θ), neutral axis depth (c), and extreme compressive fiber strain (ε_c)—can be derived from three equilibrium equations ($\sum P_u = 0; \sum M_{ux} = 0; \sum M_{uy} = 0$) through an iterative process. Figure 5.1 presents the strain and stress distribution of the column section in the elastic state under the biaxial flexural loading.
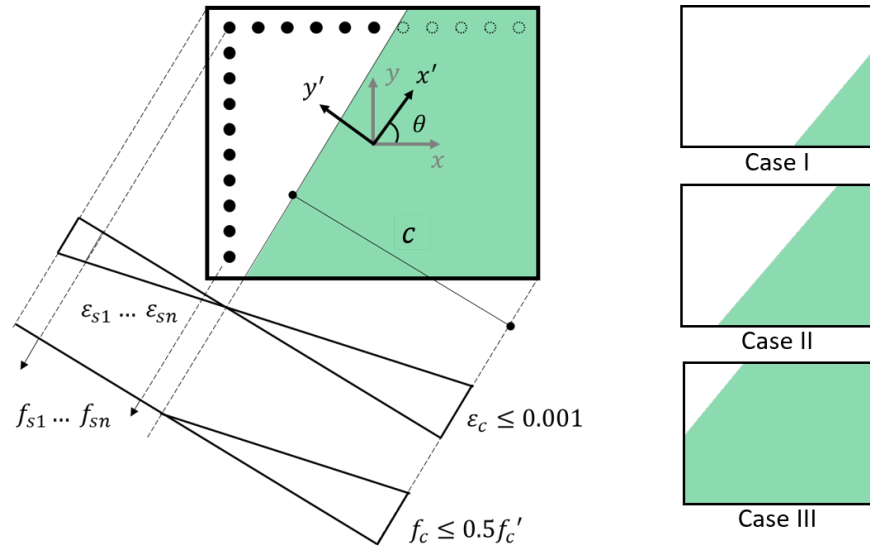
Figure 5.1 Strain and stress distribution over the column section under biaxial flexural loading and types of compressive region shape

In the 3D strut-and-tie models employed in the design example of Yi et al. (2022), the resultant forces at the interface were subdivided into four force components to proportion the optimal amount of the bottom mat reinforcement and perform nodal capacity checks at CCC nodes. The subdivided nodes should be compatible with the reactions at four drilled shafts and satisfy force and moment equilibriums at the interface. Accordingly, subdividing resultant forces should consider the internal force flow of the footing and actual stress distribution at the interface, which are challenging for the scenarios with biaxial flexure loading. The different shape of the compressive region at the interface (Figure 5.1) further complicates the procedure; therefore, designers should put in significant computational effort even when designing a drilled shaft footing for one biaxial flexural load case using the equivalent force system, comprising two struts and two ties. Since a drilled shaft footing is designed with many biaxial flexural load cases, it is not practical to establish an equivalent force system comprising multiple force components.

Based on this fact, the research team proposes using an equivalent force system consisting of a single compressive force and a single tensile force. This approach decreases the strut inclinations and results in an increase in strut and tie forces relative to those obtained from the equivalent force system with multiple struts and ties, leading to a conservative design of drilled shaft footings. Under this equivalent force system, the vertical strut is positioned at the resultant compressive force, while the tie is at the resultant tensile force. The exact locations at the interface are derived from the sectional analysis. To simplify the procedure, the tensile capacity of the concrete and compressive reinforcement contribution are neglected, and only

the column reinforcing bars at two adjacent tensile column faces are considered for the sectional analysis to determine the equivalent force system.

5.1.2. 3D Strut-and-Tie Model

5.1.2.1. LC6: Axial Force Combined with Moderate Biaxial Flexure

Figure 5.2 presents the 3D strut-and-tie model for drilled shaft footings under axial force combined with moderate flexural loading. The recommendations regarding nodal elevations of the 3D strut-and-tie model remain the same as those summarized in Section 4.1.
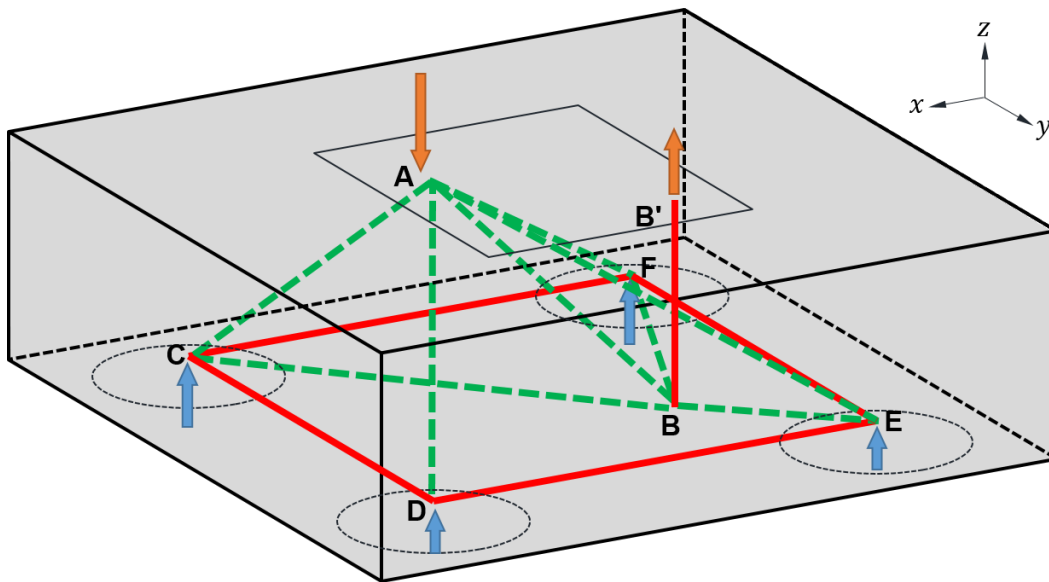
Figure 5.2 3D strut-and-tie model for drilled shaft footing under Load Case VI

The resultant compressive force of the established equivalent force system is transmitted through four diagonal struts (Struts AC, AD, AE, and AF in Figure 5.2) spreading from the CCC node to the four drilled shafts, respectively. A tie ring (Ties CD, DE, EF, and CF in Figure 5.2) is necessary to resist the lateral force component of the diagonal struts. A vertical column tie (Tie BB' in Figure 5.2) representing the resultant tensile force of the equivalent force system extends down to the plane of the bottom tie ring. To satisfy the vertical force equilibrium, an additional diagonal strut (Strut AB in Figure 5.2) is provided, connecting the CCC node and the bottom end node of the column tie element. The diagonal struts (Struts BC, BE, and BF in Figure 5.2) on the horizontal plane of the bottom tie ring are required to satisfy the horizontal force equilibrium at the CTT nodes. The configuration of the 3D strut-and-tie model is almost the same as that proposed by Ballestrino et al. (2011) (Figure 2.2). However, the internal force flow of drilled shaft footings subjected to the biaxial flexural loading cases is no longer symmetric.

Therefore, the configuration of the diagonal struts for the horizontal force equilibrium is not fixed but varies depending on the footing geometry and equivalent force system, as illustrated in Figure 5.3.

(a) *y*-force component of
Strut AC < Strut AD

(b) *y*-force component of
Strut AC > Strut AD

(c) *y*-force component of
Strut AC = Strut AD
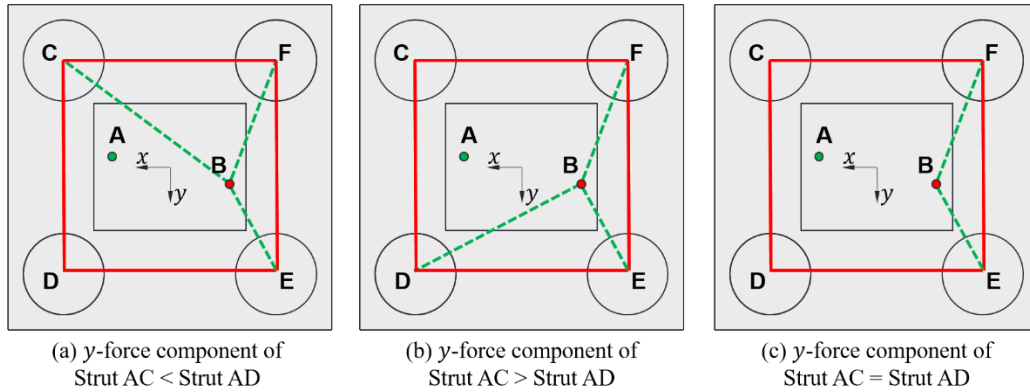
Figure 5.3 Two different configurations of horizontal struts on the bottom tie ring plane

5.1.2.2. LC7: Axial Force Combined with Large Biaxial Flexure

The biaxial flexural loading induces tension at one of four drilled shafts and has the most complicated internal force flow among the loading scenarios. The 3D strut-and-tie model for this biaxial load case has not been investigated so far. The research team developed a simplified 3D strut-and-tie model to understand the internal force flow of drilled shaft footings resulting from this extreme biaxial flexural loading condition, as shown in Figure 5.4.
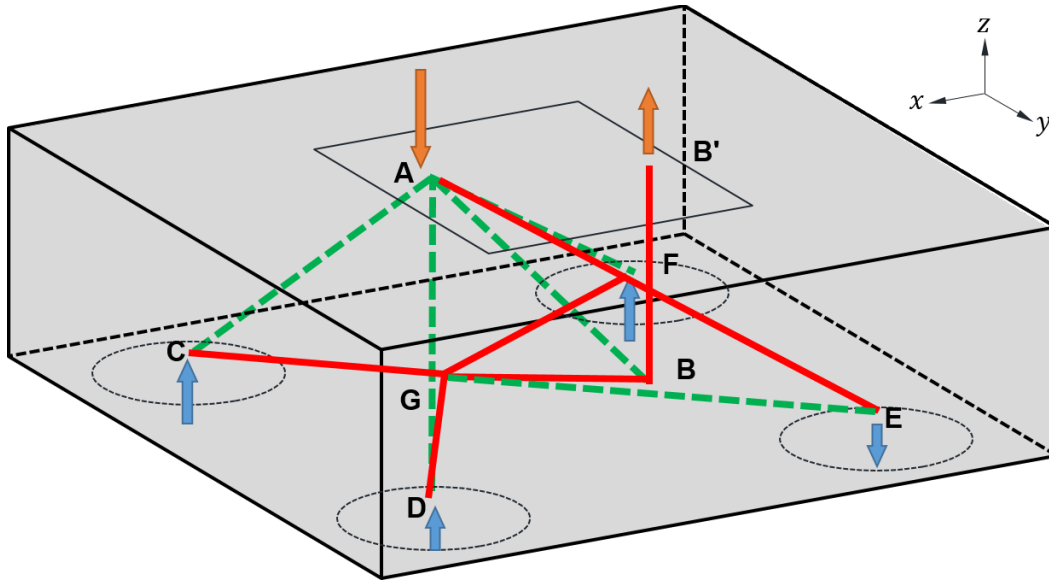
Figure 5.4 Simplified 3D strut-and-tie model for drilled shaft footing under Load Case VII

One tensile and the other three compressive reactions at the four drilled shafts are carried by the resultant compressive force at the equivalent force system through one diagonal tie (Tie AE in Figure 5.4) and three diagonal struts (Struts AC, AD, and AF in Figure 5.4), respectively. The vertical column tie (Tie BB' in Figure 5.4) resulting from the tensile resultant force of the equivalent force system is also carried by the resultant compressive force through a diagonal strut (Strut AB in Figure 5.4). All of the aforementioned diagonal elements are connected to the CCC node beneath the column (Node A in Figure 5.4), and their lateral force components satisfy the equilibrium. Similarly, the horizontal elements (Ties BG, CG, DG, and FG and Strut EG in Figure 5.4) placed on the bottom tie ring plane are required to satisfy the equilibrium at the nodes above drilled shafts (Nodes C through F in Figure 5.4). Those elements also meet at the node (Node G in Figure 5.4) where the CCC node is projected on the bottom tie ring plane and satisfy the equilibrium at Node G.
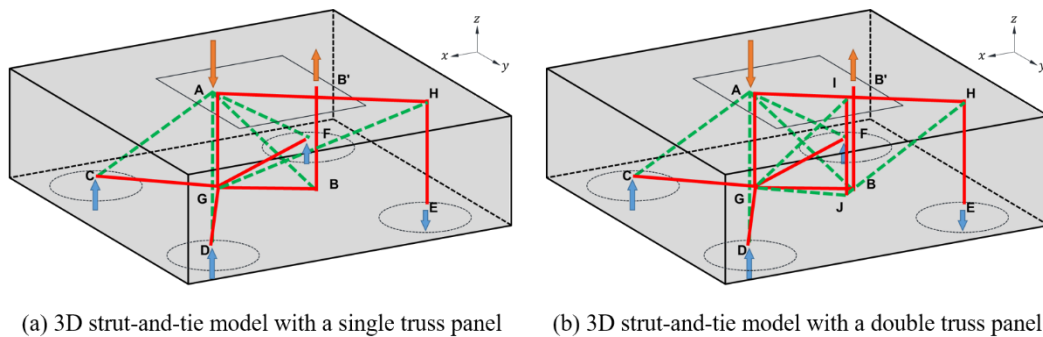
(a) 3D strut-and-tie model with a single truss panel   (b) 3D strut-and-tie model with a double truss panel

Figure 5.5 3D strut-and-tie models with a truss panel to transfer drilled shaft tie force

A triangular truss panel for transmitting the tensile reaction is substituted with a single rectangular truss panel (Figure 5.5a), which indicates that the truss panels of the column tie force transfer mechanism and of the drilled shaft tie force mechanism do not overlap each other. Nevertheless, the force transfer mechanism representing the non-contact lap splice behavior between the drilled shaft reinforcement and some column reinforcing bars (Tie IJ in Figure 5.5b) can be identified from the model expressed with two rectangular truss panels (Figure 5.5b). However, subdividing the column tie element into two ties requires computational effort, as described in Section 5.1.1.
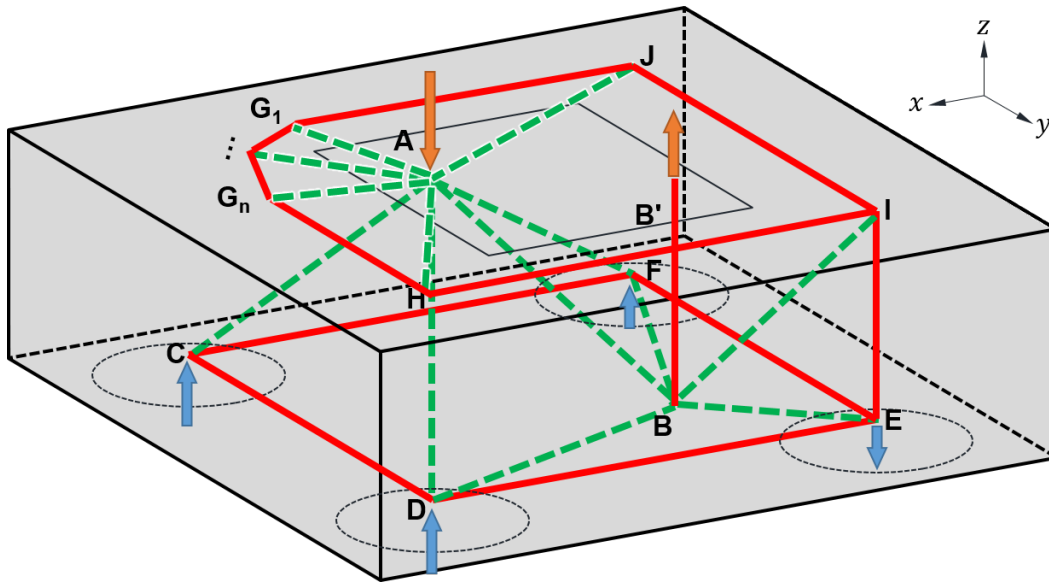
Figure 5.6 Idealized 3D strut-and-tie model for drilled shaft footing under Load Case VII

Figure 5.6 presents an idealized 3D strut-and-tie model by disassembling the diagonal ties in Figure 5.4 into orthogonal ties to facilitate designing the top and bottom mat reinforcement. Unlike the simplified model, the planes of the column and tie force transfer mechanisms are integrated together in the idealized model, and this discrepancy leads to inequilibrium at the CTT node of the drilled shaft under tension (Node E in Figure 5.6). The error caused by the inequilibrium can be estimated by shifting the nodal position of Node E to satisfy the equilibrium. The externally applied moments are compared with those estimated from the reactions of the shifted nodal position. The error was estimated in the design example covered in Section 6.2.2 and was found to be insignificant, at less than 1.0% (0.6%). Furthermore, the strut that induces the inequilibrium (Strut BE in Figure 5.6) is not used for the nodal strength checks; therefore, the inequilibrium problem does not greatly impact the design procedure.

One more thing that needs to be considered in the idealized model is positioning the top nodes (Nodes G_1, G_2, ... and G_n in Figure 5.6) for the top tie elements.

Whereas the 3D strut-and-tie model of the uniaxial flexural case resulting in tension at two of four drilled shafts has a rectangular-shaped top tie ring owing to the symmetric configuration of the model, the 3D strut-and-tie model of the biaxial flexural case inducing tension at one drilled shaft is no longer symmetric. The lateral force component of the diagonal strut representing the non-contact lap splice behavior (Strut BI in Figure 5.6) is transferred to the CCC node underneath the column through a top tie ring (Ties G_nH, HI, IJ, and G_1J in Figure 5.6) and horizontal struts stemming from the corners of the top tie ring (Struts AH, AJ, and AG_1 … AG_n in Figure 5.6). The second and third top nodes comprising the top tie ring (Nodes H and J in Figure 5.6) are positioned on the center axes of two drilled shafts adjacent to the drilled shaft under tension. On the other hand, the fourth node cannot be positioned on the center axis of the drilled shaft to transfer the tie forces and satisfy the equilibrium at Node A. Instead, a series of struts and ties are required to be formed near the corner; however, determining the number of nodes to be provided and their nodal positions for satisfying the requirements is overly complicated. Therefore, since the strut-and-tie model configuration near the corner varies significantly depending on the applied loading, the force component of each strut and tie in this region is not considered. Nevertheless, the drilled shaft footing design based on the idealized model is made possible by resolving the widespread struts (Struts AG_1 … AG_n in Figure 5.6) into a single diagonal strut (Strut AG) whose force can be derived from the equilibrium at Node A. The top mat reinforcement can also be designed from the orthogonal ties (Ties G_nH, HI, IJ, and G_1J in Figure 5.6) of the model.

5.2. Perform Nodal Strength Check at CCC Node

5.2.1. Modified Equivalent Square Bearing Face

Before describing the proposed approach to defining the CCC nodal bearing face under the biaxial loading scenarios that cause tension in the column section, the research team reviewed the assumptions used to define the CCC nodal bearing face for the other loading scenarios. The approaches employed to develop the recommendations of Yi et al. (2022) for defining the bearing faces of the CCC node in the drilled shaft footings under various load conditions are summarized below.

For a load case in which the entire column section is subjected to compression, the column section is subdivided into four sections based on the actual stress distribution according to the determined equivalent force system. Each of these subdivided sections becomes the bearing face of the CCC node. The bearing faces could have complex shapes depending on the load case (Load Case V in Figure 3.1); therefore, each subdivided section is replaced with an equivalent square bearing

face to develop the proposed 3D nodal geometry. Each equivalent bearing face is considered to be subjected to uniformly distributed stress, regardless of the actual stress distribution, when estimating its nodal strength. This approach is reasonable since the entire column section is under compression, and the sum of the capacities of the equivalent bearing faces is identical to the bearing capacity of the entire column section.

On the other hand, the dimension of the bearing face of the CCC node is determined based on the actual stress distribution when tensile stresses act on the part of the column section due to flexure. For the continuously changing neutral axis, Yi et al. (2022) defined the bearing face of the CCC node conservatively using the compressive stress block region, which is smaller than the actual compressive region over the column section, determined by equivalent stress block factors proposed by Collins and Mitchell (1992). This approach is limited to the uniaxial load cases (Load Case III and IV in Figure 3.1) since the equivalent stress factors were not verified for the cases with biaxial flexural loading. The nodal strength check was performed based on the 3D nodal geometry developed using the rectangular-shaped bearing face of the CCC node.

However, the two aforementioned approaches cannot be directly applied to the scenarios with biaxial loading in this research because not only is the entire column section not subjected to compression, but the shape of the compressive region changes depending on the applied load. Furthermore, the equivalent stress block factors verified only for the cases under uniaxial flexural loading cannot be used. As an alternative, in this study, the bearing face of the CCC node is defined through a conservative approach. We assumed that the maximum stress value of the compressive stress region over the column section derived from the sectional analysis (f_c in Figure 5.1) is uniformly distributed over the bearing face of the CCC node. Therefore, a modified bearing area of the CCC node can be obtained by dividing the resultant compressive force by the maximum stress value. After that, the modified bearing area is replaced with an equivalent square-shaped bearing face to cover the varying compressive region of the column section under the biaxial flexural loading (Figure 5.1). Consequently, the derived square-shaped bearing face is much smaller than the actual area of the compressive region but results in a much simpler and conservative estimate of the CCC nodal strength. The research team defined this simplified bearing face of the CCC node as the modified equivalent square bearing face.

Nevertheless, the confinement modification factor described in Section 4.3.1 is determined based on a square bearing face, equivalent to the actual compressive area derived from the sectional analysis. As illustrated in Figure 5.7, this approach

leads to a conservative design compared to the confinement modification factors determined from the equivalent square bearing face and actual compressive area.
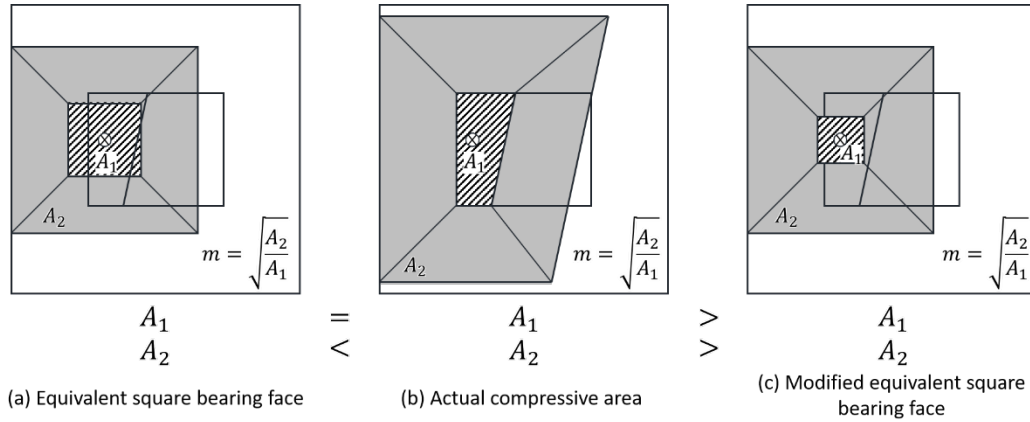
Figure 5.7 Comparison of approaches defining confinement modification factor

Table 5.1 summarizes the approaches employed to define the bearing faces of the CCC node in drilled shaft footings under different loading scenarios.

Table 5.1 Different approaches for defining bearing face of CCC node in drilled shaft footings depending on loading scenario

	Load Case I	*Load Case II*	*Load Case III*	*Load Case IV*
Load Combination	Axial Compression	Axial Compression + Mild Uniaxial Flexure	Axial Compression + Moderate Uniaxial Flexure	Axial Compression + Large Uniaxial Flexure
Compressive Stress Distribution	Uniform	Linear/Nonlinear	Uniform (Equivalent stress block)	Uniform (Equivalent stress block)
Shape of Compressive Region	Entire Section	Entire Section	Partial (Rectangular)	Partial (Rectangular)
Approach for Bearing Face of CCC Node	Equivalent Square Bearing Face	Equivalent Square Bearing Face	Equivalent Stress Block	Equivalent Stress Block

	Load Case V	**Load Case VI**	**Load Case VII**
Load Combination	Axial Compression + Mild Biaxial Flexure	**Axial Compression + Moderate Biaxial Flexure**	**Axial Compression + Large Biaxial Flexure**
Compressive Stress Distribution	Linear/Nonlinear	**Linear/Nonlinear**	**Linear/Nonlinear**
Shape of Compressive Region	Entire Section	**Partial (3 Different types)**	**Partial (3 Different types)**
Approach for Bearing Face of CCC Node	Equivalent Square Bearing Face	**Modified Equivalent Square Bearing Face**	**Modified Equivalent Square Bearing Face**

5.2.2. Development of 3D Nodal Geometry

Under the proposed equivalent force system, the 3D strut-and-tie model has only one CCC node connected with multiple struts acting in different directions. The diagonal struts must be resolved to reduce the number of force components acting at the CCC node to three for developing the 3D nodal geometry proposed by Yi et al. (2022). However, when struts acting at only one CCC node are resolved to a single strut, its lateral force component converges to be zero. Hence, it is impossible to develop the 3D nodal geometry without additional modification. A bent cap design example using the 2D STM proposed by Williams et al. (2012) subdivided a node connected with multiple struts in opposite directions to develop the nodal geometry to address a similar problem. The node was subdivided based on the ratio of the vertical force components of the struts acting in the opposite direction, as shown in Figure 5.8.

(a) 3D strut-and-tie model of Load Case VI   (b) 3D strut-and-tie model of Load Case VII

⬤⬤⬤ Struts carried by subdivided CCC nodes on Node F and D-sides
⬤⬤⬤ Struts carried by subdivided CCC nodes on Node F-side
⬤⬤⬤ Struts carried by subdivided CCC nodes on Node D-side
▮ Internal force flow carried by subdivided CCC node on Node F-side
▮ Internal force flow carried by Node D-side
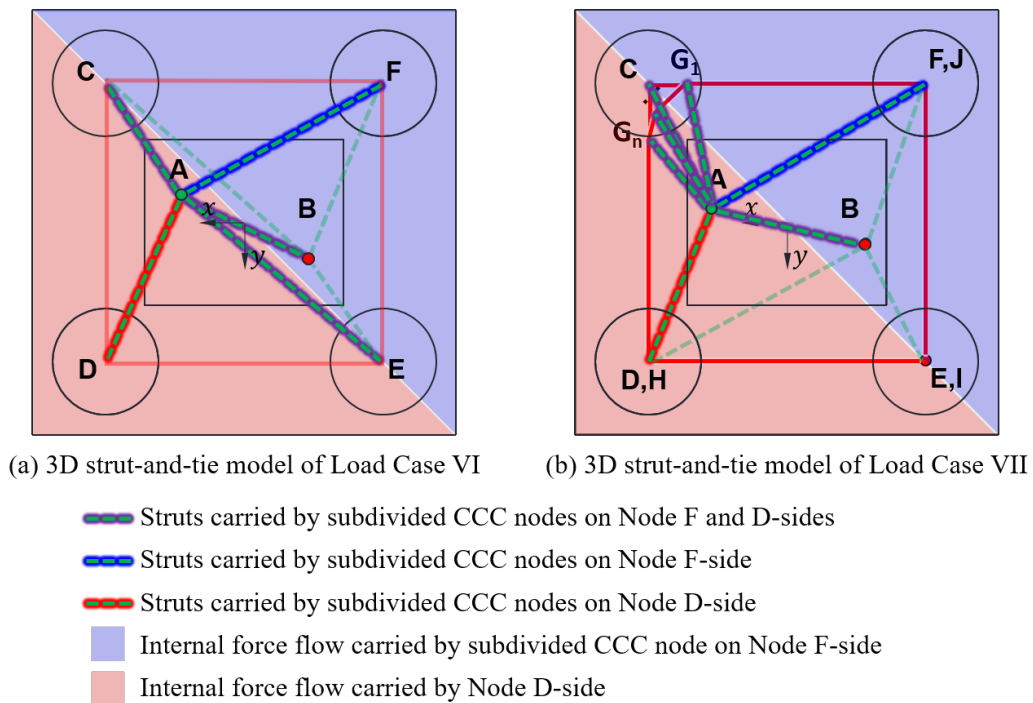
Figure 5.8 Subdividing struts acting at CCC node to develop 3D nodal geometry

The research team also subdivided the CCC node of the 3D strut-and-tie models for the scenarios with biaxial loading to develop its 3D nodal geometry. The forces acting at the CCC node are subdivided into two groups based on the diagonal sectional plane of the footing connecting the drilled shafts under the largest and smallest reaction forces. The diagonal struts in the vicinity of this plane are disassembled by the ratio of the reaction forces acting on the other two drilled shafts, and the struts in each group are resolved into a single diagonal strut. The width of the resultant compressive force and the modified equivalent square bearing face of

the CCC node is also subdivided by the ratio of the reaction force acting on those two drilled shafts. As a result, three force components (subdivided resultant compressive force, resolved diagonal strut, and lateral force component of the resolved diagonal strut) act at the two subdivided CCC nodes. Therefore, the 3D nodal geometries of those two subdivided CCC nodes can be developed based on the specified dimensions, as illustrated in Figure 5.9 and Figure 5.10.
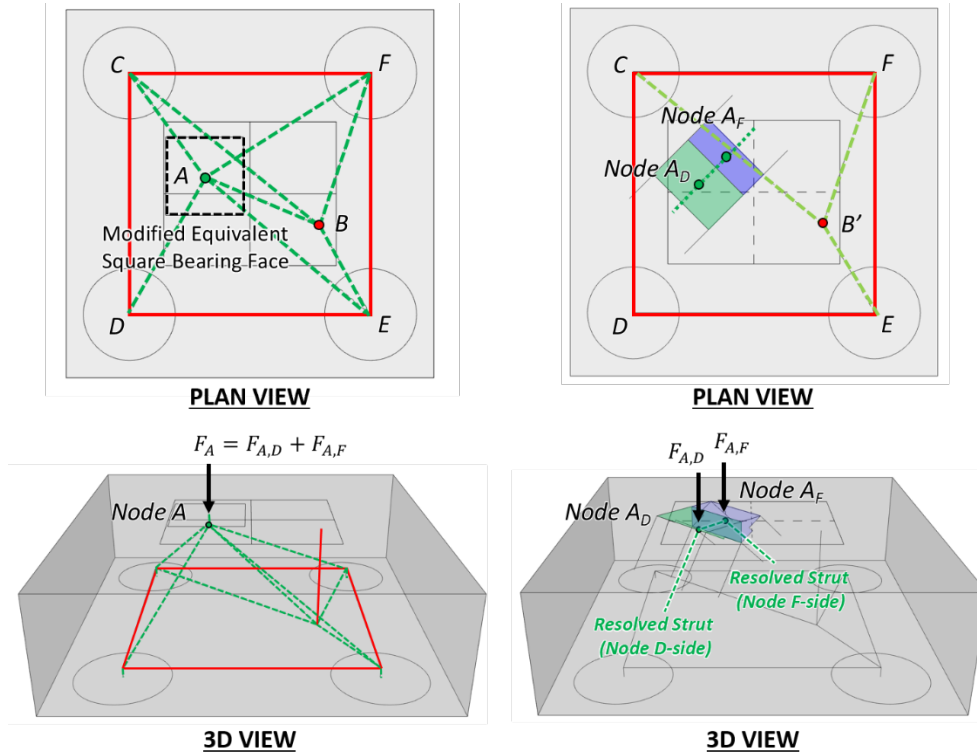
Figure 5.9 Development of 3D nodal geometry for CCC node in drilled shaft footing under Load Case VI

PLAN VIEW

PLAN VIEW

$$F_A = F_{A,D} + F_{A,F}$$

3D VIEW

3D VIEW
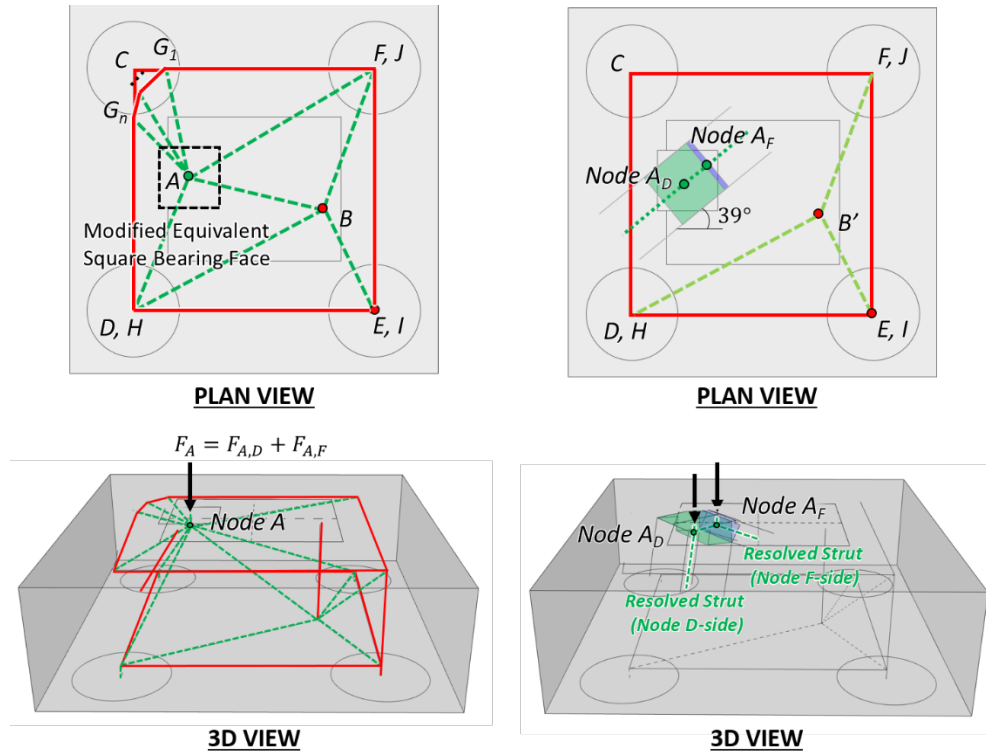
Figure 5.10 Development of 3D nodal geometry for CCC node in drilled shaft footing under Load Case VII

31

Chapter 6. Design Example

6.1. Summary of Previously Published Design Example

6.1.1. Drilled Shaft Footing Geometry
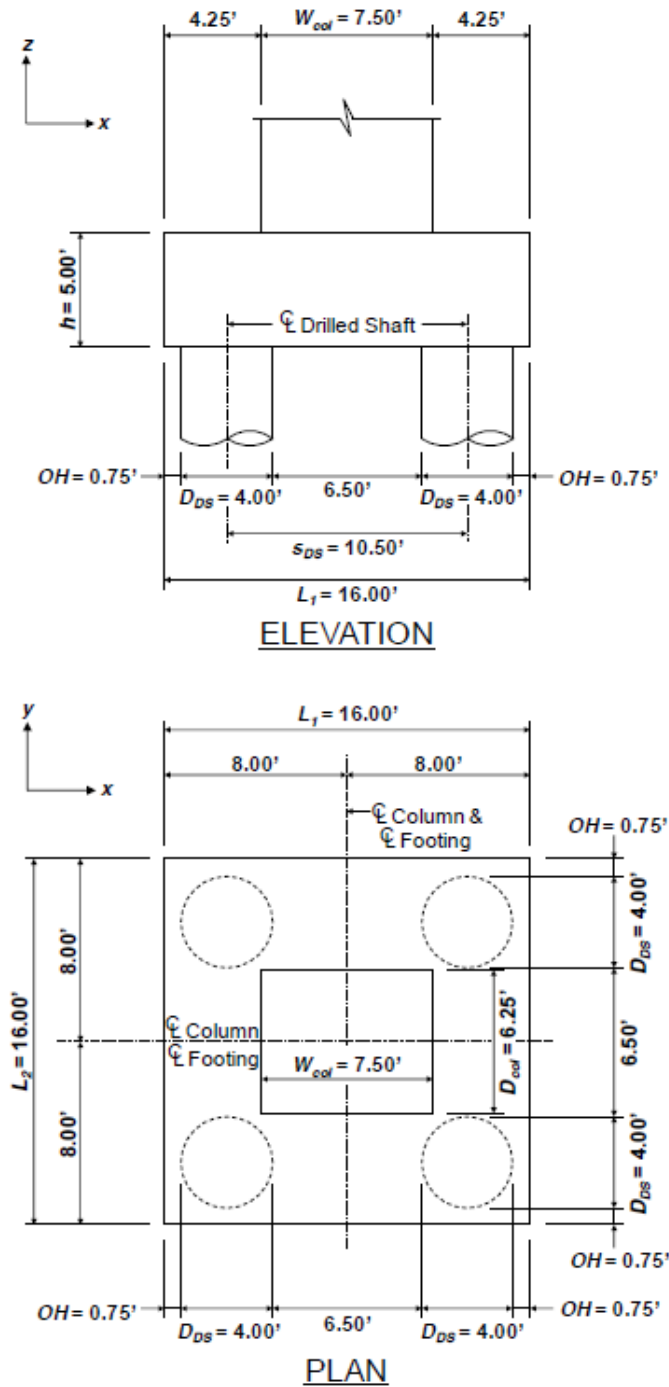
Figure 6.1 Geometry of the drilled shaft footing for the design example (Williams et al., 2012)

The design example of TxDOT 0-6953 (Yi et al., 2022) is a drilled shaft footing with the same geometry as Williams et al. (2012). The 16-foot-square drilled shaft footing is 5 feet tall and supported by four 4-foot-diameter drilled shafts, with a span of 10.50 feet. The footing has a rectangular column with a dimension of 7.50 by 6.25 feet. The footing and the column are doubly symmetric with respect to x- and y-axes, as illustrated in Figure 6.1.

6.1.2. Load Cases

The drilled shaft footing of the design example of Yi et al. (2022) has five different loading scenarios. Figure 6.2 shows the factored load combinations of the five loading scenarios.
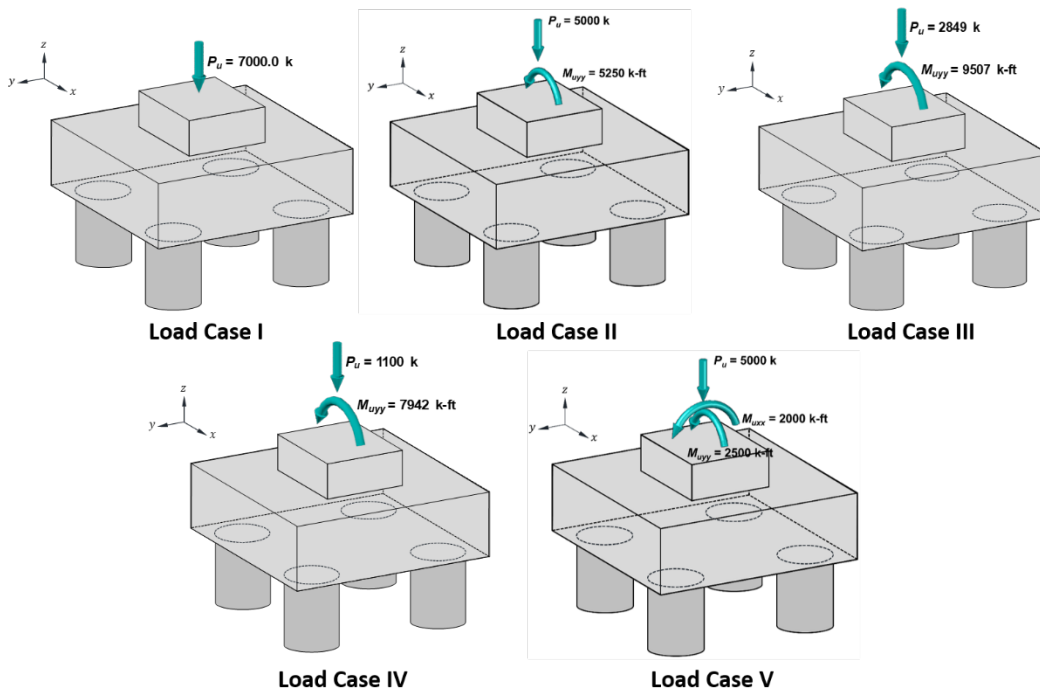
Figure 6.2 Factored load combinations used for design example of Yi et al. (2022)

6.1.3. Designed Reinforcement Detail

The reinforcement details designed from the five loading scenarios are summarized in Table 6.1.

Table 6.1 Summary of reinforcement designed with Load Case I through V

	Reinforcement Amount	Anchorage Detail	Governing Load Case
Bottom Mat Reinforcement	38-No.11 @ 5.00 in.	Straight	Load Case I
Top Mat Reinforcement	20-No.6 @ 10.00 in.	Straight	Minimum Shrinkage and Temperature Reinforcement (0.18%)
Vertical Side Face Reinforcement	20-No.6 @ 10.00 in.	90-Degree Hook	
Horizontal Side Face Reinforcement	5-No.6 @ 10.00 in.	90-Degree Hook	
Column Reinforcement	44-No.11	90-Degree Hook	N/A*
Drilled Shaft Reinforcement	4-No.9 (Embedded in footing)	180-Degree Hook	Load Case IV

*Column reinforcement layout is already given

6.2. Design Task

To supplement the design example of Yi et al. (2022), the research team designed the same drilled shaft footing with two additional biaxial loading scenarios using the proposed design guidelines. Therefore, the research team used the same concrete compressive strength ($f'_c = 3.6$ ksi) and yield strength of reinforcement ($f_y = 60$ ksi) as those of the previous design example.

One of the reviewed in-practice drilled shaft footings (Footing A in Table 3.1) has the same geometry as the footing designed in this section. Therefore, the extreme biaxial load cases classified as Load Case VI and VII (refer to Figure 3.1) are selected for the design example.

Based on the refined design recommendations introduced in Chapter 5, the drilled shaft footing is designed with a biaxial flexural loading following the general STM procedure below:

Step 1: Determine loads

Step 2: Analyze structural components

Step 3: Develop strut-and-tie model

Step 4: Proportion ties

Step 5: Perform strength checks

Step 6: Proportion the shrinkage and temperature reinforcement

Step 7: Provide necessary anchorage for ties

6.2.1. Design Calculations: Load Case VI

Figure 6.3 illustrates the factored load case where the column is subjected to axial compression combined with moderate biaxial flexure. This loading combination leads to tension at one corner of the column and non-uniform compression in drilled shafts.
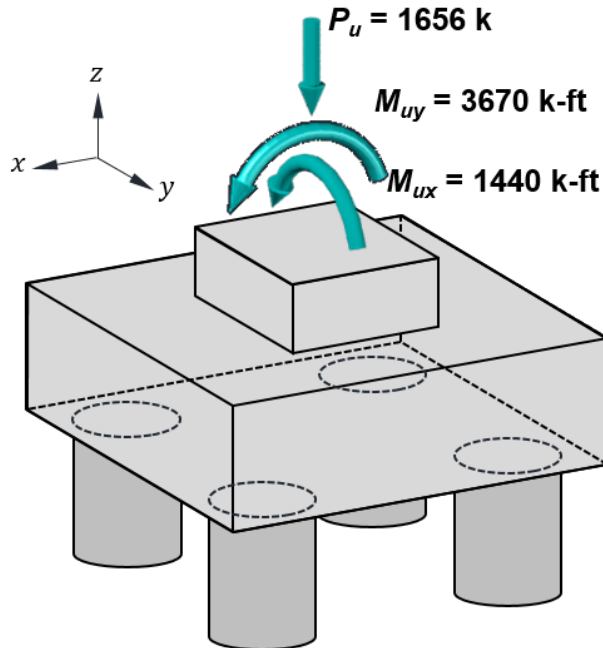
Figure 6.3 Factored load: Load Case VI

6.2.1.1. Step 1: Determine the Loads

Based on the given loading combination, a sectional analysis is conducted to determine the equivalent force system over the column section. Three unknowns (neutral axis depth (c); neutral axis inclination (θ); and extreme compressive fiber strain (ε_c)) are derived from three equilibrium equations ($\sum P_u = 0$; $\sum M_{ux} = 0$; $\sum M_{uy} = 0$) through an iterative process. The calculation procedure is provided in Appendix A. Figure 6.4 presents the derived strain and stress distribution over the column section, and the compressive and tensile resultant forces of the section determines the equivalent force system.
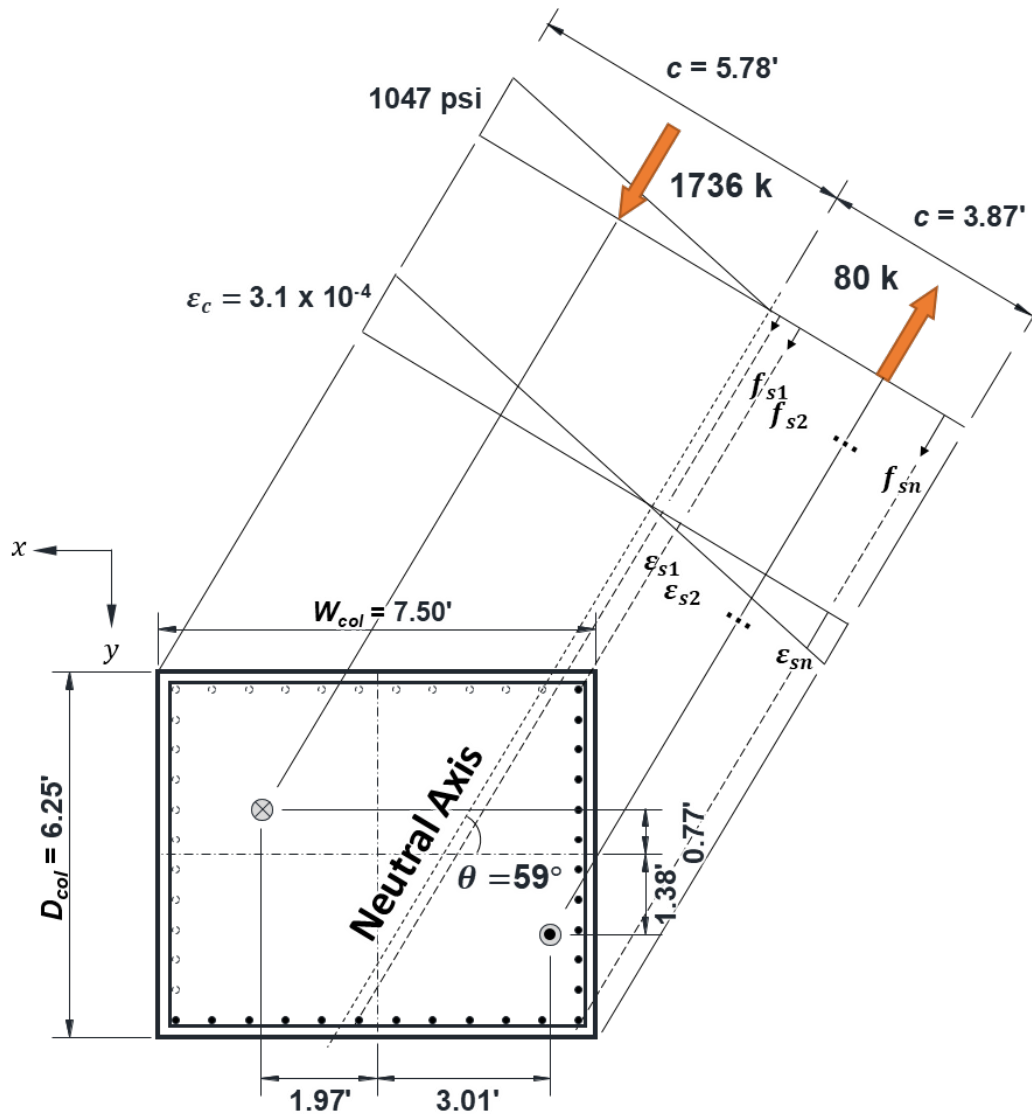
Figure 6.4 Stress distribution over the column section: Load Case VI

6.2.1.2. Step 2: Analyze Structural Component

The reaction forces in drilled shafts can be derived from the equilibrium conditions of the external loading. Figure 6.5 presents the results of the structural analysis.

$$R_1 = \frac{P_u}{4} + \frac{1}{2}\left(\frac{M_{ux}}{S_{DS,x}}\right) + \frac{1}{2}\left(\frac{M_{uy}}{S_{DS,y}}\right)$$
$$= \frac{1656 \text{ kip}}{4} + \frac{1}{2}\left(\frac{1440 \text{ k–ft}}{10.50 \text{ ft}}\right) + \frac{1}{2}\left(\frac{3670 \text{ k–ft}}{10.50 \text{ ft}}\right) = 657.3 \text{ kip (Compression)}$$
$$R_2 = \frac{P_u}{4} - \frac{1}{2}\left(\frac{M_{ux}}{S_{DS,x}}\right) + \frac{1}{2}\left(\frac{M_{uy}}{S_{DS,y}}\right)$$
$$= \frac{1656 \text{ kip}}{4} - \frac{1}{2}\left(\frac{1440 \text{ k–ft}}{10.50 \text{ ft}}\right) + \frac{1}{2}\left(\frac{3670 \text{ k–ft}}{10.50 \text{ ft}}\right) = 520.2 \text{ kip (Compression)}$$

$$R_3 = \frac{P_u}{4} - \frac{1}{2}\left(\frac{M_{ux}}{S_{DS,x}}\right) - \frac{1}{2}\left(\frac{M_{uy}}{S_{DS,y}}\right)$$

$$= \frac{1656 \text{ kip}}{4} - \frac{1}{2}\left(\frac{1440 \text{ k–ft}}{10.50 \text{ ft}}\right) - \frac{1}{2}\left(\frac{3670 \text{ k–ft}}{10.50 \text{ ft}}\right) = 307.8 \text{ kip (Compression)}$$

$$R_4 = \frac{P_u}{4} + \frac{1}{2}\left(\frac{M_{ux}}{S_{DS,x}}\right) - \frac{1}{2}\left(\frac{M_{uy}}{S_{DS,y}}\right)$$

$$= \frac{1656 \text{ kip}}{4} + \frac{1}{2}\left(\frac{1440 \text{ k–ft}}{10.50 \text{ ft}}\right) - \frac{1}{2}\left(\frac{3670 \text{ k–ft}}{10.50 \text{ ft}}\right) = 170.7 \text{ kip (Compression)}$$
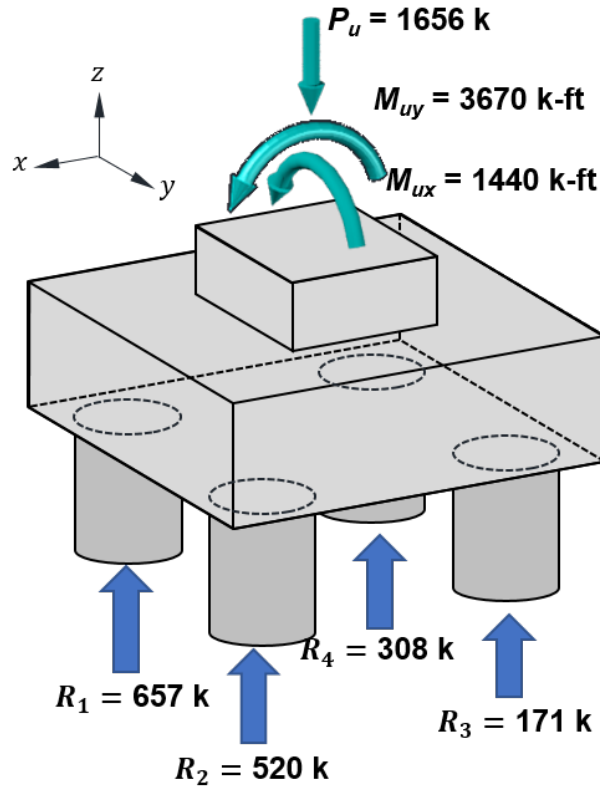
Figure 6.5 Applied loading and reaction forces: Load Case VI

6.2.1.3. Step 3: Develop Strut-and-Tie Model

The research team developed a 3D strut-and-tie model corresponding to the applied loading condition following the basic principle of the 3D STM specified in Section 5.1.2.1. The strut-and-tie configuration on the bottom plane of this design example is different from that of Ballestrino et al. (2011). This difference results from the discrepancy between lateral force components of the diagonal struts flowing down to drilled shafts. As illustrated in Figure 6.6, the y-directional lateral force component of Strut AD is higher than that of Strut AC; therefore, a horizontal strut (Strut BC) must be connected to Node C to satisfy the equilibrium.

Based on the strut-and-tie model configuration, strut forces and tie forces satisfying the equilibrium of each axis at each node can be computed, as shown in Figure 6.7 and Figure 6.8. The calculation procedure to derive the elemental forces is provided in Appendix B.
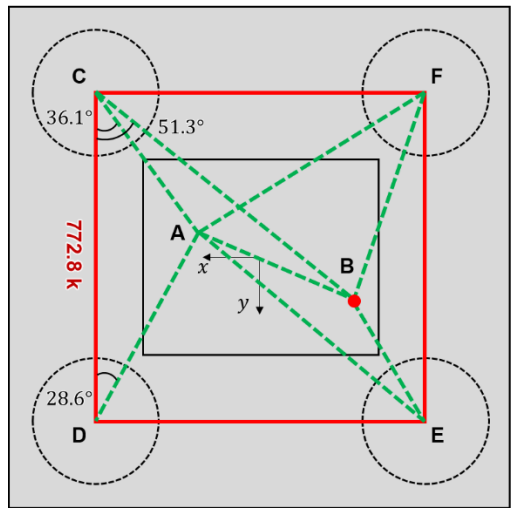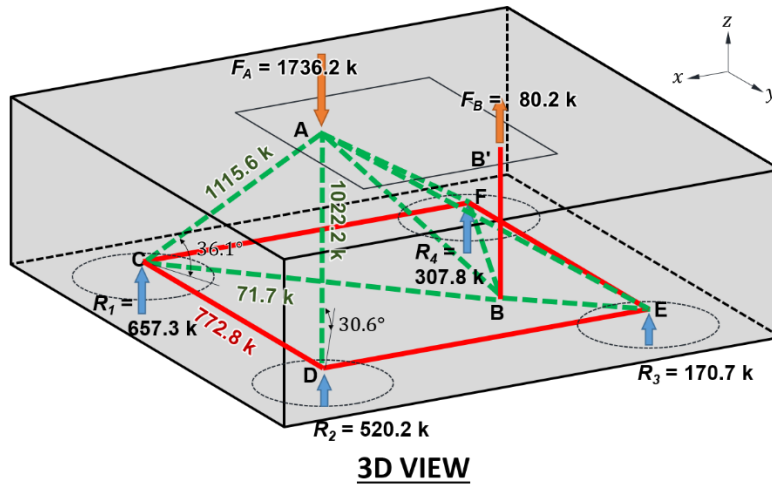
3D VIEW

y-force component of Strut AC
$$= 1115.6 \cos 36.1° \cos 36.1° = 728.0 \text{ kip}$$

y-force component of Strut AB
$$= 1022.2 \cos 30.6° \cos 28.6° = 772.8 \text{ kip}$$

Strut BC is required to satisfy
the y-directional force equilibrium

y-force component of Strut BC
$$= 71.7 \cos 51.3° = 44.9 \text{ kip}$$

PLAN VIEW

Figure 6.6 Determination of the strut-and-tie model configuration: Load Case VI

38
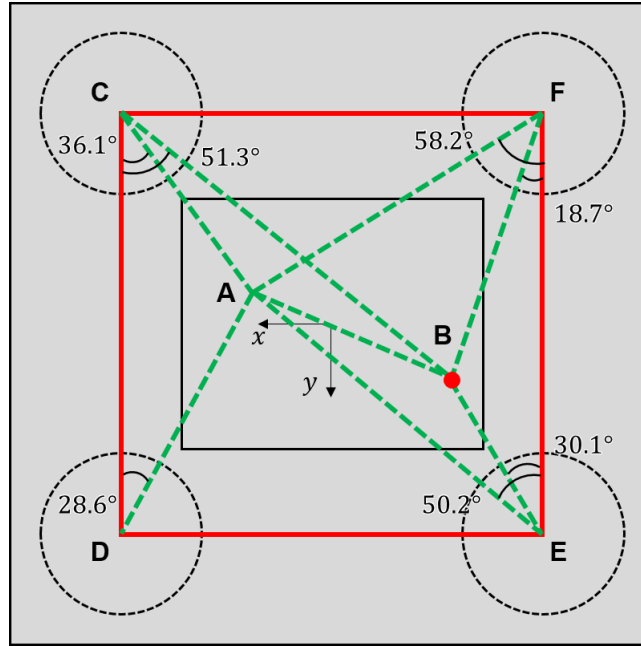
Figure 6.7 3D strut-and-tie model (plan view): Load Case VI
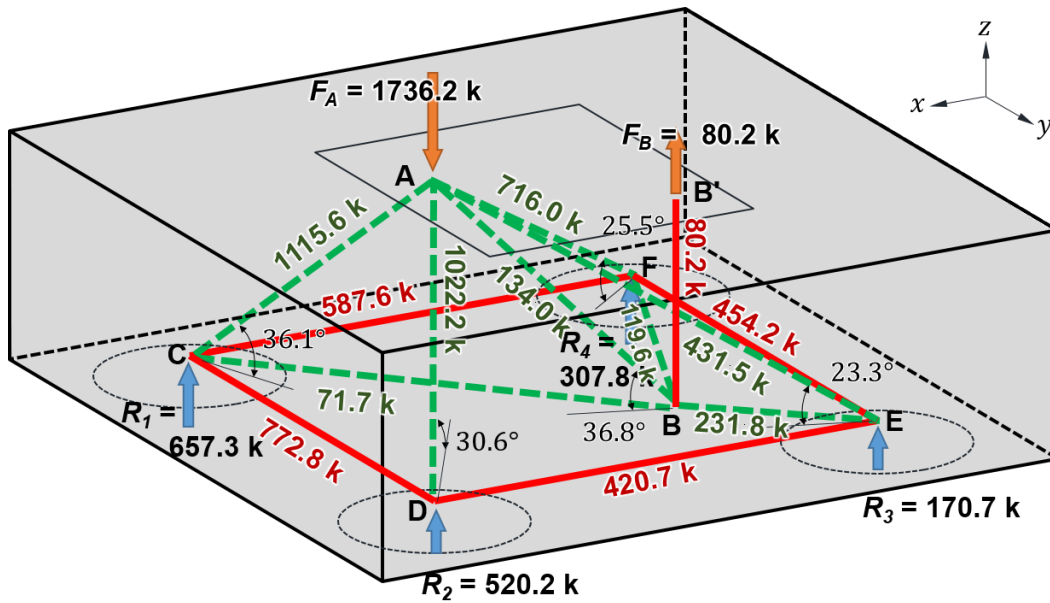
Figure 6.8 3D strut-and-tie model (axonometric view): Load Case VI

6.2.1.4. Step 4: Proportion Ties

The required number of No. 11 reinforcing bars for the bottom mat reinforcement can be estimated from the computed bottom tie forces. Furthermore, the researchers examined the capacity of the column-reinforcing bars in the tension side of the column to verify whether they can carry the computed column tie force based on the given column reinforcement layout and the derived stress distribution over the column section.

Tie CD (Bottom Mat Reinforcement)

Factored tie force: $\qquad$ $F_{u,tie} = 772.8$ kip

Tie capacity:
$$\phi \cdot f_y \cdot A_{st} = F_{u,tie}$$
$$(0.9)(60 \text{ ksi})A_{st} = 772.8 \text{ kip}$$
$$A_{st} = 14.31 \text{ in.}^2$$

Number of No. 11 bars required: $\qquad 14.31 \text{ in.}^2 / 1.56 \text{ in.}^2 = 10$ bars

Tie DE (Bottom Mat Reinforcement)

Factored tie force: $\qquad$ $F_{u,tie} = 420.7$ kip

Tie capacity:
$$\phi \cdot f_y \cdot A_{st} = F_{u,tie}$$
$$(0.9)(60 \text{ ksi})A_{st} = 420.7 \text{ kip}$$
$$A_{st} = 7.79 \text{ in.}^2$$

Number of No. 11 bars required: $\qquad 7.79 \text{ in.}^2 / 1.56 \text{ in.}^2 = 5$ bars

Tie EF (Bottom Mat Reinforcement)

Factored tie force: $\qquad$ $F_{u,tie} = 454.2$ kip

Tie capacity:
$$\phi \cdot f_y \cdot A_{st} = F_{u,tie}$$
$$(0.9)(60 \text{ ksi})A_{st} = 454.2 \text{ kip}$$
$$A_{st} = 8.41 \text{ in.}^2$$

Number of No. 11 bars required: $\qquad 8.41 \text{ in.}^2 / 1.56 \text{ in.}^2 = 6$ bars

Tie CF (Bottom Mat Reinforcement)

Factored tie force: $\qquad$ $F_{u,tie} = 587.6$ kip

Tie capacity:
$$\phi \cdot f_y \cdot A_{st} = F_{u,tie}$$
$$(0.9)(60 \text{ ksi})A_{st} = 587.6 \text{ kip}$$
$$A_{st} = 10.88 \text{ in.}^2$$

Number of No. 11 bars required: $\qquad 10.88 \text{ in.}^2 / 1.56 \text{ in.}^2 = 7$ bars

Tie BB' (Column Reinforcement)

Factored tie force: $\qquad$ $F_{u,tie} = 80.2$ kip

Tie capacity: $\qquad$ $\phi \cdot f_y \cdot A_{st} = F_{u,tie}$
$(0.9)(60 \text{ ksi})A_{st} = 80.2$ kip
$A_{st} = 1.49$ in.^{2}

Number of No. 11 bars required: $\qquad$ $1.49 \text{ in.}^2 / 1.56 \text{ in.}^2 = 1$ bars
(18 bars are under tension)

As summarized in Table 6.1, the bottom mat reinforcement determined in Load Case I (19 bars per tie element) still governs the design. In addition, the column reinforcing bars under tension are sufficient to carry the column tie force.

6.2.1.5. Step 5: Perform Strength Checks

The nodal strength checks for one CCC node (Node A in Figure 6.8) and four CTT nodes (C, D, E, and F) are performed in this step. Whereas the nodal strength check procedure for the CTT nodes is identical to that of Yi et al. (2022), that of the CCC node is performed following the proposed design procedure of this research owing to the single strut-based equivalent force system.

- *Node A (CCC node)*

The extreme compressive fiber stress and resultant compressive force over the column section derived from the sectional analysis are used to develop the modified equivalent square-shaped bearing face of the CCC node that is proposed in this research. The area of the modified equivalent square bearing face (A_{mc}) and its width (W_{eq}) can be derived from the below equation. It is much smaller than that of the actual compressive region (A_c) of the column, as depicted in Figure 6.9. The area represents the conservativeness of the proposed approach to perform the nodal capacity check for the CCC node.

$$A_{mc} = \frac{F_A}{f_c} = \frac{1736.2 \text{ kip}}{1.05 \text{ ksi}} = 1658 \text{ in.}^2$$

$$W_{eq} = \sqrt{A_{mc}} = 40.7 \text{ in.}$$
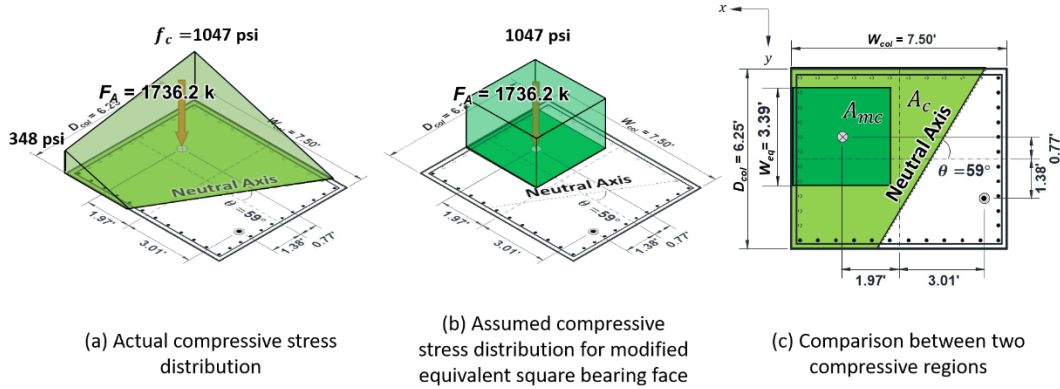
Figure 6.9 Derivation of modified equivalent square bearing face of CCC node (Node A): Load Case VI

The diagonal struts acting at Node A are subdivided diagonally based on the reaction forces at Node D and F, as described in Section 5.2.2, to develop the nodal geometry of the CCC node, as follows:

Node D-side

$$F_{AC,D} = F_{AC}\left(\frac{R_D}{R_D + R_F}\right) = (1115.6)\left(\frac{520.2}{520.2 + 307.8}\right) = 700.9 \text{ kip}$$

$$F_{AE,D} = F_{AE}\left(\frac{R_D}{R_D + R_F}\right) = (431.5)\left(\frac{520.2}{520.2 + 307.8}\right) = 271.1 \text{ kip}$$

$$F_{AB,D} = F_{AB}\left(\frac{R_D}{R_D + R_F}\right) = (134.0)\left(\frac{520.2}{520.2 + 307.8}\right) = 84.2 \text{ kip}$$

Node F-side

$$F_{AC,F} = F_{AC}\left(\frac{R_F}{R_D + R_F}\right) = (1115.6)\left(\frac{307.8}{520.2 + 307.8}\right) = 414.7 \text{ kip}$$

$$F_{AE,F} = F_{AE}\left(\frac{R_F}{R_D + R_F}\right) = (431.5)\left(\frac{307.8}{520.2 + 307.8}\right) = 160.4 \text{ kip}$$

$$F_{AB,F} = F_{AB}\left(\frac{R_F}{R_D + R_F}\right) = (134.0)\left(\frac{307.8}{520.2 + 307.8}\right) = 49.8 \text{ kip}$$

42

Similarly, the resultant compressive force and the modified bearing face are also subdivided into two components (Figure 6.10). The subdivided compressive forces are applied to the centroid of each subdivided bearing face, and the centroids are considered to be subdivided nodes of the CCC node (Nodes A_D and A_F).
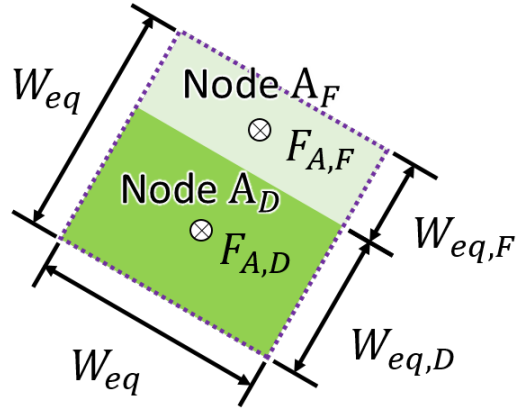
Figure 6.10 Subdivided bearing face of CCC node (Node A): Load Case VI

$$F_{A,D} = F_A \left(\frac{R_D}{R_D + R_F}\right) = (1736.2)\left(\frac{520.2}{520.2 + 307.8}\right) = 1090.7 \text{ kip}$$

$$F_{A,F} = F_A \left(\frac{R_F}{R_D + R_F}\right) = (1736.2)\left(\frac{307.8}{520.2 + 307.8}\right) = 645.4 \text{ kip}$$

$$W_{eq,D} = W_{eq}\frac{F_{A,D}}{F_A} = (40.7)\left(\frac{1090.7}{1736.2}\right) = 25.6 \text{ in.}$$

$$W_{eq,F} = W_{eq}\frac{F_{A,F}}{F_A} = (40.7)\left(\frac{645.4}{1736.2}\right) = 15.1 \text{ in.}$$

The two subdivided groups of internal forces are resolved into two diagonal struts ($F_{Ad,D}$ and $F_{Ad,F}$).

	Strut	Force component*, kip			Strut Force, kip
		x	y	z	($\sqrt{x^2 + y^2 + z^2}$)
	$F_{AC,D}$	-334.0	457.3	413.0	700.9
Node D-side	$F_{AE,D}$	191.3	-159.3	107.2	271.1
	$F_{AB,D}$	62.1	-26.7	50.4	84.2
	F_{AD}	-420.7	-772.8	520.2	1022.2
Resolved Strut	$F_{Ad,D}$	-501.5	-501.5	1090.8	1301.0
Strut Angle (atan($z/\sqrt{x^2 + y^2}$)), DEG					57.0

*The sign of a number is based on the coordinate specified in Figure 6.8

	Strut	Force component*, kip			Strut Force, kip
		x	y	z	$(\sqrt{x^2 + y^2 + z^2})$
Node F-side	$F_{AC,F}$	-197.6	270.6	244.4	414.7
	$F_{AE,F}$	113.2	-94.3	63.4	160.4
	$F_{AB,D}$	36.7	-15.8	29.8	49.8
	F_{AF}	549.2	340.9	307.8	716.0
Resolved Strut	$F_{Ad,F}$	501.5	501.5	645.4	958.9
Strut Angle (atan($z/\sqrt{x^2 + y^2}$)), DEG					42.3

*The sign of a number is based on the coordinate specified in Figure 6.8

Therefore, each subdivided node is subjected to three force components: subdivided resultant compressive force, resolved diagonal strut, and horizontal force component of the resolved diagonal strut. Following the design recommendations of Yi et al. (2022), the 3D nodal geometry of two subdivided nodes can be developed based on the specified dimensions, as depicted in Figure 6.11, Figure 6.13, and Figure 6.14.

PLAN VIEW   **3D VIEW**
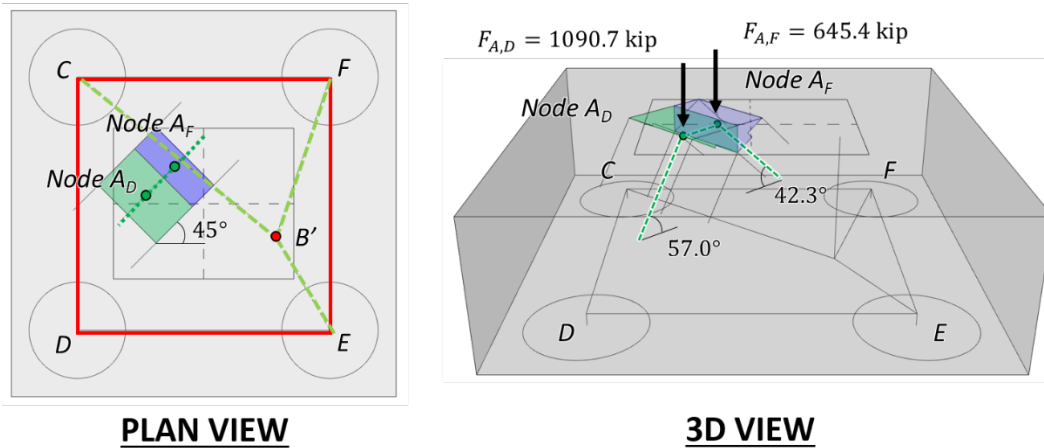
Figure 6.11 Subdivided and resolved internal forces to develop 3D nodal geometry of CCC node: Load Case VI

The triaxial confinement factor, *m,* can be computed from the equivalent square bearing face with the same area of the actual compressive region of the column section (Figure 6.12). The center of the assumed bearing area coincides with the resultant compressive force position derived from the sectional analysis described in Section 6.2.1.1.
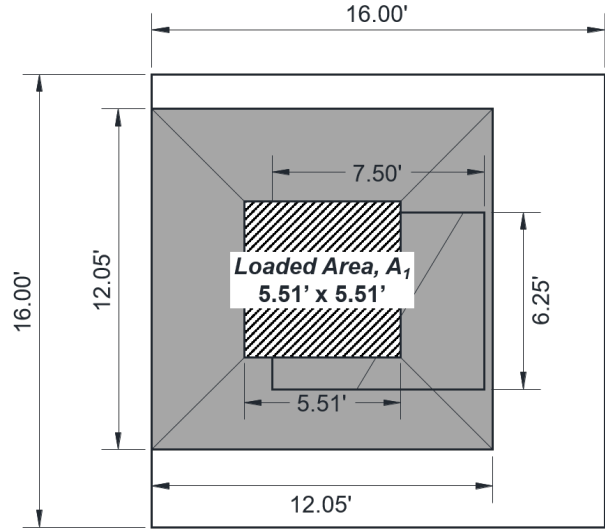
Figure 6.12 Determination of confinement modification factor, m, for Node A: Load Case VI

$$m = \sqrt{\frac{A_2}{A_1}} = \sqrt{\frac{12.05 \times 12.05}{5.51 \times 5.51}} = 2.19 \leq 3 \qquad \therefore \text{se } m = 2.19$$

Concrete efficiency factor, ν, is determined in accordance with Table 5.8.2.5.3a-1 of AASHTO LRFD (2020). The footing will be designed accordingly to satisfy the minimum side face reinforcement requirement ($> 0.18\%$); therefore, the concrete efficiency factor does not have to decrease to 0.45.
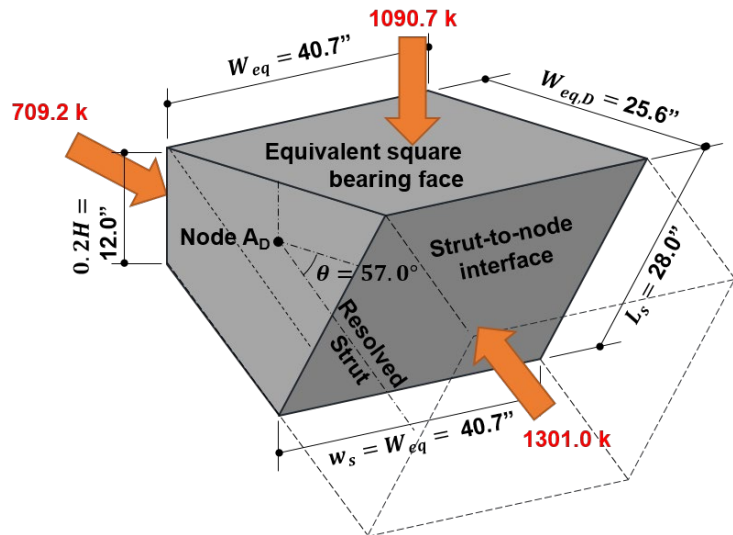
Figure 6.13 Details of 3D nodal geometry at Node A_D: Load Case VI

45

NODAL STRENGTH AT BEARING FACE (Node A_D)

Factored load:	$F_{u,bearing} = 1090.7$ kip
Concrete efficiency factor:	$\nu = 0.85$
Concrete capacity:	$f_{cu} = m \cdot \nu \cdot f_c' = (2.19)(0.85)(3.6 \text{ ksi})$ $= 6.70$ ksi
Nodal capacity:	$\phi F_{n,bearing} = \phi f_{cu} W_{eq} W_{eq,D}$ $= (0.7)(6.70 \text{ ksi})(1042 \text{ in.}^2)$ $= 4886.8 \text{ kip} > 1090.7 \text{ kip}$ **OK**

NODAL STRENGTH AT BACK FACE (Node A_D)

Factored load:	$F_{u,back} = 709.2$ kip
Effective area:	$A_{cn,back} = W_{eq} \cdot 0.2H = (40.7 \text{ in.})(12.0 \text{ in.})$ $= 489 \text{ in}^2$
Concrete efficiency factor:	$\nu = 0.85$
Concrete capacity:	$f_{cu} = m \cdot \nu \cdot f_c' = (2.19)(0.85)(3.6 \text{ ksi})$ $= 6.70$ ksi
Nodal capacity:	$\phi F_{n,back} = \phi f_{cu} A_{cn,back}$ $= (0.7)(6.70 \text{ ksi})(489 \text{ in.}^2)$ $= 2292.2 \text{ kip} > 709.2 \text{ kip}$ **OK**

NODAL STRENGTH AT STRUT-TO-NODE INTERFACE (Node A_D)

Factored load:	$F_{u,SNI} = 1301.0$ kip
Effective area:	$A_{cn,SNI} = W_{eq} \cdot L_S = (40.7 \text{ in.})(28.0 \text{ in.})$ $= 1140 \text{ in.}^2$
Concrete efficiency factor:	$\nu = 0.85 - f_c'/20 \text{ ksi} = 0.85 - 3.6 \text{ ksi}/20 \text{ ksi}$ $= 0.67 > 0.65 \qquad \therefore \text{se } \nu = 0.65$
Concrete capacity:	$f_{cu} = m \cdot \nu \cdot f_c' = (2.19)(0.65)(3.6 \text{ ksi})$ $= 5.12$ ksi
Nodal capacity:	$\phi F_n = \phi f_{cu} A_{cn,SNI}$ $= (0.7)(5.12 \text{ ksi})(1140 \text{ in}^2)$ $= 4088.5 \text{ kip} > 1301.0 \text{ kip}$ **OK**
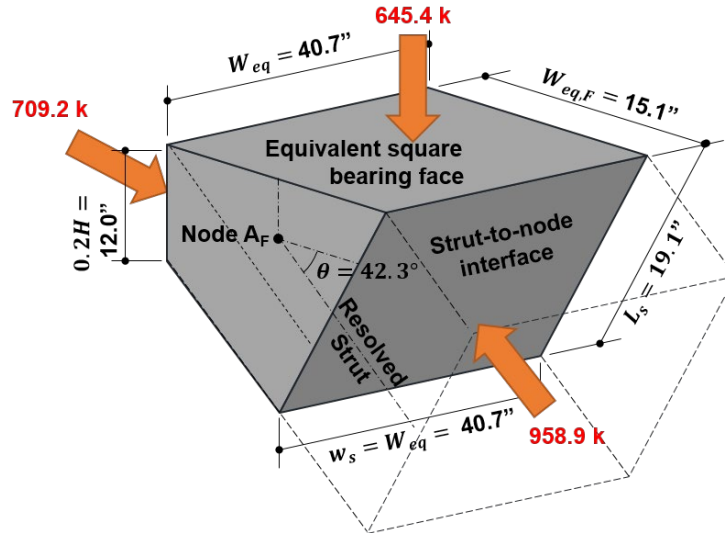
Figure 6.14 Details of 3D nodal geometry at Node A_F: Load Case VI

NODAL STRENGTH AT BEARING FACE (Node A_F)

Factored load:	$F_{u,bearing} = 645.4$ kip
Concrete efficiency factor:	$\nu = 0.85$
Concrete capacity:	$f_{cu} = m \cdot \nu \cdot f_c' = (2.19)(0.85)(3.6 \text{ ksi})$
	$= 6.70$ ksi
Nodal capacity:	$\phi F_{n,bearing} = \phi f_{cu} W_{eq} W_{eq,F}$
	$= (0.7)(6.70 \text{ ksi})(616 \text{ in.}^2)$
	$= 2891.6$ kip > 645.4 kip **OK**

NODAL STRENGTH AT BACK FACE (Node A_F)

Factored load:	$F_{u,back} = 709.2$ kip
Effective area:	$A_{cn,back} = W_{eq} \cdot 0.2H = (40.7 \text{ in.})(12.0 \text{ in.})$
	$= 489$ in^2
Concrete efficiency factor:	$\nu = 0.85$
Concrete capacity:	$f_{cu} = m \cdot \nu \cdot f_c' = (2.19)(0.85)(3.6 \text{ ksi})$
	$= 6.70$ ksi
Nodal capacity:	$\phi F_{n,back} = \phi f_{cu} A_{cn,back}$
	$= (0.7)(6.70 \text{ ksi})(489 \text{ in.}^2)$
	$= 2292.2$ kip > 709.2 kip **OK**

NODAL STRENGTH AT STRUT-TO-NODE INTERFACE (Node A_F)

Factored load:	$F_{u,SNI} = 958.9$ kip
Effective area:	$A_{cn,SNI} = W_{eq} \cdot L_S = (40.7 \text{ in.})(19.1 \text{ in.})$
	$= 776$ in.^{2}

47

Concrete efficiency factor: $v = 0.85 - {f'_c}/{20 \text{ ksi}} = 0.85 - {3.6 \text{ ksi}}/{20 \text{ ksi}}$
$= 0.67 > 0.65 \qquad \therefore \text{se } v = 0.65$

Concrete capacity: $f_{cu} = m \cdot v \cdot f'_c = (2.19)(0.65)(3.6 \text{ ksi})$
$= 5.12 \text{ ksi}$

Nodal capacity: $\phi F_n = \phi f_{cu} A_{cn,SNI}$
$= (0.7)(5.12 \text{ ksi})(776 \text{ in}^2)$
$= 2784.7 \text{ kip} > 958.9 \text{ kip} \quad \textbf{OK}$

- *Node C (CTT Node)*

Figure 6.15 illustrates the dimension and applying forces after resolving struts AC and BC at Node C in three dimensions based on the proposed recommendations of this study. Two diagonal struts (F_{CA} and F_{CB}) are resolved into one diagonal strut as summarized in the following table.

| | Strut | Force component*, kip | | | Strut Force, kip $(\sqrt{x^2 + y^2 + z^2})$ |
		x	y	z	
Diagonal struts	F_{CA}	-531.7	728.0	657.3	1115.6
	F_{CB}	-55.9	44.9	0.0	71.7
Resolved Strut	$F_{u,C}$	-587.6	772.8	657.3	1172.4
	Strut Angle (atan($z/\sqrt{x^2 + y^2}$)), DEG				34.1

*The sign of a number is based on the coordinate specified in Figure 6.8

The confinement modification factor of the bottom nodes (Nodes C through F) is 1.55 as illustrated in Figure 6.16. For the CTT node, the concrete efficiency factors at each face are identical to the following:

$v = 0.85 - {f'_c}/{20 \text{ ksi}} = 0.85 - {3.6 \text{ ksi}}/{20 \text{ ksi}} = 0.67 > 0.65 \qquad \therefore \text{se } v = 0.65$

Note that the nodal strength check at back faces is not necessary since an adequate development length that satisfies the anchorage requirement is provided in this example.
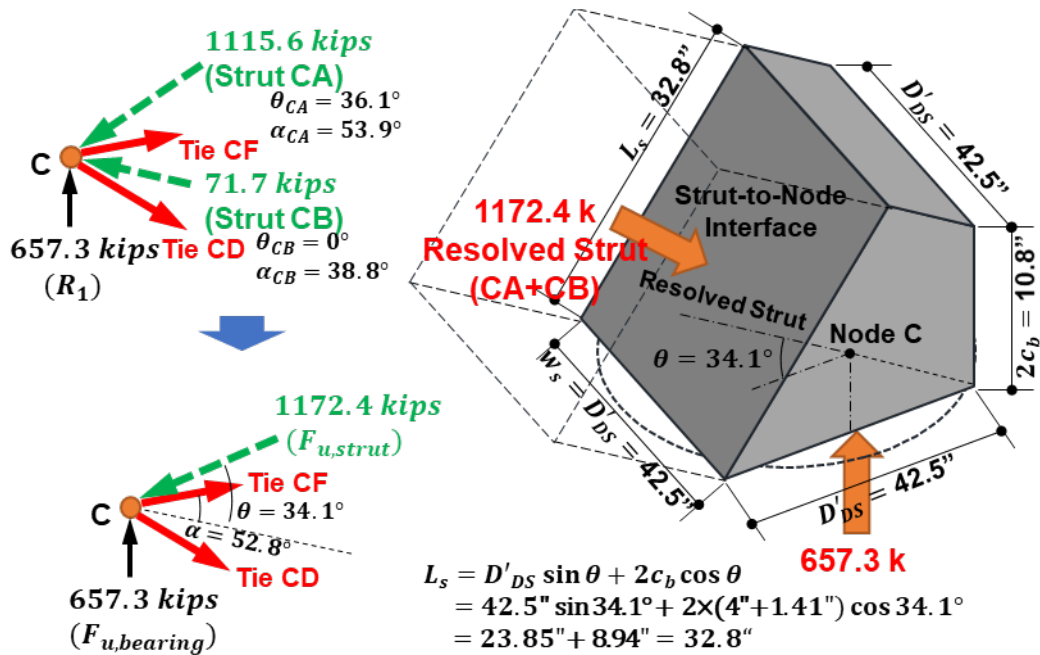
Figure 6.15 Resolving the strut forces (left) and details of 3D nodal geometry and applied forces (right) at Node C

$$L_s = D'_{DS} \sin\theta + 2c_b \cos\theta$$
$$= 42.5" \sin 34.1° + 2\times(4"+1.41")\cos 34.1°$$
$$= 23.85" + 8.94" = 32.8"$$
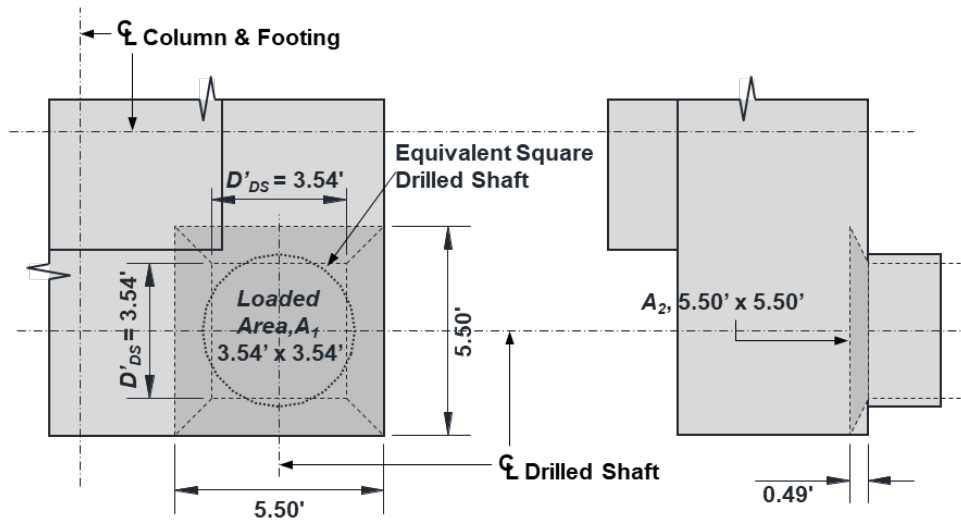
Figure 6.16 Determination of the confinement modification factor, m, for bottom nodes (Nodes C through F)

$$m = \sqrt{\frac{A_2}{A_1}} = \sqrt{\frac{5.50 \times 5.50}{3.54 \times 3.54}} = 1.55 \leq 2 \qquad \therefore se\ m = 1.55$$

49

NODAL STRENGTH AT BEARING FACE

Factored load: $F_{u,bearing} = 1165.0 \text{ kip}$

Concrete efficiency factor: $v = 0.65$

Concrete capacity: $f_{cu} = m \cdot v \cdot f_c' = (1.55)(0.65)(3.6 \text{ ksi})$
$= 3.63 \text{ ksi}$

Nodal capacity: $\phi F_{n,bearing} = \phi f_{cu} A_{cn,bearing}$
$= (0.7)(3.63 \text{ ksi})(1809.6 \text{ in.}^2)$
$= 4598.8 \text{ kip} > 657.3 \text{ kip}$ **OK**

NODAL STRENGTH AT STRUT-TO-NODE INTERFACE

Factored load: $F_{u,SNI} = 1756.1 \text{ kip}$

Concrete efficiency factor: $v = 0.65$

Effective area: $A_{cn,SNI} = w_s \cdot L_S = (42.5 \text{ in.})(32.8 \text{ in.})$
$= 1395.7 \text{ in.}^2$

Concrete capacity: $f_{cu} = m \cdot v \cdot f_c' = (1.55)(0.65)(3.6 \text{ ksi})$
$= 3.63 \text{ ksi}$

Nodal capacity: $\phi F_{n,SNI} = \phi f_{cu} A_{cn,SNI}$
$= (0.7)(3.63 \text{ ksi})(1395.7 \text{ in}^2)$
$= 3546.5 \text{ kip} > 1172.4 \text{ kip}$ **OK**

- *Node D (CTT Node)*

Figure 6.17 illustrates the dimensions and applying forces at Node D in three dimensions based on the proposed recommendations of this study. The confinement modification factor and the concrete efficiency factor of Node D are the same as those of Node C ($m = 1.55$ and $v = 0.65$).
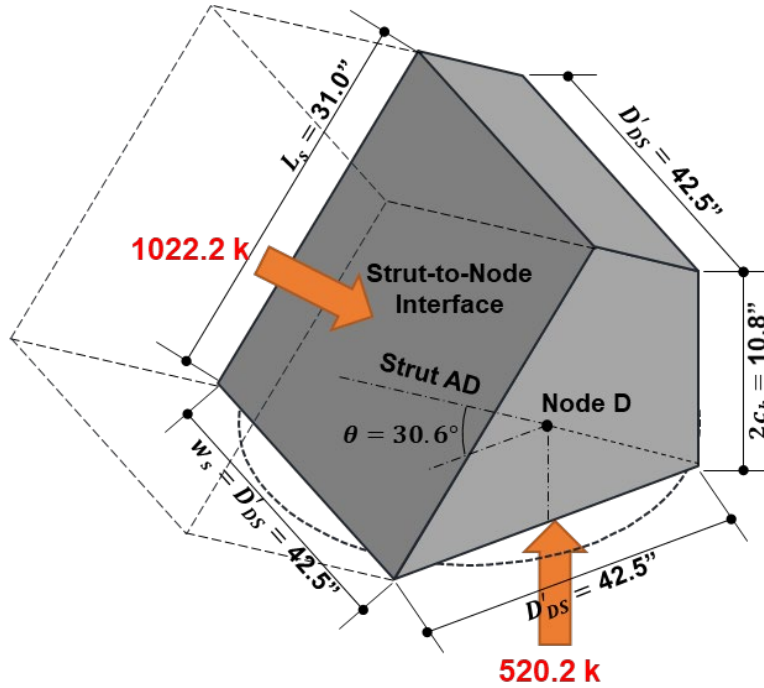
$$L_s = D'_{DS} \sin\theta + 2c_b \cos\theta$$
$$= 42.5'' \sin 30.6° + 2\times(4''+1.41'') \cos 30.6°$$
$$= 21.65'' + 9.30'' = 31.0''$$

Figure 6.17 Details of 3D nodal geometry and applied forces at Node D

NODAL STRENGTH AT BEARING FACE

Factored load:	$F_{u,bearing} = 520.2$ kip
Concrete efficiency factor:	$v = 0.65$
Concrete capacity:	$f_{cu} = m \cdot v \cdot f'_c = (1.55)(0.65)(3.6 \text{ ksi})$
	$= 3.63$ ksi
Nodal capacity:	$\phi F_{n,bearing} = \phi f_{cu} A_{cn,bearing}$
	$= (0.7)(3.63 \text{ ksi})(1809.6 \text{ in.}^2)$
	$= 4598.8 \text{ kip} > 520.2 \text{ kip}$ **OK**

51

Factored load:	$F_{u,SNI} = 1756.1$ kip
Concrete efficiency factor:	$v = 0.65$
Effective area:	$A_{cn,SNI} = w_s \cdot L_S = (42.5 \text{ in.})(31.0 \text{ in.})$ $= 1317.1 \text{ in.}^2$
Concrete capacity:	$f_{cu} = m \cdot v \cdot f_c' = (1.55)(0.65)(3.6 \text{ ksi})$ $= 3.63 \text{ ksi}$
Nodal capacity:	$\phi F_{n,SNI} = \phi f_{cu} A_{cn,SNI}$ $= (0.7)(3.63 \text{ ksi})(1544.9 \text{ in}^2)$ $= 3346.8 \text{ kip} > 1022.2 \text{ kip}$ **OK**

- *Node E (CTT Node)*

Figure 6.18 illustrates the dimensions and applying forces at Node E in three dimensions based on the proposed recommendations of this study. The confinement modification factor and the concrete efficiency factor of Node E are the same as those of Node C ($m = 1.55$ and $v = 0.65$). Two diagonal struts (F_{EA} and F_{EB}) are resolved into one diagonal strut as summarized in the following table.

	Strut	Force component*, kip			Strut Force, kip $(\sqrt{x^2 + y^2 + z^2})$
		x	y	z	
Diagonal struts	F_{EA}	304.4	-253.5	170.6	431.3
	F_{EB}	116.3	-200.8	0.0	232.0
Resolved Strut	$F_{u,E}$	420.7	-454.2	170.6	642.2
	Strut Angle (atan$(z/\sqrt{x^2 + y^2})$), DEG				15.4

*The sign of a number is based on the coordinate specified in Figure 6.8
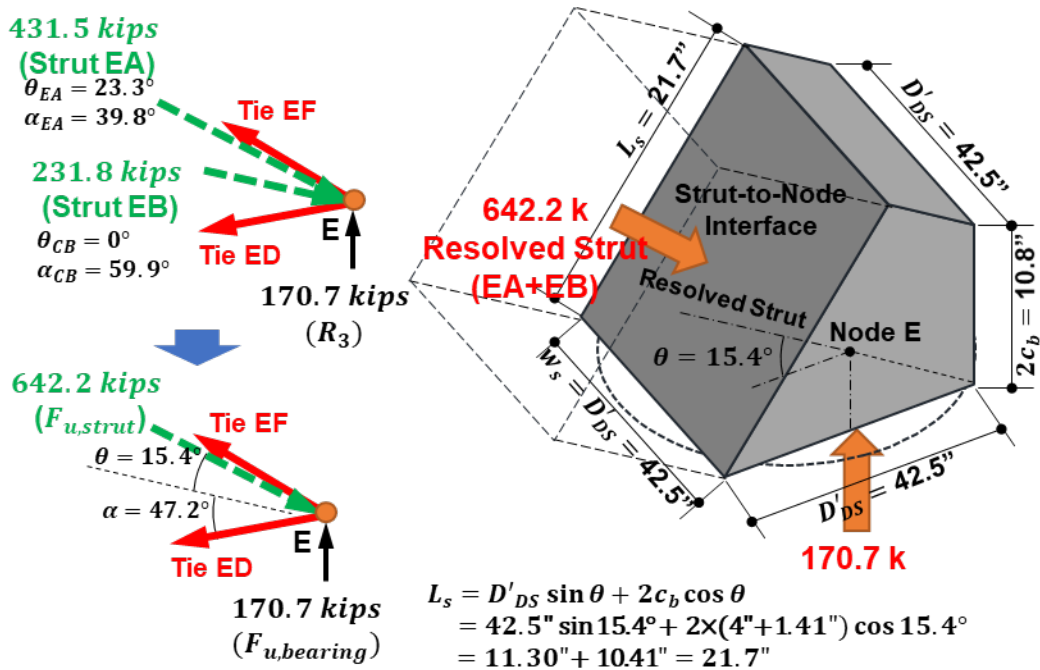
Figure 6.18 Resolving the forces (left) and details of 3D nodal geometry and applied forces (right) at Node E

NODAL STRENGTH AT BEARING FACE

Factored load:	$F_{u,bearing} = 170.7$ kip
Concrete efficiency factor:	$\nu = 0.65$
Concrete capacity:	$f_{cu} = m \cdot \nu \cdot f'_c = (1.55)(0.65)(3.6 \text{ ksi})$ $= 3.63$ ksi
Nodal capacity:	$\phi F_{n,bearing} = \phi f_{cu} A_{cn,bearing}$ $= (0.7)(3.63 \text{ ksi})(1809.6 \text{ in.}^2)$ $= 4598.8$ kip > 170.7 kip **OK**

NODAL STRENGTH AT STRUT-TO-NODE INTERFACE

Factored load:	$F_{u,SNI} = 642.2$ kip
Concrete efficiency factor:	$\nu = 0.65$
Effective area:	$A_{cn,SNI} = w_s \cdot L_S = (42.5 \text{ in.})(21.7 \text{ in.})$ $= 924.6 \text{ in.}^2$
Concrete capacity:	$f_{cu} = m \cdot \nu \cdot f'_c = (1.55)(0.65)(3.6 \text{ ksi})$ $= 3.63$ ksi
Nodal capacity:	$\phi F_{n,SNI} = \phi f_{cu} A_{cn,SNI}$ $= (0.7)(3.63 \text{ ksi})(924.6 \text{ in}^2)$ $= 2349.4$ kip > 642.2 kip **OK**

- *Node F (CTT Node)*

Figure 6.19 illustrates the dimensions and applying forces at Node F in three dimensions based on the proposed recommendations of this study. The confinement modification factor and the concrete efficiency factor of Node F are the same as those of Node C ($m = 1.55$ and $v = 0.65$). Two diagonal struts (F_{FA} and F_{FB}) are resolved into one diagonal strut as summarized in the following table.

	Strut	Force component*, kip			Strut Force, kip $(\sqrt{x^2 + y^2 + z^2})$
		x	y	z	
Diagonal struts	F_{FA}	549.2	340.9	307.8	716.0
	F_{FB}	38.4	113.4	0.0	119.6
Resolved Strut	$F_{u,F}$	587.6	454.2	307.8	803.9
Strut Angle (atan$(z/\sqrt{x^2 + y^2})$), DEG					22.5

*The sign of a number is based on the coordinate specified in Figure 6.8

$$L_s = D'_{DS} \sin\theta + 2c_b \cos\theta$$
$$= 42.5" \sin 22.5° + 2\times(4"+1.41") \cos 22.5°$$
$$= 16.29" + 9.98" = 26.3"$$
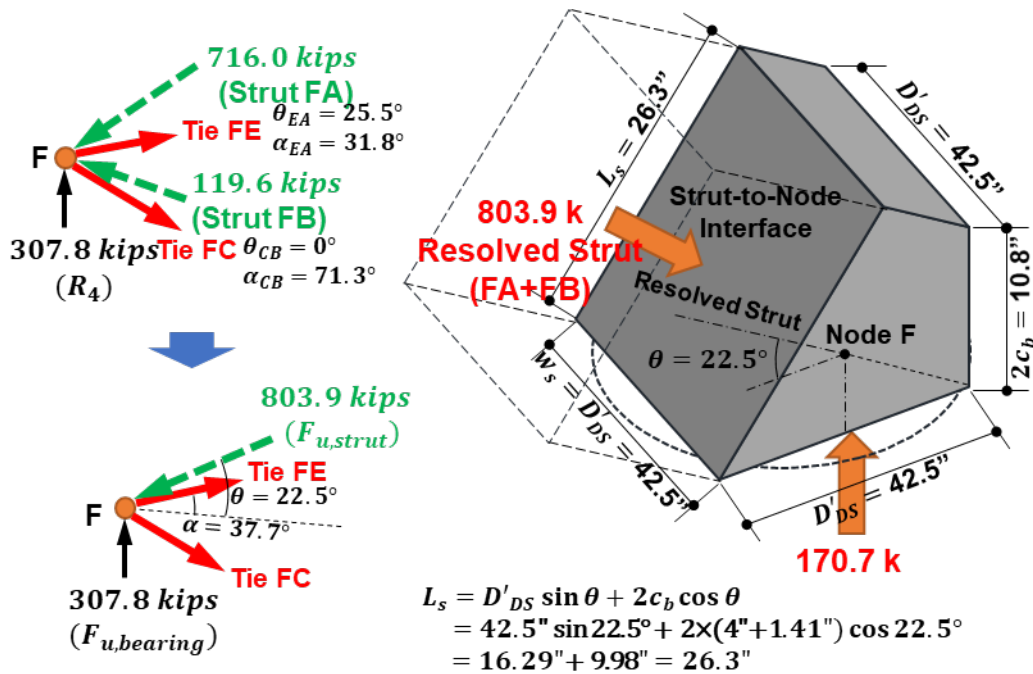
Figure 6.19 Resolving the forces (left) and details of 3D nodal geometry and applied forces (right) at Node F

NODAL STRENGTH AT BEARING FACE

Factored load:	$F_{u,bearing} = 307.8$ kip
Concrete efficiency factor:	$\nu = 0.65$
Concrete capacity:	$f_{cu} = m \cdot \nu \cdot f_c' = (1.55)(0.65)(3.6 \text{ ksi})$ $= 3.63$ ksi
Nodal capacity:	$\phi F_{n,bearing} = \phi f_{cu} A_{cn,bearing}$ $= (0.7)(3.63 \text{ ksi})(1809.6 \text{ in.}^2)$ $= 4598.8$ kip > 307.8 kip **OK**

NODAL STRENGTH AT STRUT-TO-NODE INTERFACE

Factored load:	$F_{u,SNI} = 803.9$ kip
Concrete efficiency factor:	$\nu = 0.65$
Effective area:	$A_{cn,SNI} = w_s \cdot L_S = (42.5 \text{ in.})(26.3 \text{ in.})$ $= 1118.1$ in.^{2}
Concrete capacity:	$f_{cu} = m \cdot \nu \cdot f_c' = (1.55)(0.65)(3.6 \text{ ksi})$ $= 3.63$ ksi
Nodal capacity:	$\phi F_{n,SNI} = \phi f_{cu} A_{cn,SNI}$ $= (0.7)(3.63 \text{ ksi})(1118.1 \text{ in}^2)$ $= 2841.1$ kip > 803.9 kip **OK**

Therefore, the nodal capacities of the CCC nodes and CTT nodes with defined nodal geometry are greater than factored loads.

6.2.1.6. Step 6: Proportion Shrinkage and Temperature Reinforcement

The widths of the footing in both directions are 192 in. and the thickness is 60 in. For this footing, 0.50 in.^{2}/ft. for side faces is required for shrinkage and temperature reinforcement, as the following calculation indicates.

$$A_s \geq \frac{1.30bh}{2(b+h)f_y} = \frac{1.30(192 \text{ in.})(60 \text{ in.})}{2(192 \text{ in.} +60 \text{ in.})(60 \text{ ksi})} = 0.50 \text{ in.}^2/\text{ft.}$$

To determine the spacing of side face reinforcement, the spacing of bottom mat reinforcement (5 in.) is doubled, for practical purposes. This spacing (10 in.) is under the maximum of 12 in. for components thicker than 36.0 in. On the side faces, No. 6 bars with 10 in. spacing ($A_s = 0.53$ in.^{2}/ft.) are provided in both horizontal and vertical directions. On the top face, No. 6 bars with 10 in. spacing in orthogonal directions are provided. The shrinkage and temperature reinforcement is not

necessary on the bottom face because uniformly distributed bottom mat reinforcement exists over the entire bottom face. The reinforcing details are provided in Section 6.2.3.

6.2.1.7. Step 7: Provide Necessary Anchorage for Ties

- *Bottom Ties*

As described in Section 4.4, all ties have to be completely developed at the section where the tie centroid intersects with the extended nodal zone. It is necessary to check whether the available development length for bottom mat reinforcement is greater than the minimum requirement. Figure 6.20 depicts the available length of Tie CD at both ends. Resolved struts were used to define the extended nodal zone, and the projected angles on XZ- and YZ-plane as summarized the following table.

Resolved Strut	Force component*, kip			Strut Force, kip $\sqrt{x^2 + y^2 + z^2}$	Projected Angle, DEG	
					XZ-Plane $\mathrm{atan}(z/x)$	YZ-Plane $\mathrm{atan}(z/y)$
	x	y	z			
CA	-587.6	772.8	657.3	1172.4	48.2	40.4
DA	-420.7	-772.8	520.2	-1022.2	51.0	33.9
EA	420.7	-454.2	170.6	642.2	22.1	20.6
FA	587.6	454.2	307.8	803.9	27.6	34.1

*The sign of a number is based on the coordinate specified in Figure 6.8
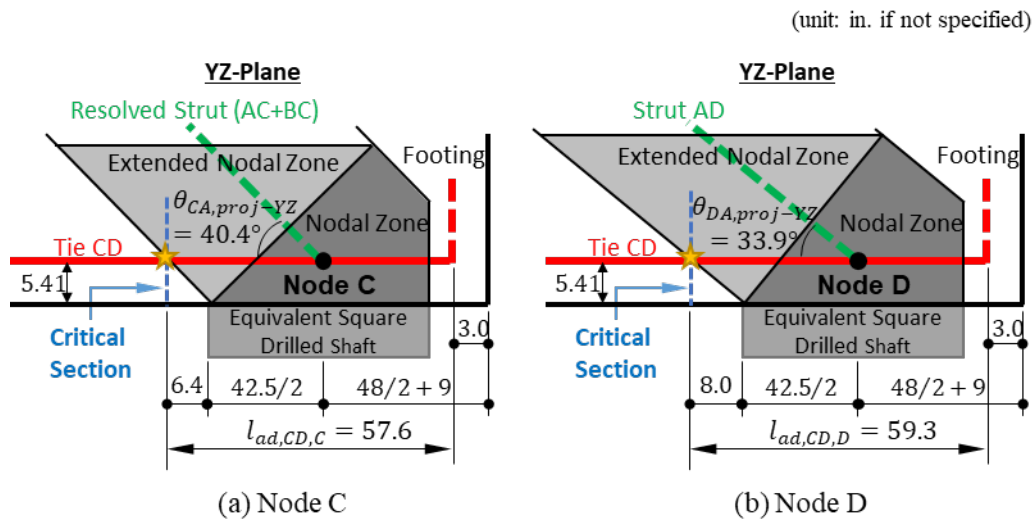
Figure 6.20 Critical sections for the development of Tie CD

56

The available development lengths for the bottom ties are indicated by the following calculation:

Tie CD

$$l_{ad,CD,C} = \frac{c_b}{\tan \theta_{CA,proj-\text{YZ}}} + D_{DS}'/2 + D_{DS}/2 + OH - c$$

$$= \frac{(5.41 \text{ in.})}{\tan 40.4°} + (42.5 \text{ in.})/2 + (48.0 \text{ in.})/2 + 9 \text{ in.} - 3 \text{ in.} = 57.6 \text{ in.}$$

$$l_{ad,CD,D} = \frac{c_b}{\tan \theta_{DA,proj-\text{YZ}}} + D_{DS}'/2 + D_{DS}/2 + OH - c$$

$$= \frac{(5.41 \text{ in.})}{\tan 33.9°} + (42.5 \text{ in.})/2 + (48.0 \text{ in.})/2 + 9 \text{ in.} - 3 \text{ in.} = 59.3 \text{ in.}$$

Tie DE

$$l_{ad,DE,D} = \frac{c_b}{\tan \theta_{DA,proj-\text{XZ}}} + D_{DS}'/2 + D_{DS}/2 + OH - c$$

$$= \frac{(5.41 \text{ in.})}{\tan 51.0°} + (42.5 \text{ in.})/2 + (48.0 \text{ in.})/2 + 9 \text{ in.} - 3 \text{ in.} = 55.6 \text{ in.}$$

$$l_{ad,DE,E} = \frac{c_b}{\tan \theta_{EA,proj-\text{XZ}}} + D_{DS}'/2 + D_{DS}/2 + OH - c$$

$$= \frac{(5.41 \text{ in.})}{\tan 22.1°} + (42.5 \text{ in.})/2 + (48.0 \text{ in.})/2 + 9 \text{ in.} - 3 \text{ in.} = 64.6 \text{ in.}$$

Tie EF

$$l_{ad,EF,E} = \frac{c_b}{\tan \theta_{EA,proj-\text{YZ}}} + D_{DS}'/2 + D_{DS}/2 + OH - c$$

$$= \frac{(5.41 \text{ in.})}{\tan 20.6°} + (42.5 \text{ in.})/2 + (48.0 \text{ in.})/2 + 9 \text{ in.} - 3 \text{ in.} = 65.7 \text{ in.}$$

$$l_{ad,EF,F} = \frac{c_b}{\tan \theta_{FA,proj-\text{YZ}}} + D_{DS}'/2 + D_{DS}/2 + OH - c$$

$$= \frac{(5.41 \text{ in.})}{\tan 34.1°} + (42.5 \text{ in.})/2 + (48.0 \text{ in.})/2 + 9 \text{ in.} - 3 \text{ in.} = 59.3 \text{ in.}$$

Tie CF

$$l_{ad,CF,C} = \frac{c_b}{\tan \theta_{CA,proj-\text{XZ}}} + D_{DS}{}'/2 + D_{DS}/2 + OH - c$$

$$= \frac{(5.41 \text{ in.})}{\tan 51.0°} + (42.5 \text{ in.})/2 + (48.0 \text{ in.})/2 + 9 \text{ in.} - 3 \text{ in.} = 55.6 \text{ in.}$$

$$l_{ad,CF,F} = \frac{c_b}{\tan \theta_{CA,proj-\text{XZ}}} + D_{DS}{}'/2 + D_{DS}/2 + OH - c$$

$$= \frac{(5.41 \text{ in.})}{\tan 27.6°} + (42.5 \text{ in.})/2 + (48.0 \text{ in.})/2 + 9 \text{ in.} - 3 \text{ in.} = 61.6 \text{ in.}$$

The minimum required development lengths of a straight bar and a 90- or 180-degree hooked bar are calculated in accordance with Article 5.10.8.2 of AASHTO LRFD (2020). Table 6.2 summarizes the calculation of the minimum development lengths for each tie and each anchorage type and compares them with the available lengths. As a result, both straight and hooked No. 11 bars are adequate for the development within proposed available lengths for all ties due to the low reinforcement excess factor λ_{er} (required reinforcement area/provided reinforcement area). Using straight reinforcing bars for the bottom mat, as is the most common current practice, is suggested.

Table 6.2 Summary of the minimum development lengths

Tie	Anchorage Type	λ_{rc}	λ_{er}	l_d or l_{dh} [in.]	$l_{ad,min}$ [in.]	Check
CD	Straight	0.56	0.48	29.1	57.6	OK
	Hooked	1.00	0.48	13.6		OK
DE	Straight	0.56	0.26	15.9	55.6	OK
	Hooked	1.00	0.26	7.4		OK
EF	Straight	0.56	0.28	17.1	59.3	OK
	Hooked	1.00	0.28	8.0		OK
CF	Straight	0.56	0.37	22.2	55.6	OK
	Hooked	1.00	0.36	10.4		OK

Note) $l_d = 2.4 d_b \frac{f_y}{\sqrt{f'_c}} \left(\frac{\lambda_{rl} \lambda_{cf} \lambda_{rc} \lambda_{er}}{\lambda} \right)$, $l_{dh} = \frac{38 d_b}{60} \frac{f_y}{\sqrt{f'_c}} \left(\frac{\lambda_{rc} \lambda_{cw} \lambda_{er}}{\lambda} \right)$

$l_{ad,min}$: the minimum of the available development length at both ends of a tie
λ_{rl}: reinforcement location factor (=1.0)
λ_{cf} or λ_{cw}: coating factor (=1.0)
λ_{rc}: reinforcement confinement factor (no transverse reinforcement assumed for straight bars and 1.0 for hooked bars)
λ_{er}: excess reinforcement factor
λ: concrete density modification factor (=1.0)

- *Vertical Tie*

The anchorage check for the vertical column tie element (Tie BB') also needs to be performed. The available length for the column reinforcement is determined by the compression field proposed by Yi et al. (2022) (Figure 6.21) and can be computed as follow:

$$l_{ad.COL} = \left(\frac{L_t}{L_s} \right) (0.9H - c_b) - (d_{b,bu}) = \left(\frac{26.9}{86.7} \right) (0.9(60) - 5.41) - (1.41) = 13.7 \text{ in.}$$
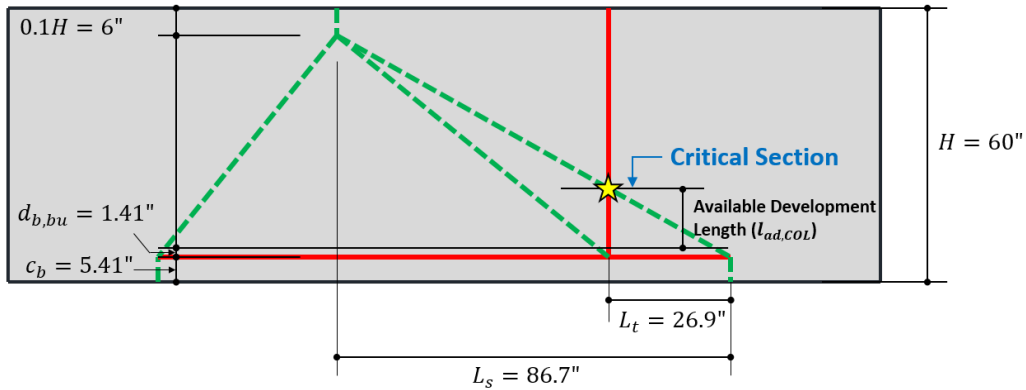
Figure 6.21 Critical section for development of column tie: Load Case VI

As designed with Load Case III and VI, 90-degree hooked bars are employed for the column reinforcement, and the column reinforcement placed for the major moment is recommended to be oriented towards the column. Even though the hooked column reinforcement placed with respect to the minor moment axis is outer-oriented, the diagonal strut existing in the strut-and-tie model of Load Case IV and VII to represent a non-contact lap splice behavior of the column and drilled shaft reinforcement can also activate the bearing action of the outer-oriented hook. Therefore, the anchorage requirement checks for both inner and outer-oriented hooked column reinforcement are performed with the required development length of hooked bars in accordance with AASHTO LRFD (2020). The reinforcement confinement factor, λ_{rc}, is 0.8 determined by given details of the column reinforcement; the coating factor, λ_{cw}, is 1.0 for uncoated reinforcement; the excess reinforcement factor, λ_{er}, is 0.048 based on the given and required column reinforcement; and the concrete density modification factor, λ, is 1.0 for normal weight concrete. The required development length of a hooked No. 11 bar is calculated below:

$$l_{dh} = \frac{38.0(1.41 \text{ in.})}{60.0} \cdot \frac{60 \text{ ksi}}{\sqrt{3.6 \text{ ksi}}} \times \left(\frac{0.8 \cdot 1.0 \cdot 0.048}{1.0}\right) = 1.1 \text{ in.} < l_{ad,COL}(= 13.6 \text{ in.})$$

Therefore, the anchorage details designed for Load Case I through V (Table 6.1) can still develop sufficient stress levels to be safe under Load Case VI.

6.2.2. Design Calculations: Load Case VII

Figure 6.22 presents the factored load case where the column is subjected to axial compression combined with large biaxial flexure. This loading combination induces tension at one corner of the column and one of four drilled shafts.
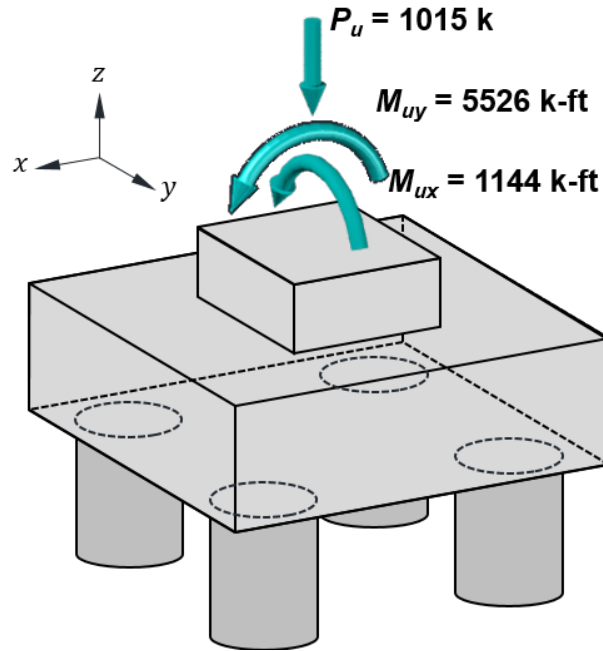
Figure 6.22 Factored load: Load Case VII

6.2.2.1. Step 1: Determine the Loads

A sectional analysis is also conducted for the load combination. Three equilibrium equations ($\sum P_u = 0$; $\sum M_{ux} = 0$; $\sum M_{uy} = 0$) can derive three unknowns (neutral axis depth (c); neutral axis inclination (θ); extreme compressive fiber strain (ε_c)) required for developing the strain and stress distribution over the column section. The calculation procedure is presented in Appendix A. Figure 6.23 illustrates the developed strain and stress distribution. The compressive and tensile resultant forces comprising the equivalent force system of the 3D strut-and-tie model can be determined from the distribution.
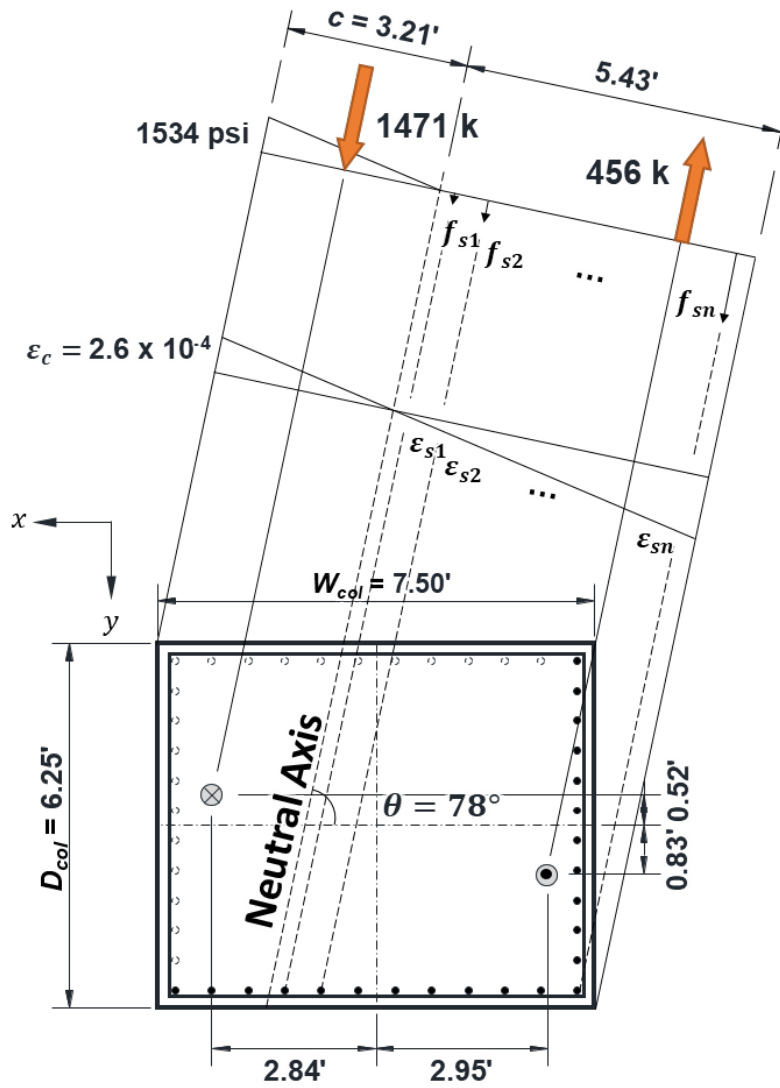
Figure 6.23 Stress distribution over the column section: Load Case VII

6.2.2.2. Step 2: Analyze Structural Component

The reaction forces in drilled shafts can be derived from the equilibrium conditions of the external loading. Figure 6.24 presents the results of the structural analysis.

$$R_1 = \frac{P_u}{4} + \frac{1}{2}\left(\frac{M_{ux}}{S_{DS,x}}\right) + \frac{1}{2}\left(\frac{M_{uy}}{S_{DS,y}}\right)$$

$$= \frac{1015 \text{ kip}}{4} + \frac{1}{2}\left(\frac{1144 \text{ k–ft}}{10.50 \text{ ft}}\right) + \frac{1}{2}\left(\frac{5526 \text{ k–ft}}{10.50 \text{ ft}}\right) = 571.4 \text{ kip (Compression)}$$

$$R_2 = \frac{P_u}{4} - \frac{1}{2}\left(\frac{M_{ux}}{S_{DS,x}}\right) + \frac{1}{2}\left(\frac{M_{uy}}{S_{DS,y}}\right)$$

$$= \frac{1015 \text{ kip}}{4} - \frac{1}{2}\left(\frac{1144 \text{ k–ft}}{10.50 \text{ ft}}\right) + \frac{1}{2}\left(\frac{5526 \text{ k–ft}}{10.50 \text{ ft}}\right) = 462.4 \text{ kip (Compression)}$$

$$R_3 = \frac{P_u}{4} - \frac{1}{2}\left(\frac{M_{ux}}{S_{DS,x}}\right) - \frac{1}{2}\left(\frac{M_{uy}}{S_{DS,y}}\right)$$

$$= \frac{1015 \text{ kip}}{4} - \frac{1}{2}\left(\frac{1144 \text{ k–ft}}{10.50 \text{ ft}}\right) - \frac{1}{2}\left(\frac{5526 \text{ k–ft}}{10.50 \text{ ft}}\right) = 63.9 \text{ kip (Tension)}$$

$$R_4 = \frac{P_u}{4} + \frac{1}{2}\left(\frac{M_{ux}}{S_{DS,x}}\right) - \frac{1}{2}\left(\frac{M_{uy}}{S_{DS,y}}\right)$$

$$= \frac{1015 \text{ kip}}{4} + \frac{1}{2}\left(\frac{1144 \text{ k–ft}}{10.50 \text{ ft}}\right) - \frac{1}{2}\left(\frac{5526 \text{ k–ft}}{10.50 \text{ ft}}\right) = 45.1 \text{ kip (Compression)}$$
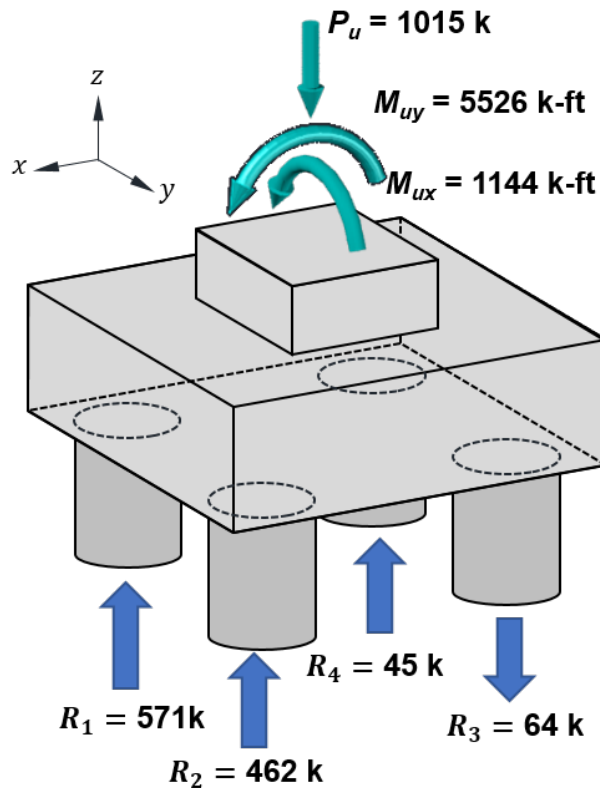
Figure 6.24 Applied loading and reaction forces: Load Case VII

6.2.2.3. Step 3: Develop Strut-and-Tie Model

As described in Section 5.1.2.2, the drilled shaft footing subjected to large biaxial flexure is designed using the idealized 3D strut-and-tie model. Figure 6.25 and Figure 6.26 present the idealized strut-and-tie model for Load Case VII. The force component of Strut BE is not considered in the design example due to the error resulting from integrating the force transfer plane offset for the column and drilled shaft ties in the idealized model. Similarly, the nodal position of Node G is determined to satisfy the equilibrium condition at Node A, as shown in Figure 6.25. The calculation procedure to derive the elemental forces is provided in Appendix B.
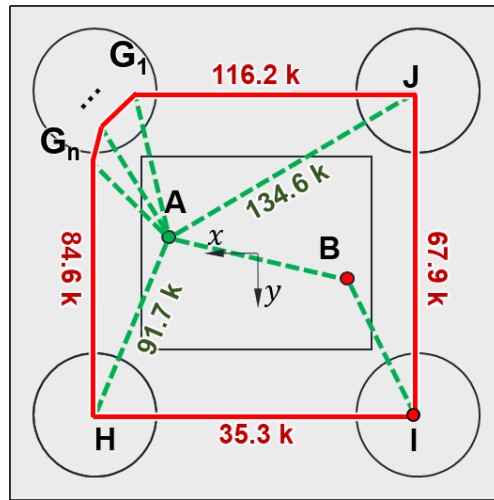
Figure 6.25 3D strut-and-tie model (plan view – top tie ring): Load Case VII
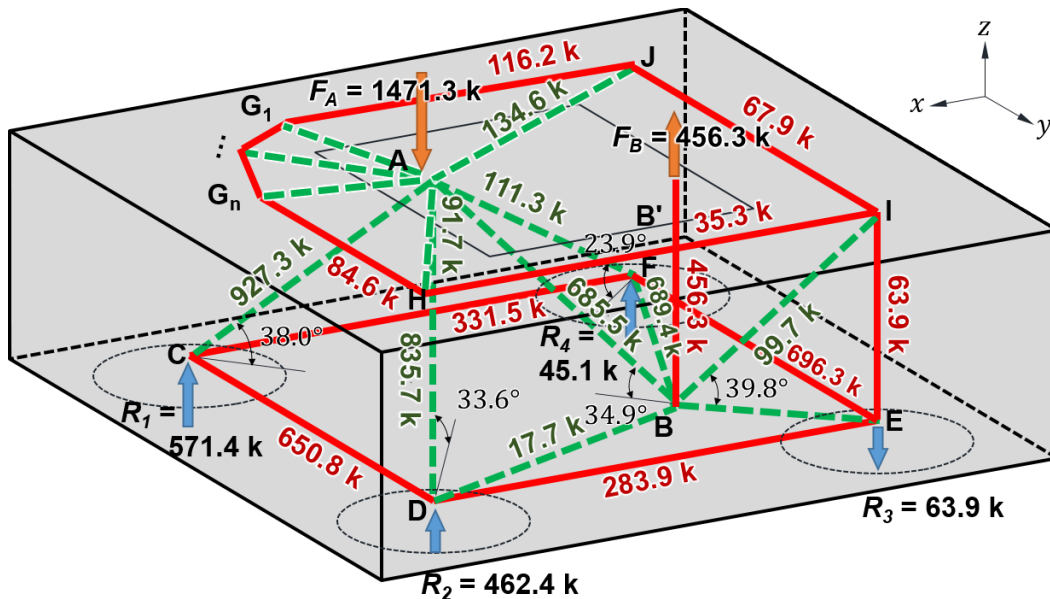
Figure 6.26 3D strut-and-tie model (axonometric view): Load Case VII

The error in the idealized model is estimated by shifting Node E on the x-axis to satisfy the equilibrium condition, as illustrated in Figure 6.27. Based on the shifted nodal position, the moment to the y-axis is computed from the reaction forces ($M_{uy,computed} = 5494$ k-ft) and compared with the factored moment ($M_{uy} = 5526$ k-ft). The error is estimated as 0.58%, which is an insignificant error. Based on the estimated error, the idealized model can be applied to the footing geometry and load case of the design example.

(a) Idealized strut-and-tie model configuration

(b) Modified strut-and-tie model configuration with shifted Node E
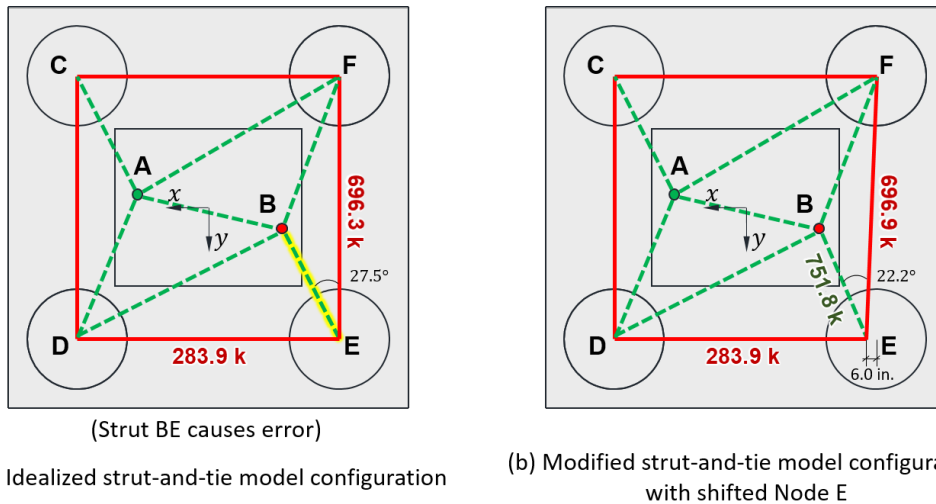
Figure 6.27 Modified strut-and-tie model configuration to estimate error in idealized model

6.2.2.4. Step 4: Proportion Ties

The reinforcement amounts of the drilled shaft, bottom mat, and top mat reinforcement are estimated from the tie forces. Even though Node G deviates from the center axis of the drilled shaft, the inclined top ties connected to the node are also considered to be carried by the top mat reinforcement placed within the half span of the footing. Similar to Load Case VI, the derived column tie force can verify the safety of the given column reinforcement design.

Tie EI (Drilled Shaft Reinforcement)

Factored tie force: $F_{u,tie} = 63.9$ kip

Tie capacity:
$\phi \cdot f_y \cdot A_{st} = F_{u,tie}$
$(0.9)(60 \text{ ksi})A_{st} = 63.9 \text{ kip}$
$A_{st} = 1.18 \text{ in.}^2$

Number of No. 9 bars required: $1.18 \text{ in.}^2 / 1.00 \text{ in.}^2 = 2$ bars

Tie CD (Bottom Mat Reinforcement)

Factored tie force:

$$F_{u,tie} = 650.8 \text{ kip}$$

Tie capacity:

$$\phi \cdot f_y \cdot A_{st} = F_{u,tie}$$
$$(0.9)(60 \text{ ksi})A_{st} = 650.8 \text{ kip}$$
$$A_{st} = 12.05 \text{ in.}^2$$

Number of No. 11 bars required:

$$12.05 \text{ in.}^2 / 1.56 \text{ in.}^2 = 8 \text{ bars}$$

Tie DE (Bottom Mat Reinforcement)

Factored tie force:

$$F_{u,tie} = 283.9 \text{ kip}$$

Tie capacity:

$$\phi \cdot f_y \cdot A_{st} = F_{u,tie}$$
$$(0.9)(60 \text{ ksi})A_{st} = 283.9 \text{ kip}$$
$$A_{st} = 5.26 \text{ in.}^2$$

Number of No. 11 bars required:

$$5.26 \text{ in.}^2 / 1.56 \text{ in.}^2 = 4 \text{ bars}$$

Tie EF (Bottom Mat Reinforcement)

Factored tie force:

$$F_{u,tie} = 696.2 \text{ kip}$$

Tie capacity:

$$\phi \cdot f_y \cdot A_{st} = F_{u,tie}$$
$$(0.9)(60 \text{ ksi})A_{st} = 696.2 \text{ kip}$$
$$A_{st} = 12.89 \text{ in.}^2$$

Number of No. 11 bars required:

$$12.89 \text{ in.}^2 / 1.56 \text{ in.}^2 = 9 \text{ bars}$$

Tie CF (Bottom Mat Reinforcement)

Factored tie force:

$$F_{u,tie} = 331.5 \text{ kip}$$

Tie capacity:

$$\phi \cdot f_y \cdot A_{st} = F_{u,tie}$$
$$(0.9)(60 \text{ ksi})A_{st} = 331.5 \text{ kip}$$
$$A_{st} = 6.14 \text{ in.}^2$$

Number of No. 11 bars required:

$$6.14 \text{ in.}^2 / 1.56 \text{ in.}^2 = 4 \text{ bars}$$

Ties G_lJ (x-directional Top Mat Reinforcement)

Factored tie force:

$$F_{u,tie} = 126.1 \text{ kip}$$

Tie capacity:

$$\phi \cdot f_y \cdot A_{st} = F_{u,tie}$$
$$(0.9)(60 \text{ ksi})A_{st} = 126.1 \text{ kip}$$
$$A_{st} = 2.33 \text{ in.}^2$$

Number of No. 6 bars required:

$$2.33 \text{ in.}^2 / 0.44 \text{ in.}^2 = 6 \text{ bars}$$

Ties G_nH (y-directional Top Mat Reinforcement)

Factored tie force: $F_{u,tie} = 107.7$ kip

Tie capacity:
$$\phi \cdot f_y \cdot A_{st} = F_{u,tie}$$
$$(0.9)(60 \text{ ksi})A_{st} = 107.7 \text{ kip}$$
$$A_{st} = 1.99 \text{ in.}^2$$

Number of No. 6 bars required: $1.99 \text{ in.}^2 / 0.44 \text{ in.}^2 = 5$ bars

Tie HI (Top Mat Reinforcement)

Factored tie force: $F_{u,tie} = 67.9$ kip

Tie capacity:
$$\phi \cdot f_y \cdot A_{st} = F_{u,tie}$$
$$(0.9)(60 \text{ ksi})A_{st} = 67.9 \text{ kip}$$
$$A_{st} = 1.26 \text{ in.}^2$$

Number of No. 6 bars required: $1.26 \text{ in.}^2 / 0.44 \text{ in.}^2 = 3$ bars

Tie IJ (Top Mat Reinforcement)

Factored tie force: $F_{u,tie} = 35.3$ kip

Tie capacity:
$$\phi \cdot f_y \cdot A_{st} = F_{u,tie}$$
$$(0.9)(60 \text{ ksi})A_{st} = 35.3 \text{ kip}$$
$$A_{st} = 0.65 \text{ in.}^2$$

Number of No. 6 bars required: $0.65 \text{ in.}^2 / 0.44 \text{ in.}^2 = 2$ bars

Tie BB' (Column Reinforcement)

Factored tie force: $F_{u,tie} = 456.3$ kip

Tie capacity:
$$\phi \cdot f_y \cdot A_{st} = F_{u,tie}$$
$$(0.9)(60 \text{ ksi})A_{st} = 456.3 \text{ kip}$$
$$A_{st} = 8.45 \text{ in.}^2$$

Number of No. 11 bars required: $8.45 \text{ in.}^2 / 1.56 \text{ in.}^2 = 6$ bars
(20 bars are under tension)

The bottom mat reinforcement amount determined from Load Case I (38-#11) is still safe for Load Case VII. Similarly, the drilled shaft design of Load Case IV (4-#9 per each drilled shaft) governs the design. Furthermore, the top mat reinforcement amount determined from the shrinkage and temperature reinforcement (20-#6) requirement also governs the top mat reinforcement design of Load Case VII. The column reinforcement design is also safe to carry the column tie force resulting from Load Case VII.

6.2.2.5. Step 5: Perform Strength Checks

- *Node A (CCC node)*

The area (A_{mc}) and width (W_{eq}) of the modified equivalent square bearing face of the CCC node can be derived from the extreme compressive fiber stress and resultant compressive force as shown below:

$$A_{mc} = \frac{F_A}{f_c} = \frac{1471.3 \text{ kip}}{1.53 \text{ ksi}} = 959 \text{ in.}^2$$

$$W_{eq} = \sqrt{A_{mc}} = 31.0 \text{ in.}$$

(a) Actual compressive stress distribution

(b) Assumed compressive stress distribution for modified equivalent square bearing face

(c) Comparison between two compressive regions
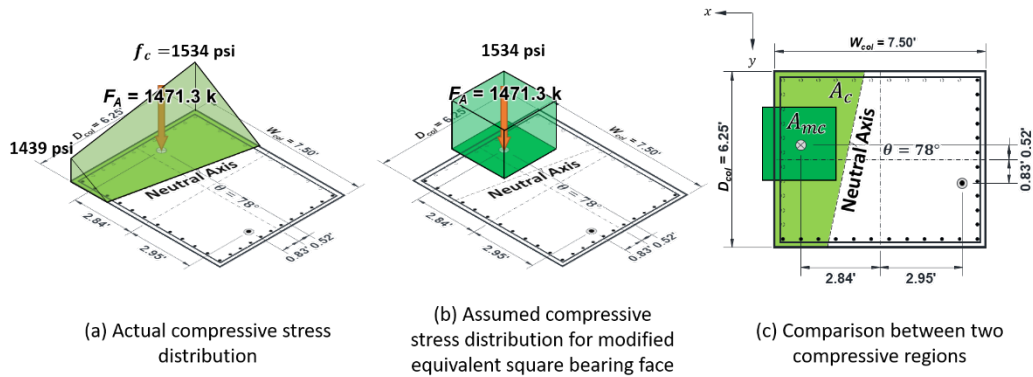
Figure 6.28 Derivation of modified equivalent square bearing face of CCC node (Node A): Load Case VII

The diagonal struts acting at Node A are subdivided into two groups depending on the reaction forces at Node D and F, as described in Section 5.2.2. The resolved strut force (Strut AG) of the widespread diagonal struts (Struts AG$_1$, $\cdots$, AG$_n$) is estimated as 143.7 kip (x-force component: 116.2 kip; y-force component: 84.6 kip) based on the equilibrium condition at Node A.

Node D-side

$$F_{AC,D} = F_{AC} \left(\frac{R_D}{R_D + R_F} \right) = (927.3) \left(\frac{462.4}{462.4 + 45.1} \right) = 844.9 \text{ kip}$$

$$F_{AG,D} = F_{AG} \left(\frac{R_D}{R_D + R_F} \right) = (143.7) \left(\frac{462.4}{462.4 + 45.1} \right) = 131.0 \text{ kip}$$

$$F_{AB,D} = F_{AB} \left(\frac{R_D}{R_D + R_F} \right) = (685.5) \left(\frac{462.4}{462.4 + 45.1} \right) = 624.6 \text{ kip}$$

Node F-side

$$F_{AC,F} = F_{AC}\left(\frac{R_F}{R_D + R_F}\right) = (927.3)\left(\frac{45.1}{462.4 + 45.1}\right) = 414.7 \text{ kip}$$

$$F_{AG,F} = F_{AG}\left(\frac{R_F}{R_D + R_F}\right) = (143.7)\left(\frac{45.1}{462.4 + 45.1}\right) = 12.8 \text{ kip}$$

$$F_{AB,F} = F_{AB}\left(\frac{R_F}{R_D + R_F}\right) = (685.5)\left(\frac{45.1}{462.4 + 45.1}\right) = 60.9 \text{ kip}$$

The resultant compressive force and the modified bearing face are also subdivided into two parts, and two subdivided nodes of the CCC node (Nodes A_D and A_F) are assigned to the centroid of each subdivided bearing face (Figure 6.29).
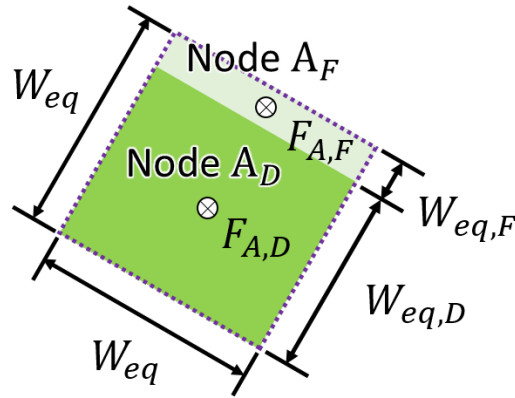
Figure 6.29 Subdivided bearing face of CCC node (Node A): Load Case VII

$$F_{A,D} = F_A\left(\frac{R_D}{R_D + R_F}\right) = (1471.3)\left(\frac{462.4}{462.4 + 45.1}\right) = 1340.6 \text{ kip}$$

$$F_{A,F} = F_A\left(\frac{R_F}{R_D + R_F}\right) = (1471.3)\left(\frac{45.1}{462.4 + 45.1}\right) = 130.7 \text{ kip}$$

$$W_{eq,D} = W_{eq}\frac{F_{A,D}}{F_A} = (31.0)\left(\frac{1340.6}{1471.3}\right) = 28.2 \text{ in.}$$

$$W_{eq,F} = W_{eq}\frac{F_{A,F}}{F_A} = (31.0)\left(\frac{130.7}{1471.3}\right) = 2.8 \text{ in.}$$

The two subdivided groups of internal forces are resolved into two diagonal struts ($F_{Ad,D}$ and $F_{Ad,F}$).

	Strut	Force component*, kip			Strut Force, kip
		x	y	z	$(\sqrt{x^2 + y^2 + z^2})$
Node D-side	$F_{AC,D}$	-302.0	592.9	520.6	844.9
	$F_{AG,D}$	-105.9	77.1	0.0	131.0
	$F_{AB,D}$	498.7	-116.4	357.6	624.6
	F_{AD}	-258.3	-642.4	462.4	835.7
	F_{AH}	-35.3	-84.6	0.0	91.7
Resolved Strut	$F_{Ad,D}$	-212.9	-173.3	1340.6	1368.4
Strut Angle (atan($z/\sqrt{x^2 + y^2}$)), DEG					78.4

*The sign of a number is based on the coordinate specified in Figure 6.8

	Strut	Force component*, kip			Strut Force, kip
		x	y	z	$(\sqrt{x^2 + y^2 + z^2})$
Node F-side	$F_{AC,F}$	-29.4	57.8	50.8	82.4
	$F_{AG,F}$	-10.3	7.5	0.0	12.8
	$F_{AB,F}$	48.6	-11.3	34.9	60.9
	F_{AF}	87.8	51.3	45.1	111.3
	F_{AJ}	116.2	67.9	0.0	134.6
Resolved Strut	$F_{Ad,F}$	212.9	173.3	130.7	304.0
Strut Angle (atan($z/\sqrt{x^2 + y^2}$)), DEG					25.5

*The sign of a number is based on the coordinate specified in Figure 6.8

Each subdivided node is subjected to three force components (subdivided resultant compressive force, resolved diagonal strut, and horizontal force component of the resolved diagonal strut). Therefore, the 3D nodal geometry of the subdivided nodes can be developed based on the design recommendations of Yi et al. (2022), as illustrated in Figure 6.30, Figure 6.32, and Figure 6.33.

PLAN VIEW   **3D VIEW**
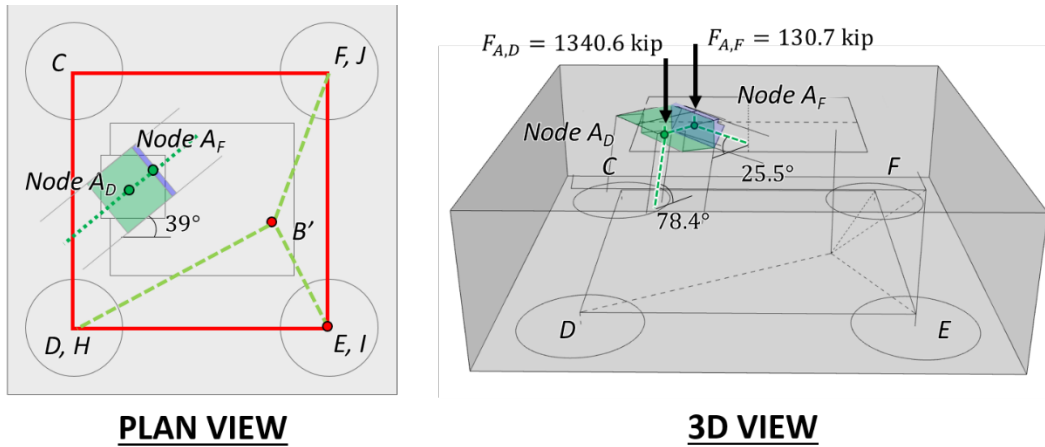
Figure 6.30 Subdivided and resolved internal forces to develop 3D nodal geometry of CCC node: Load Case VII

The triaxial confinement factor, *m*, can be computed from the equivalent square bearing face, which has the same area as the actual compressive region of the column section. The center of the assumed bearing area coincides with the resultant compressive force position derived from the sectional analysis described in Section 6.2.2.1.
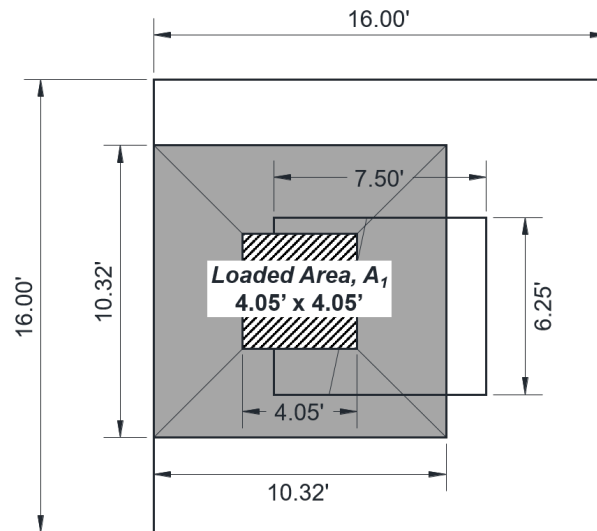
Figure 6.31 Determination of confinement modification factor, m, for Node A: Load Case VII

$$m = \sqrt{\frac{A_2}{A_1}} = \sqrt{\frac{10.32 \times 10.32}{4.05 \times 4.05}} = 2.55 \leq 3 \qquad \therefore \text{se } m = 2.55$$

Concrete efficiency factor, ν, is determined in accordance with Table 5.8.2.5.3a-1 of AASHTO LRFD (2020) and must satisfy the minimum side face reinforcement requirement (>0.18%).
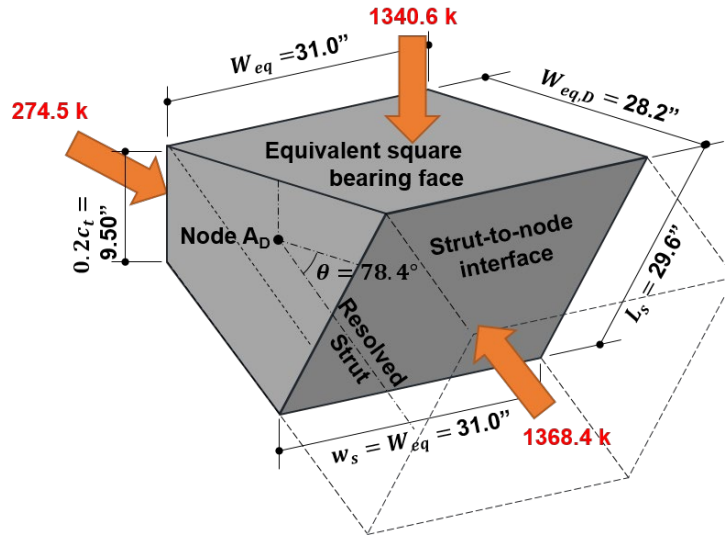
Figure 6.32 Details of 3D nodal geometry at Node A_D: Load Case VII

NODAL STRENGTH AT BEARING FACE (Node A_D)

Factored load: $\quad\quad\quad\quad\quad\quad\quad\quad\quad F_{u,bearing} = 1340.6 \text{ kip}$

Concrete efficiency factor: $\quad\nu = 0.85$

Concrete capacity: $\quad\quad\quad\quad\quad f_{cu} = m \cdot \nu \cdot f'_c = (2.55)(0.85)(3.6 \text{ ksi})$
$$= 7.80 \text{ ksi}$$

Nodal capacity: $\quad\quad\quad\quad\quad \phi F_{n,bearing} = \phi f_{cu} W_{eq} W_{eq,D}$
$$= (0.7)(7.80 \text{ ksi})(874 \text{ in.}^2)$$
$$= 4770.4 \text{ kip} > 1340.6 \text{ kip} \quad \textbf{OK}$$

NODAL STRENGTH AT BACK FACE (Node A_D)

Factored load: $\quad\quad\quad\quad\quad\quad\quad\quad\quad F_{u,back} = 274.5 \text{ kip}$

Effective area: $\quad\quad\quad\quad\quad\quad\quad A_{cn,back} = W_{eq} \cdot 0.2H = (31.0 \text{ in.})(12.0 \text{ in.})$
$$= 294 \text{ in}^2$$

Concrete efficiency factor: $\quad\nu = 0.85$

Concrete capacity: $\quad\quad\quad\quad\quad f_{cu} = m \cdot \nu \cdot f'_c = (2.55)(0.85)(3.6 \text{ ksi})$
$$= 7.80 \text{ ksi}$$

Nodal capacity: $\quad\quad\quad\quad\quad \phi F_{n,back} = \phi f_{cu} A_{cn,back}$
$$= (0.7)(7.80 \text{ ksi})(294 \text{ in.}^2)$$
$$= 1605.9 \text{ kip} > 274.5 \text{ kip} \quad \textbf{OK}$$

NODAL STRENGTH AT STRUT-TO-NODE INTERFACE (Node A_D)

Factored load: $F_{u,SNI} = 1368.4$ kip

Effective area:
$$A_{cn,SNI} = W_{eq} \cdot L_S = (31.0 \text{ in.})(29.6 \text{ in.})$$
$$= 915 \text{ in.}^2$$

Concrete efficiency factor:
$$\nu = 0.85 - {f_c'}/{20 \text{ ksi}} = 0.85 - {3.6 \text{ ksi}}/{20 \text{ ksi}}$$
$$= 0.67 > 0.65 \qquad \therefore \text{ se } \nu = 0.65$$

Concrete capacity:
$$f_{cu} = m \cdot \nu \cdot f_c' = (2.55)(0.65)(3.6 \text{ ksi})$$
$$= 5.96 \text{ ksi}$$

Nodal capacity:
$$\phi F_n = \phi f_{cu} A_{cn,SNI}$$
$$= (0.7)(5.96 \text{ ksi})(915 \text{ in}^2)$$
$$= 3820.1 \text{ kip} > 1368.4 \text{ kip} \quad \textbf{OK}$$
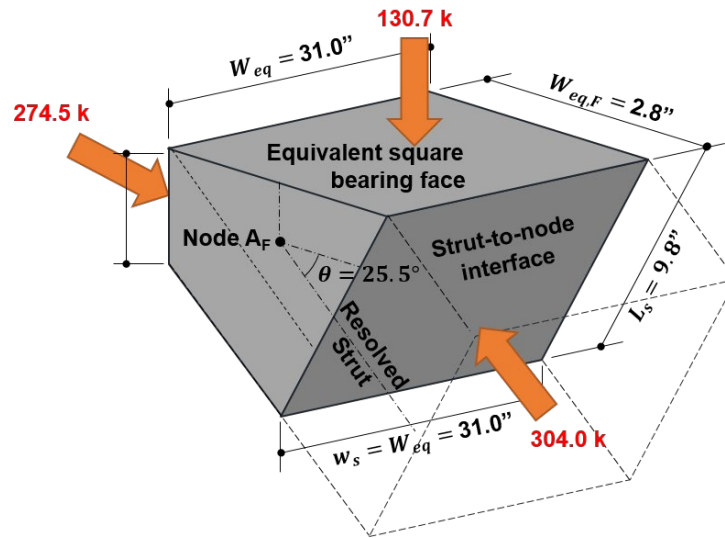
Figure 6.33 Details of 3D nodal geometry at Node A_F: Load Case VII

NODAL STRENGTH AT BEARING FACE (Node A_F)

Factored load: $F_{u,bearing} = 130.7$ kip

Concrete efficiency factor: $\nu = 0.85$

Concrete capacity:
$$f_{cu} = m \cdot \nu \cdot f_c' = (2.55)(0.85)(3.6 \text{ ksi})$$
$$= 7.80 \text{ ksi}$$

Nodal capacity:
$$\phi F_{n,bearing} = \phi f_{cu} W_{eq} W_{eq,F}$$
$$= (0.7)(7.80 \text{ ksi})(85 \text{ in.}^2)$$
$$= 465.1 \text{ kip} > 130.7 \text{ kip} \quad \textbf{OK}$$

NODAL STRENGTH AT BACK FACE (Node A$_F$)

Factored load: $\qquad\qquad\qquad$ $F_{u,back} = 274.5$ kip

Effective area: $\qquad\qquad\quad$ $A_{cn,back} = W_{eq} \cdot 0.2H = (31.0 \text{ in.})(12.0 \text{ in.})$
$$= 294 \text{ in}^2$$

Concrete efficiency factor: $\quad$ $v = 0.85$

Concrete capacity: $\qquad\quad$ $f_{cu} = m \cdot v \cdot f'_c = (2.55)(0.85)(3.6 \text{ ksi})$
$$= 7.80 \text{ ksi}$$

Nodal capacity: $\qquad\quad\;$ $\phi F_{n,back} = \phi f_{cu} A_{cn,back}$
$$= (0.7)(7.80 \text{ ksi})(294 \text{ in.}^2)$$
$$= 1605.9 \text{ kip} > 274.5 \text{ kip} \quad \textbf{OK}$$

NODAL STRENGTH AT STRUT-TO-NODE INTERFACE (Node A$_F$)

Factored load: $\qquad\qquad\qquad$ $F_{u,SNI} = 304.0$ kip

Effective area: $\qquad\qquad\quad$ $A_{cn,SNI} = W_{eq} \cdot L_S = (31.0 \text{ in.})(9.8 \text{ in.})$
$$= 302 \text{ in.}^2$$

Concrete efficiency factor: $\quad$ $v = 0.85 - {f'_c}/{20 \text{ ksi}} = 0.85 - {3.6 \text{ ksi}}/{20 \text{ ksi}}$
$$= 0.67 > 0.65 \qquad \therefore \text{ se } v = 0.65$$

Concrete capacity: $\qquad\quad$ $f_{cu} = m \cdot v \cdot f'_c = (2.55)(0.65)(3.6 \text{ ksi})$
$$= 5.96 \text{ ksi}$$

Nodal capacity: $\qquad\quad\;$ $\phi F_n = \phi f_{cu} A_{cn,SNI}$
$$= (0.7)(5.96 \text{ ksi})(302 \text{ in}^2)$$
$$= 1261.7 \text{ kip} > 304.0 \text{ kip} \quad \textbf{OK}$$

- *Node C (CTT Node)*

Figure 6.34 illustrates the dimension and applying forces after resolving struts AC and BC at Node C in three dimensions based on the proposed recommendations of this study. The confinement modification factor and the concrete efficiency factor of Node C are the same as those in Load Case VI ($m = 1.55$ and $v = 0.65$). Note that the nodal strength check at back faces is not necessary since an adequate development length that satisfies the anchorage requirement is provided in this example.

$$L_s = D'_{DS} \sin\theta + 2c_b \cos\theta$$
$$= 42.5" \sin 38.0° + 2\times(4"+1.41") \cos 38.0°$$
$$= 26.21" + 8.52" = 34.7"$$
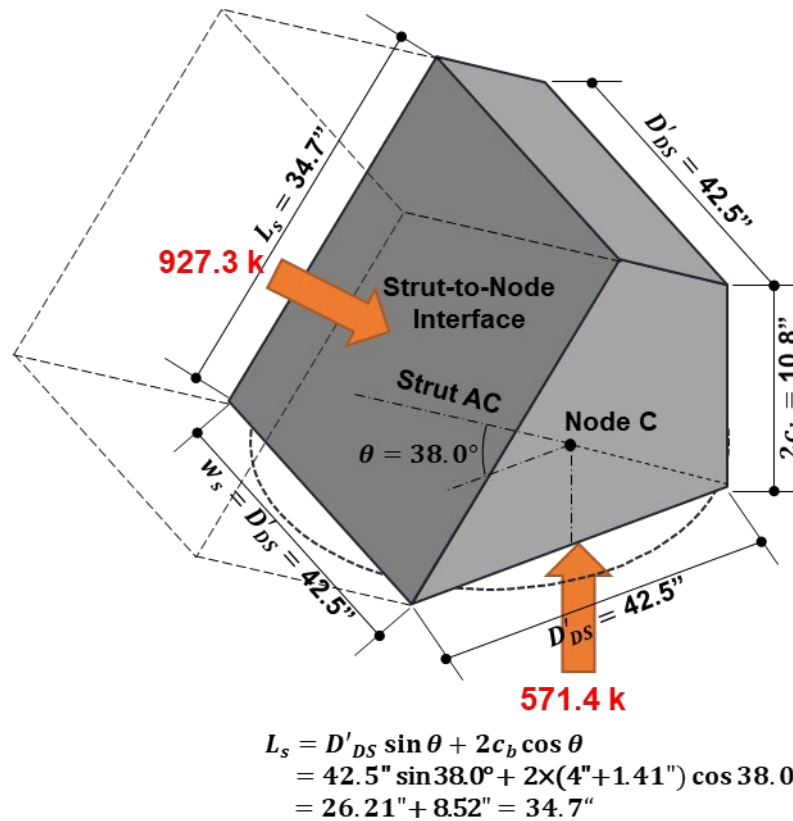
Figure 6.34 Details of 3D nodal geometry and applied forces at Node C

NODAL STRENGTH AT BEARING FACE

Factored load:	$F_{u,bearing} = 571.4$ kip
Concrete efficiency factor:	$v = 0.65$
Concrete capacity:	$f_{cu} = m \cdot v \cdot f'_c = (1.55)(0.65)(3.6 \text{ ksi})$ $= 3.63$ ksi
Nodal capacity:	$\phi F_{n,bearing} = \phi f_{cu} A_{cn,bearing}$ $= (0.7)(3.63 \text{ ksi})(1809.6 \text{ in.}^2)$ $= 4598.8$ kip > 571.4 kip **OK**

NODAL STRENGTH AT STRUT-TO-NODE INTERFACE

Factored load: $\qquad$ $F_{u,SNI} = 927.3$ kip

Concrete efficiency factor: $\quad v = 0.65$

Effective area: $\qquad A_{cn,SNI} = w_s \cdot L_S = (42.5 \text{ in.})(34.7 \text{ in.})$
$$= 1477.5 \text{ in.}^2$$

Concrete capacity: $\qquad f_{cu} = m \cdot v \cdot f_c' = (1.55)(0.65)(3.6 \text{ ksi})$
$$= 3.63 \text{ ksi}$$

Nodal capacity: $\qquad \phi F_{n,SNI} = \phi f_{cu} A_{cn,SNI}$
$$= (0.7)(3.63 \text{ ksi})(1477.5 \text{ in}^2)$$
$$= 3755.0 \text{ kip} > 927.3 \text{ kip} \quad \textbf{OK}$$

- ### Node D (CTT Node)

Figure 6.35 illustrates the dimension and applying forces at Node D in three dimensions based on the proposed recommendations of this study. The confinement modification factor and the concrete efficiency factor of Node D are the same as those of Node C ($m = 1.55$ and $v = 0.65$). Two diagonal struts (F_{DA} and F_{DB}) are resolved into one diagonal strut as summarized in the following table.

| | Strut | Force component*, kip | | | Strut Force, kip |
		x	y	z	$(\sqrt{x^2 + y^2 + z^2})$
Diagonal struts	F_{DA}	268.3	642.4	462.4	835.7
	F_{DB}	15.4	8.3	0.0	17.7
Resolved Strut	$F_{u,D}$	283.7	650.7	462.4	847.3
	Strut Angle ($\text{atan}(z/\sqrt{x^2 + y^2})$), DEG				33.1

*The sign of a number is based on the coordinate specified in Figure 6.8
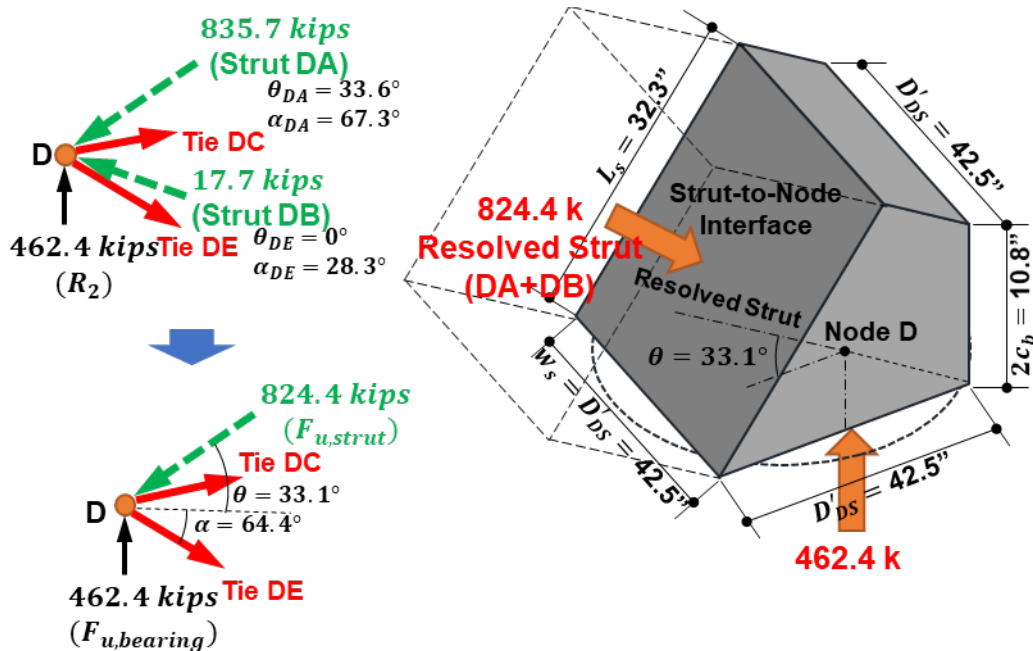
Figure 6.35 Resolving the forces (left) and details of 3D nodal geometry and applied forces (right) at Node D

NODAL STRENGTH AT BEARING FACE

Factored load: $F_{u,bearing} = 462.4 \text{ kip}$

Concrete efficiency factor: $\nu = 0.65$

Concrete capacity: $f_{cu} = m \cdot \nu \cdot f'_c = (1.55)(0.65)(3.6 \text{ ksi})$
$$= 3.63 \text{ ksi}$$

Nodal capacity: $\phi F_{n,bearing} = \phi f_{cu} A_{cn,bearing}$
$$= (0.7)(3.63 \text{ ksi})(1809.6 \text{ in.}^2)$$
$$= 4598.8 \text{ kip} > 462.4 \text{ kip} \quad \textbf{OK}$$

NODAL STRENGTH AT STRUT-TO-NODE INTERFACE

Factored load: $F_{u,SNI} = 824.4 \text{ kip}$

Concrete efficiency factor: $\nu = 0.65$

Effective area: $A_{cn,SNI} = w_s \cdot L_S = (42.5 \text{ in.})(32.3 \text{ in.})$
$$= 1373.4 \text{ in.}^2$$

Concrete capacity: $f_{cu} = m \cdot \nu \cdot f'_c = (1.55)(0.65)(3.6 \text{ ksi})$
$$= 3.63 \text{ ksi}$$

Nodal capacity: $\phi F_{n,SNI} = \phi f_{cu} A_{cn,SNI}$
$$= (0.7)(3.63 \text{ ksi})(1373.4 \text{ in}^2)$$
$$= 3490.2 \text{ kip} > 824.4 \text{ kip} \quad \textbf{OK}$$

- *Node F (CTT Node)*

Figure 6.36 illustrates the dimension and applying forces at Node F in three dimensions based on the proposed recommendations of this study. The confinement modification factor and the concrete efficiency factor of Node F are the same as those of Node C ($m = 1.55$ and $v = 0.65$). Two diagonal struts (F_{FA} and F_{FB}) are resolved into one diagonal strut as summarized in the following table.

Strut		Force component*, kip			Strut Force, kip $(\sqrt{x^2 + y^2 + z^2})$
		x	y	z	
Diagonal struts	F_{FA}	-87.8	-51.3	-45.1	111.3
	F_{FB}	-243.7	-644.9	0.0	689.5
Resolved Strut	$F_{u,F}$	-331.5	-696.3	-45.1	772.5
Strut Angle ($\text{atan}(z/\sqrt{x^2 + y^2})$), DEG					3.3

*The sign of a number is based on the coordinate specified in Figure 6.8
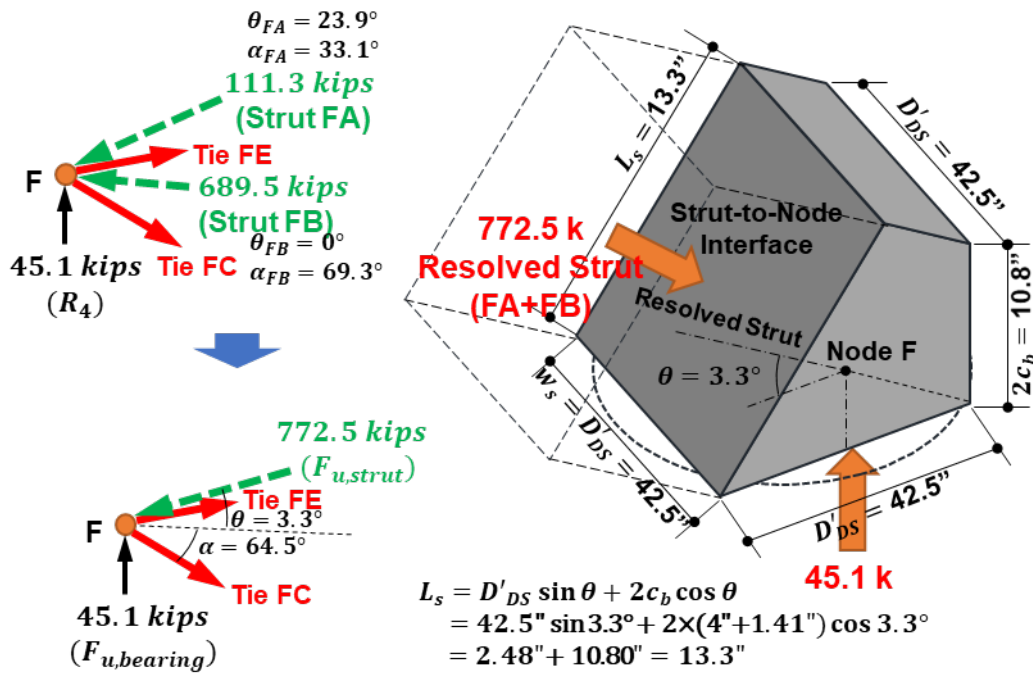
Figure 6.36 Resolving the forces (left) and details of 3D nodal geometry and applied forces (right) at Node F

78

NODAL STRENGTH AT BEARING FACE

Factored load:	$F_{u,bearing} = 45.1$ kip
Concrete efficiency factor:	$v = 0.65$
Concrete capacity:	$f_{cu} = m \cdot v \cdot f'_c = (1.55)(0.65)(3.6 \text{ ksi})$ $= 3.63$ ksi
Nodal capacity:	$\phi F_{n,bearing} = \phi f_{cu} A_{cn,bearing}$ $= (0.7)(3.63 \text{ ksi})(1809.6 \text{ in.}^2)$ $= 4598.8$ kip > 45.1 kip **OK**

NODAL STRENGTH AT STRUT-TO-NODE INTERFACE

Factored load:	$F_{u,SNI} = 772.5$ kip
Concrete efficiency factor:	$v = 0.65$
Effective area:	$A_{cn,SNI} = w_s \cdot L_S = (42.5 \text{ in.})(13.3 \text{ in.})$ $= 565.1$ in.^{2}
Concrete capacity:	$f_{cu} = m \cdot v \cdot f'_c = (1.55)(0.65)(3.6 \text{ ksi})$ $= 3.63$ ksi
Nodal capacity:	$\phi F_{n,SNI} = \phi f_{cu} A_{cn,SNI}$ $= (0.7)(3.63 \text{ ksi})(565.1 \text{ in}^2)$ $= 1436.1$ kip > 772.5 kip **OK**

Therefore, the nodal capacities of the CCC nodes and CTT nodes with defined nodal geometry are greater than factored loads.

6.2.2.6. Step 6: Proportion Shrinkage and Temperature Reinforcement

The necessary shrinkage and temperature reinforcement for the footing was specified in Section 6.2.1.6 On the side faces, No. 6 bars with 10 in. spacing ($A_s = 0.53$ in.^{2}/ft.) are required in both horizontal and vertical directions. On the top face, No. 6 bars with 10 in. spacing A_s (0.53 in.^{2}/ft.) are provided. No. 6 bars with 10 in. spacing as the top mat reinforcement are sufficient for the required strength as calculated in Section 6.2.1.6. Therefore, the original reinforcement plan (No. 6 bars with 10 in. spacing) will be used.

6.2.2.7. Step 7: Provide Necessary Anchorage for Ties

- *Bottom Ties*

Proper anchorage of the bottom mat reinforcement (Ties CD, DE, EF, and FC) was discussed in Section 6.2.1.7. These ties are properly anchored with the use of straight bars. Bottom ties connected with Node E need to be checked in the anchorage because Node E is a smeared node where the boundary of a node is not determined by the bearing plate. Figure 6.37 illustrates the available length at Node E, confirming that straight bars are anchored properly there.

(Unit: in. if not specified)
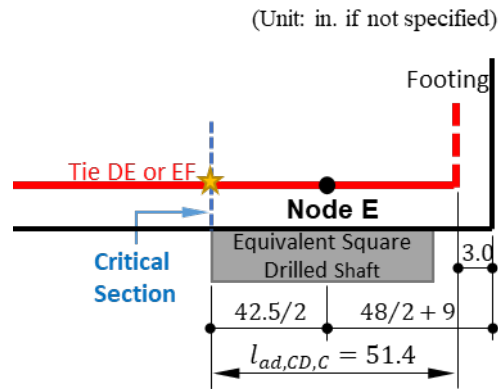
Figure 6.37 Critical sections for the development of ties at Node E

- *Top Ties*

Each top tie (Ties GH, HI, IJ, and JG) is connected with smeared nodes (Nodes G through J) at both ends. The available development length is the same as that at Node E, as shown in Figure 6.37. The minimum development length of a No.6 straight bar is 22.8 in. even if λ_{er}, excess reinforcement factor, is not considered ($\lambda_{er} = 1.0$) in accordance with AASHTO LRFD (2020). Therefore, top mat reinforcement can be sufficiently developed in the given load case.

- *Vertical Ties*

The 3D strut-and-tie model for Load Case VII contains vertical ties for the column (Tie BB') and drilled shaft reinforcement (Tie EI). The available lengths for those tie elements are estimated from the compression field proposed by Yi et al. (2022), as depicted in Figure 6.38.

$$
\begin{aligned}
l_{ad,COL} &= H - (c_b + c_t) - (d_{b,bu}) - z_s \tan 25° \\
&= (60 \text{ in.}) - (5.41 \text{ in.} + 4.75 \text{ in.}) - (1.41 \text{ in.}) - (59.8 \text{ in.}) \tan 25° \\
&= 20.6 \text{ in.}
\end{aligned}
$$

$$l_{ad,DS} = H - (c_b + c_t) - (d_{b,tl}) - z_s \tan 25°$$
$$= (60 \text{ in.}) - (5.41 \text{ in.} + 4.75 \text{ in.}) - (0.75 \text{ in.}) - (59.8 \text{ in.}) \tan 25°$$
$$= 21.2 \text{ in.}$$
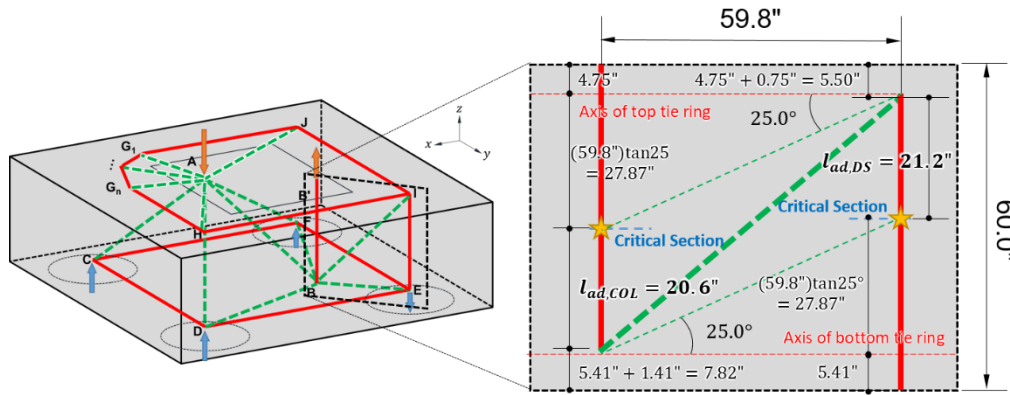
Figure 6.38 Critical section for the development of column ties and drilled shaft ties

The anchorage requirement for the column and drilled shaft reinforcement can be satisfied by employing hooked reinforcement. The proposed critical section of the column reinforcement indicates the hooked column reinforcement oriented towards the column is not effective. However, the diagonal strut flowing down from the column (Strut AB in Figure 6.38) can activate the bearing action of the inner-oriented hooked column reinforcement. Therefore, the anchorage requirement check for the 90-degree hooked column reinforcement is performed with the minimum required development length of hooked bars, regardless of the hook orientation. The required development lengths for 90-degree and 180-degree hooked bars are computed in accordance with AASHTO LRFD (2020). The reinforcement confinement factor, λ_{rc}, is 0.8 determined from given details of the column reinforcement; the coating factor, λ_{cw}, is 1.0 for uncoated reinforcement; the excess reinforcement factor, λ_{er}, is 0.244 based on the designed column reinforcement; and the concrete density modification factor, λ, is 1.0 for normal weight concrete. The required development length of a hooked No. 11 bar is calculated below:

$$l_{dh,COL} = \frac{38.0(1.41 \text{ in.})}{60.0} \times \frac{60 \text{ ksi}}{\sqrt{3.6 \text{ ksi}}} \times \left(\frac{0.8 \cdot 1.0 \cdot 0.244}{1.0}\right)$$
$$= 5.5 \text{ in.} < l_{ad,COL}(= 20.6 \text{ in.})$$

The drilled shaft reinforcement also uses No. 9 hooked bars to satisfy the anchorage requirement. The orientation of the 180-degree hook does not affect the development length. The same equation is used to calculate the development length of a hooked No. 9 bar with excess reinforcement factor, λ_{er}, of 0.532 based on the designed drilled shaft reinforcement:

81

$$l_{dh,DS} = \frac{38.0(1.128 \text{ in.})}{60.0} \times \frac{60 \text{ ksi}}{\sqrt{3.6 \text{ ksi}}} \times \left(\frac{0.8 \cdot 1.0 \cdot 0.532}{1.0} \right)$$

$$= 9.6 \text{ in.} < l_{ad,DS}(= 21.2 \text{ in.})$$

Therefore, the research team confirms that all reinforcing bars of the footing designed for Load Case VII are safe for the applied loading condition.

6.2.3. Reinforcement Layout

The reinforcement details designed for Load Case I through V are sufficient to resist the internal force resulting from the biaxial flexural load cases: Load Case VI and VII. Therefore, the details remain the same as those proposed by Yi et al. (2022) and depicted in Figure 6.39 through Figure 6.43.

, including locations
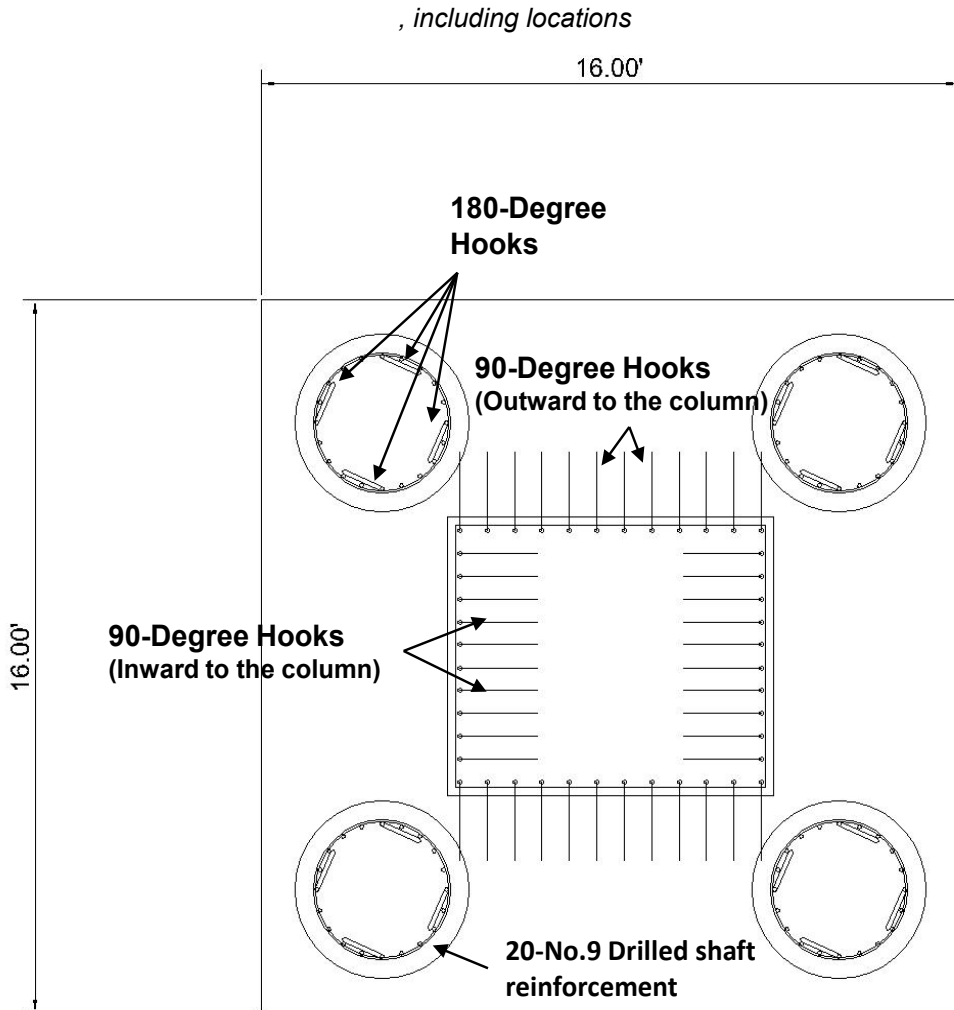
Figure 6.39 Reinforcement details for anchorage of vertical ties
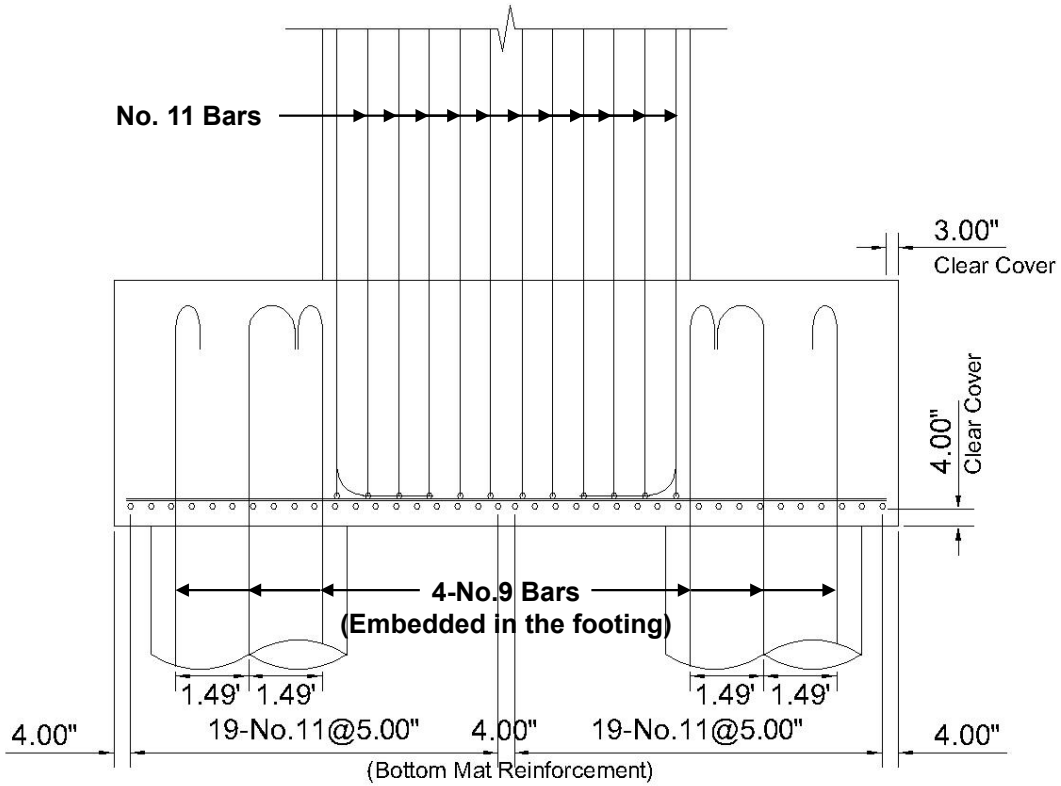
Figure 6.40 Reinforcement details for ties: elevation view
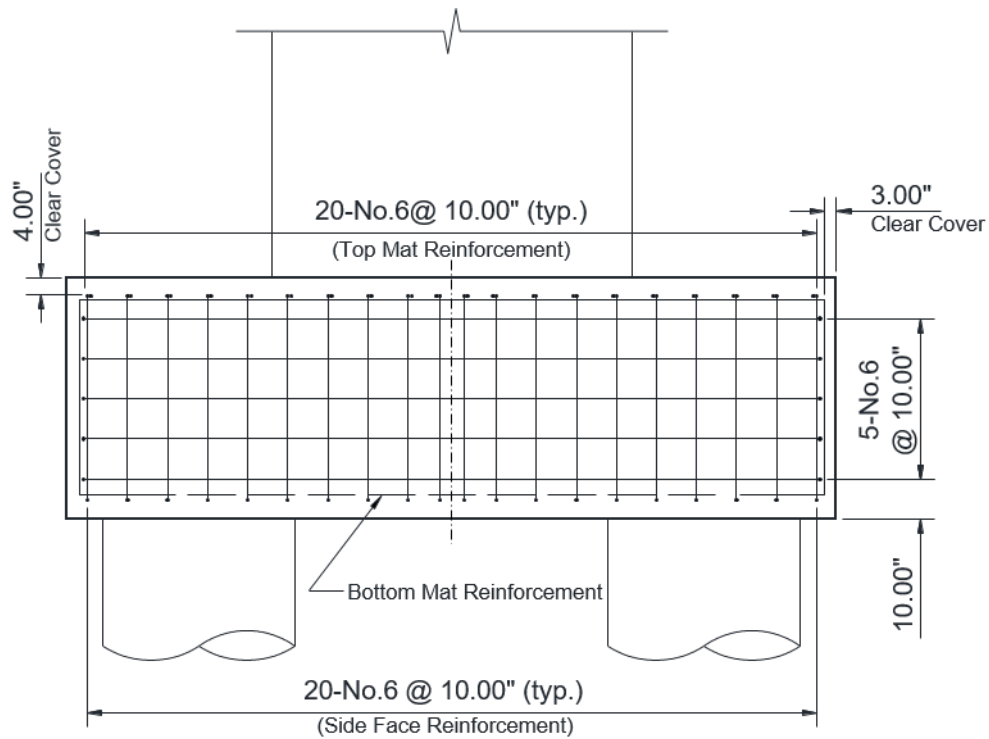
Figure 6.41 Details for shrinkage and temperature reinforcement: elevation view
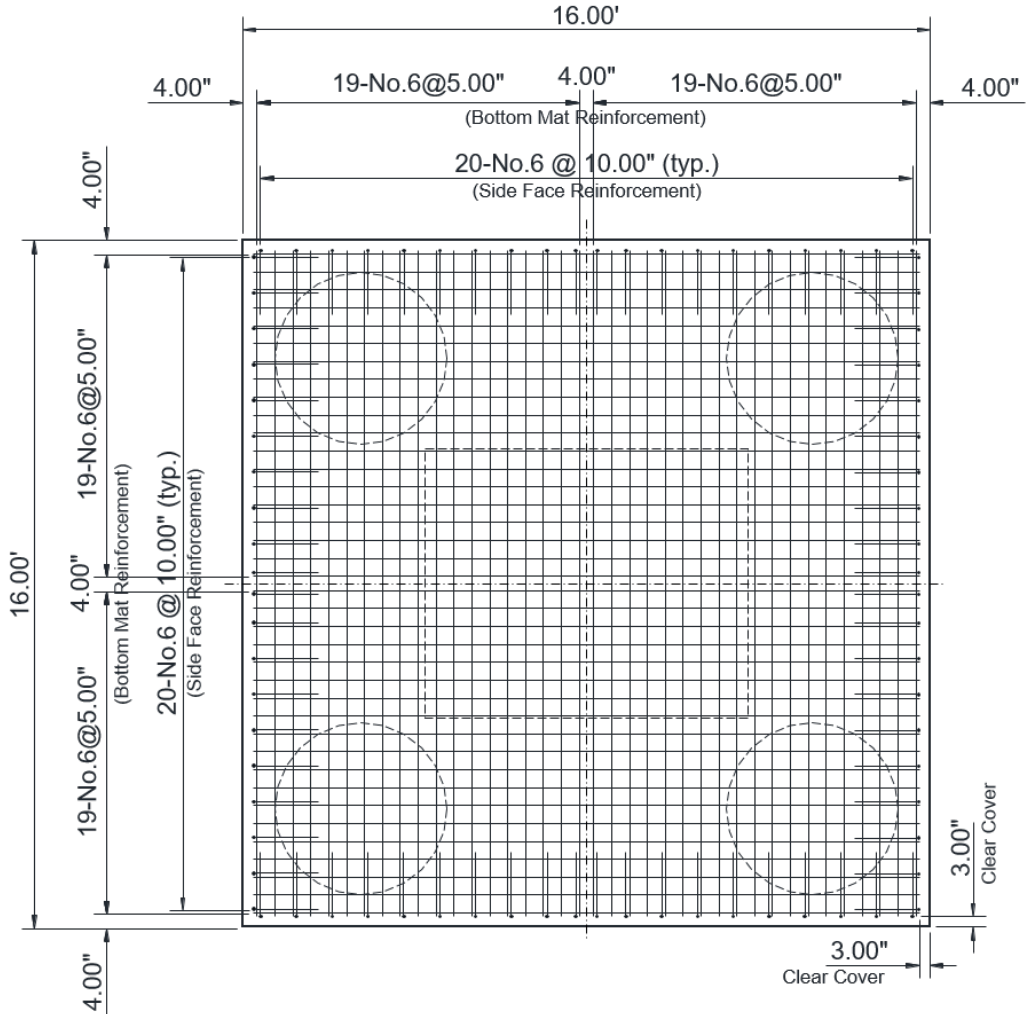
Figure 6.42 Details for bottom mat reinforcement: plan view
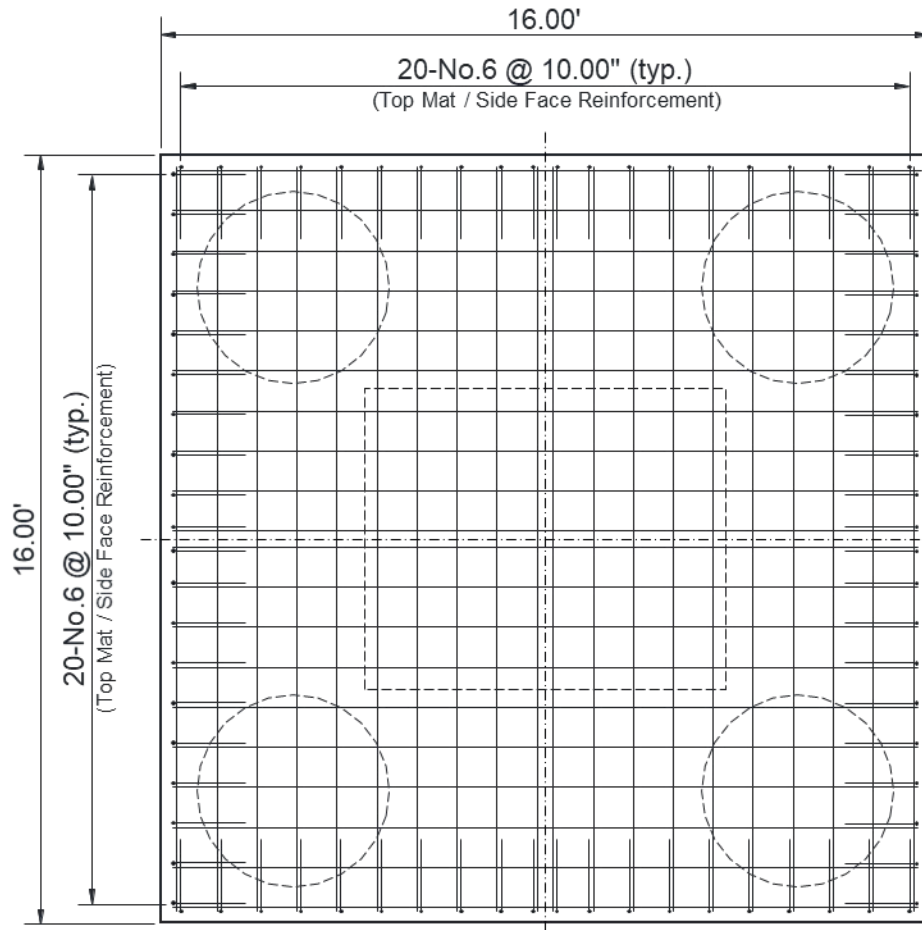
Figure 6.43 Details for top mat reinforcement: plan view

Chapter 7. Summary and Conclusions

This research has developed design recommendations for drilled shaft footings subjected to biaxial flexural loading scenarios (Load Case VI: axial compression combined with moderate biaxial flexure; Load Case VII: axial compression combined with large biaxial flexure) using the 3D STM in a conservative way. Due to the lack of previous studies, the recommendations were mostly refined from those proposed by Yi et al. (2022) for drilled shaft footings subjected to uniaxial loading scenarios, and they are summarized as follows:

Equivalent Force System: Single Strut and Single Tie Equivalent Force System

Yi et al. (2022) proposed determining the equivalent force system of the 3D strut-and-tie model for drilled shaft footings based on the actual stress distribution corresponding to the applied loading condition. Complex biaxial flexural loading leads to complex stress distribution over the column section, requiring complicated calculations and decisions to establish the equivalent force system comprising multiple struts and ties. Therefore, the research team simplified the procedure by employing the single strut and single tie equivalent force system. The strut-and-tie model developed from the proposed equivalent force system also leads to a conservative design owing to decreased strut inclinations.

Development of 3D Strut-and-Tie Models for Load Cases VI and VII

According to the established equivalent force system and the reactions at drilled shafts resulting from the biaxial flexural loading conditions, the research team developed 3D strut-and-tie models for Load Case VI and Load Case VII. The configurations of the models were determined based on the asymmetric internal force flow in drilled shaft footings. The 3D strut-and-tie model of Load Case VII was idealized to a strut-and-tie model configuration, similar to that of Load Case III, familiar to designers. The idealized model has a deficiency: it cannot consider the offset between the truss panels of the column tie transfer mechanism and those of the drilled shaft tie transfer mechanism; however, the error resulting from the deficiency was insignificant.

Modified Equivalent Square Bearing Face for CCC Node

The bearing face of the CCC node is conservatively determined using the extreme compressive fiber stress derived from the sectional analysis for the equivalent force system. Assuming the extreme compressive fiber stress is uniformly distributed over the bearing face of the CCC node leads it to become much smaller than the actual compressive area over the column section. Furthermore, the modified

bearing face is assumed to be an equivalent square-shaped bearing face, which is proposed as the modified equivalent square bearing face in this research, to develop the nodal geometry of the CCC node.

Development of 3D Nodal Geometry (CCC Node)

The research team proposed subdividing the CCC node into two parts for developing the 3D nodal geometry. The diagonal struts acting at the CCC node are divided by the ratio of the reaction force acting on the drilled shaft of each part with respect to the diagonal plane of the foundation. Similarly, the modified equivalent square bearing face and the vertical strut from the column are also subdivided. The research team resolved all diagonal struts on each side into one diagonal strut; therefore, the number of forces acting at each subdivided CCC node becomes three: subdivided resultant compressive force, resolved diagonal strut, and lateral force component of the resolved diagonal strut. The 3D nodal geometry of each subdivided node can be established following the recommendations of Yi et al. (2022).

Although many load cases subjected to biaxial flexural loading are considered in the design of in-practice drilled shaft footings, little research on the application of the 3D STM to the footings has been conducted. Since the research team conservatively refined the design recommendations established based on large-scale tests conducted by Yi et al. (2022), drilled shaft footings can be designed for safety using the proposed methods. Designers can design even drilled shaft footings with complicated internal force flow using the 3D STM based on the outcomes of this research.

However, even though the proposed recommendations were established conservatively, it must be acknowledged that they have not been experimentally verified. Additional experimental studies on drilled shaft footings subjected to biaxial loading scenarios can verify the conservativeness of the proposed recommendations and further refine them.

Appendix A Determination of Equivalent Force System

The biaxial flexural loading scenarios corresponding to Load Case VI and VII induces complex strain and stress distributions over the column section. This section describes the calculation procedure of the sectional analysis to derive the distributions.

Three unknowns (neutral axis depth (c); neutral axis inclination (θ); and extreme compressive fiber strain (ε_c)) are required to develop the strain and stress distributions over the column section and can be resolved iteratively using three equilibrium equations ($\sum P_u = 0$; $\sum M_{ux} = 0$; $\sum M_{uy} = 0$).

As illustrated in Figure A.1, the analysis is performed using the coordinate system with the centroid of the column as the origin. The coordinates ($x - y$ coordinate in Figure #) of all four corners of the column and tensile column reinforcing bars are transformed to new coordinates ($x' - y'$ coordinate in Figure A.1) rotated by the neutral axis inclination (θ).

$$\text{Coordinate Transformation } (x, \, y) \; \rightarrow (x', \, y')$$

$$x' = x \cos\theta + y \sin\theta$$

$$y' = y \cos\theta - x \sin\theta$$

Therefore, the neutral axis depth (c) is expressed with the offset from the rotated coordinate system ($y'_n \, (=abs(y'_b - c)$ in Figure A.1) for the analysis. The column reinforcing bars subjected to compression and at the compressive faces of the column ($A - B$ and $B - D$ faces in Figure A.1) are not considered in the analysis to simplify the calculation.
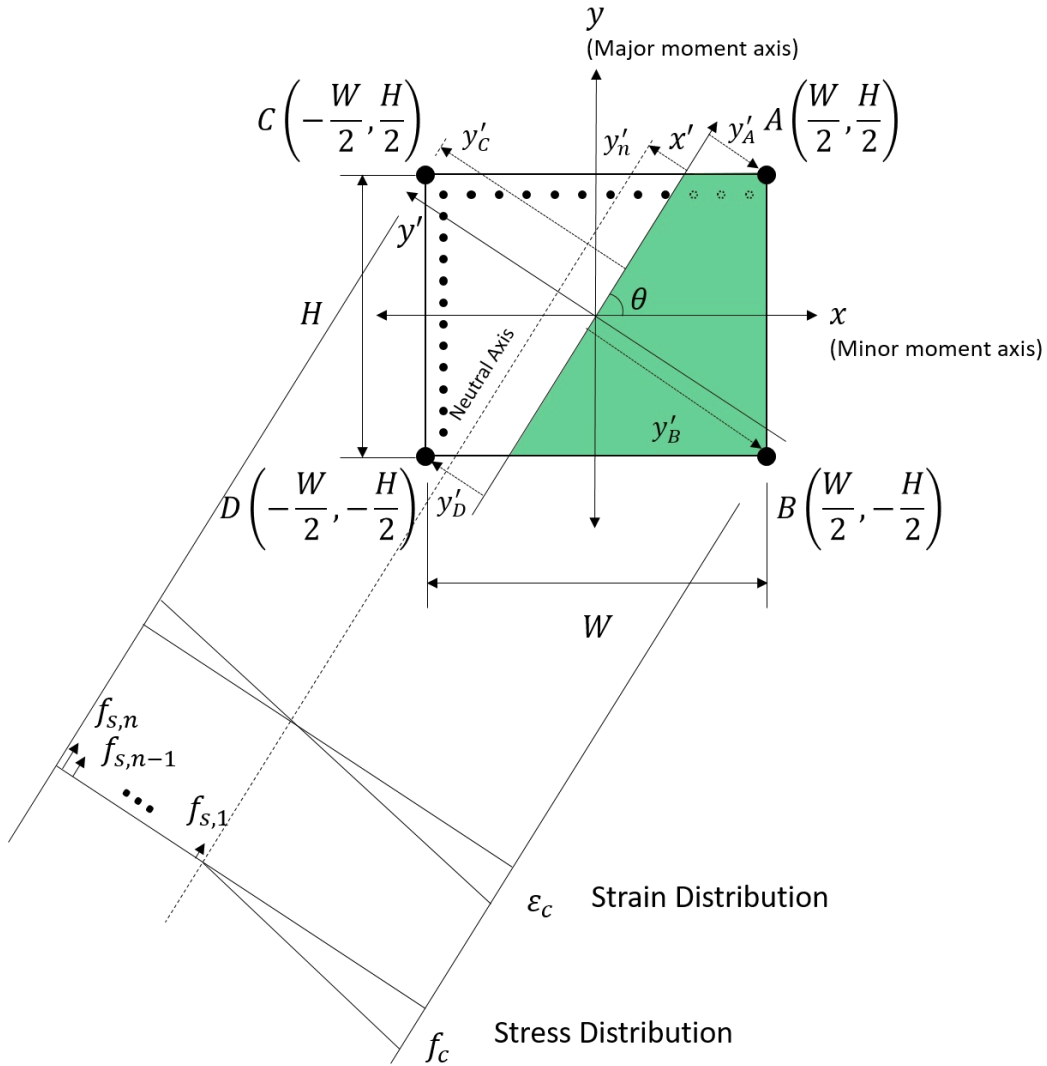
Figure A.1 Stress distribution over the column section under biaxial flexural loading

The shape of the compressive region varies depending on the neutral axis position; therefore, this report computes the compressive resultant force and its centroid position for each shape geometrically. Figure A.2 presents different shapes of the compressive region available over the column section.
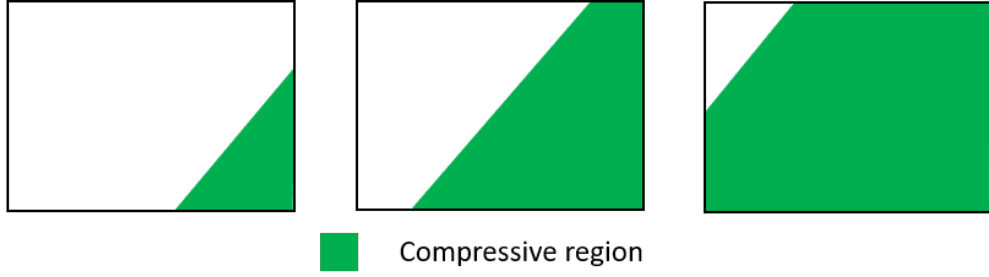
Figure A.2 Different shapes of compressive region depending on neutral axis depth

For each case, the resultant compressive force (C) and its centroid position ($\bar{x}$ and $\bar{y}$ in $x - y$ coordinate) can be derived as below using three assumed values (y'_n, θ, and ε_c).
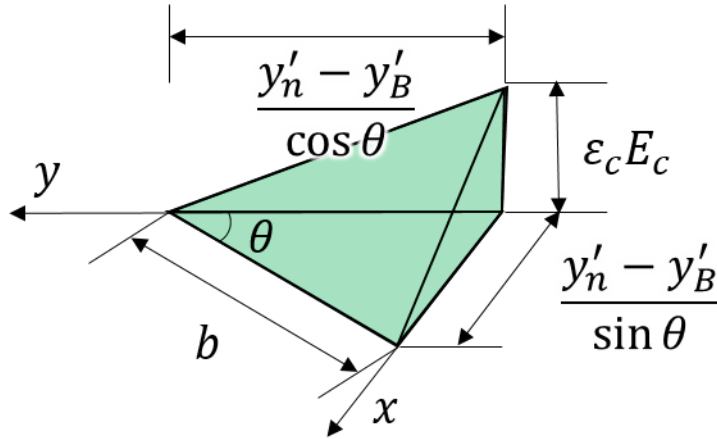
Case I

$$b : \frac{H}{\sin \theta} = (y'_n - y'_B) : H \cos \theta$$

$$b = \frac{y'_n - y'_B}{\cos \theta \sin \theta}$$

$$C_c = \left(\frac{1}{3}\right)\left(b \frac{y'_n - y'_B}{2}(\varepsilon_c E_c)\right)$$

$$\bar{x} = \left(\frac{W}{2} - \left(\frac{y'_n - y'_B}{4 \sin \theta}\right)\right); \bar{y} = \left(-\frac{H}{2} + \left(\frac{y'_n - y'_B}{4 \cos \theta}\right)\right)$$

91

Case II

The compressive region is subdivided into three parts to simplify the calculation.

Region 1 **Region 2** **Region 3**
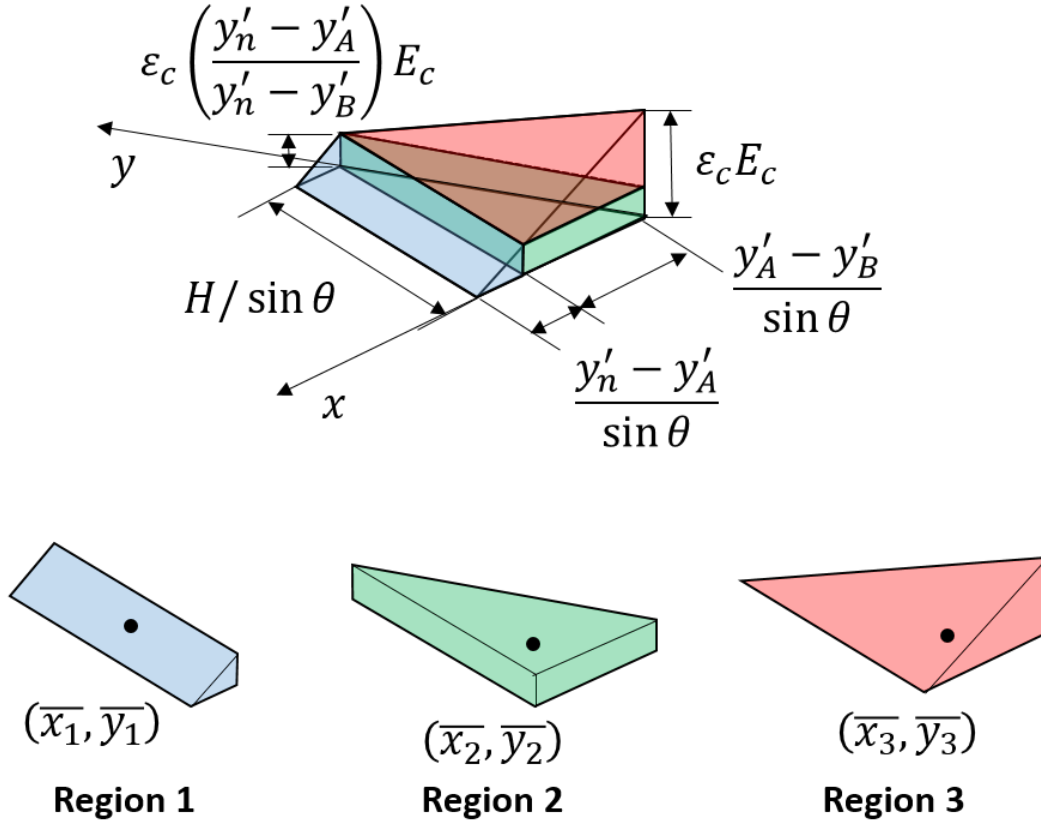
Region 1

$$C_1 = \frac{1}{2} \left(\varepsilon_c \left(\frac{y_n' - y_A'}{y_n' - y_B'} \right) E_c \left(\frac{y_n' - y_A'}{\sin \theta} \right) \right) H$$

$$\overline{x_1} = \frac{y_A'}{\sin \theta} - \left(\frac{y_n' - y_A'}{3 \sin \theta} \right)$$

$$\overline{y_1} = 0$$

Region 2

$$C_2 = \frac{1}{2}\left(\frac{y_A' - y_B'}{\sin\theta}H\right)\left(\varepsilon_c\left(\frac{y_n' - y_A'}{y_n' - y_B'}\right)E_c\right)$$

$$\overline{x_2} = \frac{W}{2} - \left(\frac{y_A' - y_B'}{3\sin\theta}\right)$$

$$\overline{y_2} = -\frac{H}{2} + \frac{H}{3} = -\frac{H}{6}$$

Region 3

$$C_3 = \frac{1}{6}\left(\frac{y_A' - y_B'}{\sin\theta}H\right)\left(\varepsilon_c E_c - \varepsilon_c abs\left(\frac{y_n' - y_A'}{y_n' - y_B'}\right)E_c\right)$$

$$\overline{x_3} = \frac{W}{2} - abs\left(\frac{y_A' - y_B'}{4\sin\theta}\right)$$

$$\overline{y_3} = -\frac{H}{2} + \frac{H}{4} = -\frac{H}{4}$$

Combining the computed results from three subdivided regions,

$$C_c = C_1 + C_2 + C_3$$

$$\bar{x} = \frac{C_1\overline{x_1} + C_2\overline{x_2} + C_3\overline{x_3}}{C}$$

$$\bar{y} = \frac{C_1\overline{y_1} + C_2\overline{y_2} + C_3\overline{y_3}}{C}$$

Case III

Similarly, the compressive region is also subdivided into six parts to simplify the calculation.

$$\varepsilon_c \left(\frac{y'_n - y'_A}{y'_n - y'_B} \right) E_c$$

$$\varepsilon_c E_c$$

$$\varepsilon_c \left(\frac{y'_n - y'_D}{y'_n - y'_B} \right) E_c$$

$$\frac{y'_A - y'_B}{\sin \theta}$$

$$\frac{y'_C - y_n}{\cos \theta \sin \theta}$$

$$\frac{y'_D - y'_A}{\sin \theta}$$

$$\frac{y'_n - y'_D}{\cos \theta}$$

$(\overline{x_1}, \overline{y_1})$	$(\overline{x_2}, \overline{y_2})$	$(\overline{x_3}, \overline{y_3})$
Region 1	**Region 2**	**Region 3**

$(\overline{x_4}, \overline{y_4})$	$(\overline{x_5}, \overline{y_5})$	$(\overline{x_6}, \overline{y_6})$
Region 4	**Region 5**	**Region 6**
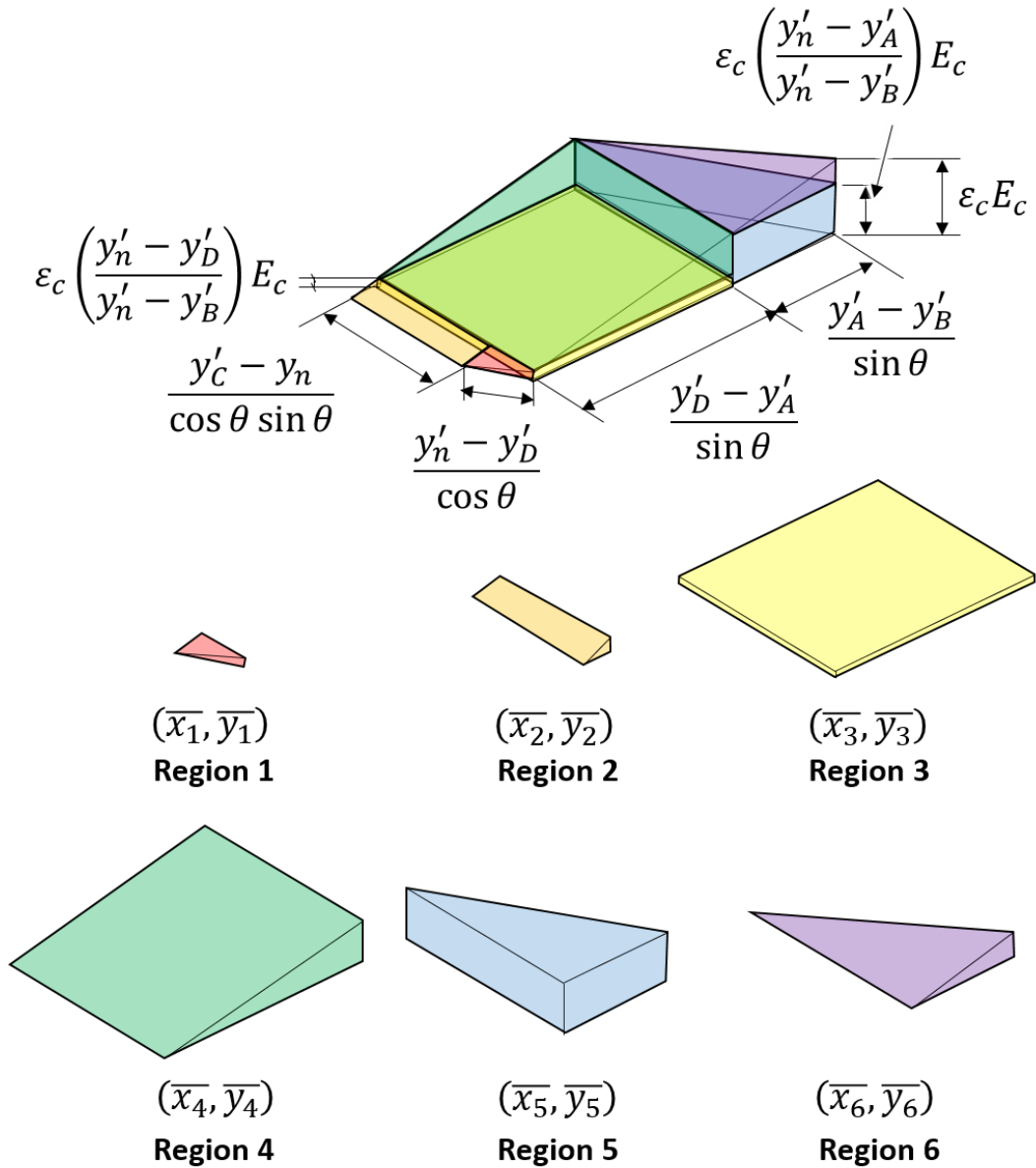
Region 1

$$C_1 = \frac{1}{3}\left(\varepsilon_c\left(\frac{y_n' - y_D'}{y_n' - y_B'}\right)E_c\left(\frac{y_n' - y_D'}{\sin\theta\cos\theta}\right)\right)(y_n' - y_D')$$

$$\overline{x_1} = -\frac{W}{2} + \frac{1}{3}\left(\frac{y_n' - y_D'}{\sin\theta}\right)$$

$$\overline{y_1} = -\frac{H}{2} + \frac{2}{3}\left(\frac{y_n' - y_D'}{\cos\theta}\right)$$

Region 2

$$C_2 = \frac{1}{2}\left(\frac{y_C' - y_n}{\cos\theta\sin\theta}\right)(y_n' - y_D')\varepsilon_c\left(\frac{y_n' - y_D'}{y_n' - y_B'}\right)E_c$$

$$\overline{x_2} = -\frac{W}{2} + \frac{2(y_n' - y_D')}{3\sin\theta} + \frac{1}{2}\left(\frac{y_C' - y_n}{\cos\theta}\right)\cot\theta$$

$$\overline{y_2} = \frac{H}{2} - \frac{1}{2}\left(\frac{y_C' - y_n}{\cos\theta}\right)$$

Region 3

$$C_3 = H\left(\frac{y_D' - y_A'}{\sin\theta}\right)\left(\varepsilon_c\left(\frac{y_n' - y_D'}{y_n' - y_B'}\right)E_c\right)$$

$$\overline{x_3} = 0$$

$$\overline{y_3} = 0$$

Region 4

$$C_4 = \frac{1}{2}H\left(\frac{y_D' - y_A'}{\sin\theta}\right)\left(\varepsilon_c\left(\frac{y_D' - y_A'}{y_n' - y_B'}\right)E_c\right)$$

$$\overline{x_4} = -\frac{W}{2} + \left(\frac{H}{2}\cot\theta\right) + \frac{2(y_D' - y_A')}{3\sin\theta}$$

$$\overline{y_4} = 0$$

Region 5

$$C_5 = \frac{1}{2}\left(\left(\frac{y'_A - y'_B}{\sin\theta}\right)H\right)\left(\varepsilon_c\left(\frac{y'_n - y'_A}{y'_n - y'_B}\right)E_c\right)$$

$$\overline{x_5} = \frac{W}{2} - \left(\frac{y'_A - y'_B}{3\sin\theta}\right)$$

$$\overline{y_5} = -\frac{H}{2} + \frac{H}{3} = -\frac{H}{6}$$

Region 6

$$C_6 = \frac{1}{6}H\left(\frac{y'_A - y'_B}{\sin\theta}\right)\left(\varepsilon_c E_c\left(1 - \frac{y'_n - y'_A}{y'_n - y'_B}\right)\right)$$

$$\overline{x_6} = \frac{W}{2} - \left(\frac{y'_A - y'_B}{4\sin\theta}\right)$$

$$\overline{y_6} = -\frac{H}{2} + \frac{H}{4} = -\frac{H}{4}$$

Combining the computed results from three subdivided regions,

$$C_c = C_1 + C_2 + C_3 + C_4 + C_5 + C_6$$

$$\bar{x} = \frac{C_1\overline{x_1} + C_2\overline{x_2} + C_3\overline{x_3} + C_4\overline{x_4} + C_5\overline{x_5} + C_6\overline{x_6}}{C}$$

$$\bar{y} = \frac{C_1\overline{y_1} + C_2\overline{y_2} + C_3\overline{y_3} + C_4\overline{y_4} + C_5\overline{y_5} + C_6\overline{y_6}}{C}$$

Based on the established equations, the calculation procedure to establish the equivalent force system of the Load Case VI example is presented in this section.

Given Load Combination (Load Case VI)

$$P_u = 1656 \text{ kip}$$
$$M_{ux} = 1440 \text{ kip} - \text{ft}$$
$$M_{uy} = 3670 \text{ kip} - \text{ft}$$

1st iteration

Neutral axis depth (y_n'): 0 in.

Neutral axis inclination (θ): 60.5° $\left(= \text{atan}\left(\frac{M_{uy}I_y}{M_{ux}I_x}\right)\right)$; Uncracked section assumed

Extreme compressive fiber strain (ε_c): -0.0001 (Elastic state)

Case II $(y_B' = -57.6 \text{ in.} < y_n' = 0 \text{ in.} < y_C' = 57.6 \text{ in.})$

Region 1

$$C_1 = \frac{1}{2}\left(\varepsilon_c\left(\frac{y_n' - y_A'}{y_n' - y_B'}\right)E_c\left(\frac{y_n' - y_A'}{\sin\theta}\right)\right)H = -109.9 \text{ kip}$$

$$\overline{x_1} = \frac{y_A'}{\sin\theta} - \left(\frac{y_n' - y_A'}{3\sin\theta}\right) = 15.9 \text{ in.}$$

$$\overline{y_1} = 0 \text{ in.}$$

Region 2

$$C_2 = \frac{1}{2}\left(\frac{y_A' - y_B'}{\sin\theta}H\right)\left(\varepsilon_c\left(\frac{y_n' - y_A'}{y_n' - y_B'}\right)E_c\right) = -195.5 \text{ kip}$$

$$\overline{x_2} = \frac{W}{2} - \left(\frac{y_A' - y_B'}{3\sin\theta}\right) = 30.9 \text{ in.}$$

$$\overline{y_2} = -\frac{H}{2} + \frac{H}{3} = -\frac{H}{6} = -12.5 \text{ in.}$$

Region 3

$$C_3 = \frac{1}{6}\left(\frac{y'_A - y'_B}{\sin\theta}H\right)\left(\varepsilon_c E_c - \varepsilon_c abs\left(\frac{y'_n - y'_A}{y'_n - y'_B}\right)E_c\right) = -116.0 \text{ kip}$$

$$\overline{x_3} = \frac{W}{2} - abs\left(\frac{y'_A - y'_B}{4\sin\theta}\right) = 34.4 \text{ in.}$$

$$\overline{y_3} = -\frac{H}{2} + \frac{H}{4} = -\frac{H}{4} = -18.8 \text{ in.}$$

Combining the computed results from three subdivided regions,

$$C_c = C_1 + C_2 + C_3 = -421.4 \text{ kip}$$

$$\bar{x} = \frac{C_1\overline{x_1} + C_2\overline{x_2} + C_3\overline{x_3}}{C} = 27.9 \text{ in.}$$

$$M_{y,c} = abs\left(\frac{C\bar{x}}{12}\right) = 979.76 \text{ kip} - \text{ft}$$

$$\bar{y} = \frac{C_1\overline{y_1} + C_2\overline{y_2} + C_3\overline{y_3}}{C} = -11.0 \text{ in.}$$

$$M_{x,c} = abs\left(\frac{C\bar{x}}{12}\right) = 386.28 \text{ kip} - \text{ft}$$

From the assumed variables, the tensile forces and moments due to the column reinforcing bars can be computed as below.

Rebar No.	x (in.)	y (in.)	Rebar size	Diameter (in.)	Area (in.²)	Distance from the neutral axis y'_t (in.)	Tensile strain $(\varepsilon_s = \varepsilon_c \frac{y'_b - y'_n}{y'_t - y_n})$	Tensile stress (ksi)	T_s (kip)	$M_{s,x}$ (kip-in.)	$M_{s,y}$ (kip-in.)
1	-41.40	33.90	#11	1.41	1.56	52.72	9.15E-05	2.65	4.14	11.69	14.28
2	-41.40	27.74	#11	1.41	1.56	49.69	8.62E-05	2.50	3.90	9.02	13.46
3	-41.40	21.57	#11	1.41	1.56	46.66	8.10E-05	2.35	3.66	6.58	12.64
4	-41.40	15.41	#11	1.41	1.56	43.62	7.57E-05	2.20	3.42	4.40	11.82
5	-41.40	9.25	#11	1.41	1.56	40.59	7.04E-05	2.04	3.19	2.46	10.99
6	-41.40	3.08	#11	1.41	1.56	37.56	6.52E-05	1.89	2.95	0.76	10.17
7	-41.40	-3.08	#11	1.41	1.56	34.53	5.99E-05	1.74	2.71	-0.70	9.35
8	-41.40	-9.25	#11	1.41	1.56	31.50	5.47E-05	1.59	2.47	-1.91	8.53
9	-41.40	-15.41	#11	1.41	1.56	28.46	4.94E-05	1.43	2.23	-2.87	7.71
10	-41.40	-21.57	#11	1.41	1.56	25.43	4.41E-05	1.28	2.00	-3.59	6.89
11	-41.40	-27.74	#11	1.41	1.56	22.40	3.89E-05	1.13	1.76	-4.06	6.07
12	-41.40	-33.90	#11	1.41	1.56	19.37	3.36E-05	0.97	1.52	-4.30	5.25
13	-33.87	33.90	#11	1.41	1.56	46.17	8.01E-05	2.32	3.62	10.24	10.23
14	-26.35	33.90	#11	1.41	1.56	39.61	6.87E-05	1.99	3.11	8.79	6.83
15	-18.82	33.90	#11	1.41	1.56	33.06	5.74E-05	1.66	2.60	7.33	4.07
16	-11.29	33.90	#11	1.41	1.56	26.51	4.60E-05	1.33	2.08	5.88	1.96
17	-3.76	33.90	#11	1.41	1.56	19.95	3.46E-05	1.00	1.57	4.43	0.49
18	3.76	33.90	#11	1.41	1.56	13.40	2.33E-05	0.67	1.05	2.97	-0.33
19	11.29	33.90	#11	1.41	1.56	6.85	1.19E-05	0.34	0.54	1.52	-0.51
20	18.82	33.90	#11	1.41	1.56	0.29	5.07E-07	0.01	0.02	0.06	-0.04
21	26.35	33.90	#11	1.41	1.56	-6.26	N/A*			
22	33.87	33.90	#11	1.41	1.56	-12.81	N/A*			
23	41.40	33.90	#11	1.41	1.56	-19.37	N/A*			
*Rebars under compression are not considered.								Sum	48.55	58.70	139.86

Therefore, three equilibrium equations can be established as below.

Force Equilibrium Equation

$$\sum P = (C_c + T_s) - P = -1283.17 \text{ kip}$$

Moment Equilibrium Equation (x-axis)

$$\sum M_x = (M_{x,c} + M_{x,s}) - M_{ux} = -996.41 \text{ kip} - \text{ft}$$

Moment Equilibrium Equation (y-axis)

$$\sum M_y = (M_{y,c} + M_{y,s}) - M_{uy} = -2549.20 \text{ kip} - \text{ft}$$

The research team used the goal seek algorithm equipped in Excel to satisfy the equilibrium equations.

1$^{\text{st}}$ Goal Seek Cycle

Step	To satisfy	By changing	Updated variables	Equilibrium Equations
1	$\sum M_y = 0$	Extreme Compressive Fiber Strain (ε_c)	$y_n' = 0$ in. (Case II) $\varepsilon_c = -0.00033$ $\theta = 60.53°$	$\sum P = -435.20 \text{ kip}$ $\sum M_x = 12.52 \text{ kip} - \text{ft}$ $\sum M_y = 0 \text{ kip} - \text{ft}$
2	$\sum P = 0$	Neutral Axis Depth (y_n')	$y_n' = 8.86$ in. (Case II) $\varepsilon_c = -0.00033$ $\theta = 60.53°$	$\sum P = 0 \text{ kip}$ $\sum M_x = 28.04 \text{ kip} - \text{ft}$ $\sum M_y = 274.44 \text{ kip} - \text{ft}$
3	$\sum M_x = 0$	Neutral Axis Inclination (θ)	$y_n' = 8.86$ in. (Case II) $\varepsilon_c = -0.00033$ $\theta = 61.19°$	$\sum P = 5.78 \text{ kip}$ $\sum M_x = 0 \text{ kip} - \text{ft}$ $\sum M_y = 305.33 \text{ kip} - \text{ft}$

2nd Goal Seek Cycle

Step	To satisfy	By changing	Updated variables	Equilibrium Equations
1	$\sum M_y = 0$	Extreme Compressive Fiber Strain (ε_c)	$y_n' = 8.86$ in. (Case II) $\varepsilon_c = -0.00030$ $\theta = 61.19°$	$\sum P = -121.86$ kip $\sum M_x = -110.60$ kip $-$ ft $\sum M_y = 0$ kip $-$ ft
2	$\sum P = 0$	Neutral Axis Depth (y_n')	$y_n' = 11.57$ in. (Case II) $\varepsilon_c = -0.00030$ $\theta = 61.19°$	$\sum P = 0$ kip $\sum M_x = -106.49$ kip $-$ ft $\sum M_y = 51.13$ kip $-$ ft
3	$\sum M_x = 0$	Neutral Axis Inclination (θ)	$y_n' = 11.57$ in. (Case II) $\varepsilon_c = -0.00030$ $\theta = 58.57°$	$\sum P = -19.25$ kip $\sum M_x = 0$ kip $-$ ft $\sum M_y = -63.92$ kip $-$ ft

3rd Goal Seek Cycle

Step	To satisfy	By changing	Updated variables	Equilibrium Equations
1	$\sum M_y = 0$	Extreme Compressive Fiber Strain (ε_c)	$y_n' = 11.57$ in. (Case II) $\varepsilon_c = -0.00031$ $\theta = 58.57°$	$\sum P = 9.76$ kip $\sum M_x = 23.53$ kip $-$ ft $\sum M_y = 0$ kip $-$ ft
2	$\sum P = 0$	Neutral Axis Depth (y_n')	$y_n' = 11.36$ in. (Case II) $\varepsilon_c = -0.00031$ $\theta = 58.57°$	$\sum P = 0$ kip $\sum M_x = 24.97$ kip $-$ ft $\sum M_y = -3.48$ kip $-$ ft
3	$\sum M_x = 0$	Neutral Axis Inclination (θ)	$y_n' = 11.36$ in. (Case II) $\varepsilon_c = -0.00031$ $\theta = 59.17°$	$\sum P = 4.25$ kip $\sum M_x = 0$ kip $-$ ft $\sum M_y = 23.61$ kip $-$ ft

After a few more cycles, three values satisfying the equilibrium conditions can be obtained as below:

$$y_n' = 11.47 \text{ in. (Case II)}$$
$$\varepsilon_c = -0.00031$$
$$\theta = 59.01°$$

Given Load Combination (Load Case VII)

$$P_u = 1015 \text{ kip}$$
$$M_{ux} = 1144 \text{ kip} - \text{ft}$$
$$M_{uy} = 5526 \text{ kip} - \text{ft}$$

1ˢᵗ iteration

Neutral axis depth (y_n'): 0 in.

Neutral axis inclination (θ): 73.4° $\left(= \text{atan}\left(\frac{M_{uy}I_y}{M_{ux}I_x}\right)\right)$; Uncracked section assumed

Extreme compressive fiber strain (ε_c): -0.0001 (Elastic state)

Case II ($y_B' = -57.6 \text{ in.} < y_n' = 0 \text{ in.} < y_C' = 57.6 \text{ in.}$)

Region 1

$$C_1 = \frac{1}{2}\left(\varepsilon_c\left(\frac{y_n' - y_A'}{y_n' - y_B'}\right)E_c\left(\frac{y_n' - y_A'}{\sin\theta}\right)\right)H = -261.1 \text{ kip}$$

$$\overline{x_1} = \frac{y_A'}{\sin\theta} - \left(\frac{y_n' - y_A'}{3\sin\theta}\right) = 22.6 \text{ in.}$$

$$\overline{y_1} = 0 \text{ in.}$$

Region 2

$$C_2 = \frac{1}{2}\left(\frac{y'_A - y'_B}{\sin\theta}H\right)\left(\varepsilon_c\left(\frac{y'_n - y'_A}{y'_n - y'_B}\right)E_c\right) = -172.6 \text{ kip}$$

$$\overline{x_2} = \frac{W}{2} - \left(\frac{y'_A - y'_B}{3\sin\theta}\right) = 37.6 \text{ in.}$$

$$\overline{y_2} = -\frac{H}{2} + \frac{H}{3} = -\frac{H}{6} = -12.5 \text{ in.}$$

Region 3

$$C_3 = \frac{1}{6}\left(\frac{y'_A - y'_B}{\sin\theta}H\right)\left(\varepsilon_c E_c - \varepsilon_c abs\left(\frac{y'_n - y'_A}{y'_n - y'_B}\right)E_c\right) = -38.0 \text{ kip}$$

$$\overline{x_3} = \frac{W}{2} - abs\left(\frac{y'_A - y'_B}{4\sin\theta}\right) = 39.4 \text{ in.}$$

$$\overline{y_3} = -\frac{H}{2} + \frac{H}{4} = -\frac{H}{4} = -18.8 \text{ in.}$$

Combining the computed results from three subdivided regions,

$$C_c = C_1 + C_2 + C_3 = -471.8 \text{ kip}$$

$$\bar{x} = \frac{C_1\overline{x_1} + C_2\overline{x_2} + C_3\overline{x_3}}{C} = 29.4 \text{ in.}$$

$$M_{y,c} = abs\left(\frac{C\bar{x}}{12}\right) = 1155.7 \text{ kip} - \text{ft}$$

$$\bar{y} = \frac{C_1\overline{y_1} + C_2\overline{y_2} + C_3\overline{y_3}}{C} = -6.1 \text{ in.}$$

$$M_{x,c} = abs\left(\frac{C\bar{x}}{12}\right) = 239.3 \text{ kip} - \text{ft}$$

From the assumed variables, the tensile forces and moments due to the column reinforcing bars can be computed as below.

Rebar No.	x (in.)	y (in.)	Rebar size	Diameter (in.)	Area (in.²)	Distance from the neutral axis y'_t (in.)	Tensile strain ($\varepsilon_s = \varepsilon_c \frac{y'_b - y'_n}{y'_t - y_n}$)	Tensile stress (ksi)	T_s (kip)	$M_{s,x}$ (kip-in.)	$M_{s,y}$ (kip-in.)
1	-41.40	33.90	#11	1.41	1.56	49.36	9.17E-05	2.66	4.15	11.72	14.31
2	-41.40	27.74	#11	1.41	1.56	47.60	8.84E-05	2.56	4.00	9.24	13.80
3	-41.40	21.57	#11	1.41	1.56	45.84	8.51E-05	2.47	3.85	6.92	13.29
4	-41.40	15.41	#11	1.41	1.56	44.08	8.19E-05	2.37	3.70	4.76	12.78
5	-41.40	9.25	#11	1.41	1.56	42.32	7.86E-05	2.28	3.56	2.74	12.27
6	-41.40	3.08	#11	1.41	1.56	40.56	7.53E-05	2.18	3.41	0.88	11.76
7	-41.40	-3.08	#11	1.41	1.56	38.79	7.21E-05	2.09	3.26	-0.84	11.25
8	-41.40	-9.25	#11	1.41	1.56	37.03	6.88E-05	1.99	3.11	-2.40	10.74
9	-41.40	-15.41	#11	1.41	1.56	35.27	6.55E-05	1.90	2.96	-3.81	10.23
10	-41.40	-21.57	#11	1.41	1.56	33.51	6.22E-05	1.81	2.82	-5.06	9.72
11	-41.40	-27.74	#11	1.41	1.56	31.75	5.90E-05	1.71	2.67	-6.17	9.20
12	-41.40	-33.90	#11	1.41	1.56	29.99	5.57E-05	1.62	2.52	-7.12	8.69
13	-33.87	33.90	#11	1.41	1.56	42.15	7.83E-05	2.27	3.54	10.00	10.00
14	-26.35	33.90	#11	1.41	1.56	34.93	6.49E-05	1.88	2.94	8.29	6.44
15	-18.82	33.90	#11	1.41	1.56	27.72	5.15E-05	1.49	2.33	6.58	3.65
16	-11.29	33.90	#11	1.41	1.56	20.51	3.81E-05	1.10	1.72	4.87	1.62
17	-3.76	33.90	#11	1.41	1.56	13.29	2.47E-05	0.72	1.12	3.16	0.35
18	3.76	33.90	#11	1.41	1.56	6.08	1.13E-05	0.33	0.51	1.44	-0.16
19	11.29	33.90	#11	1.41	1.56	-1.14	N/A*				
20	18.82	33.90	#11	1.41	1.56	-8.35	N/A*				
21	26.35	33.90	#11	1.41	1.56	-15.56	N/A*				
22	33.87	33.90	#11	1.41	1.56	-22.78	N/A*				
23	41.40	33.90	#11	1.41	1.56	-29.99	N/A*				
*Rebars under compression are not considered.								Sum	52.16	45.21	159.93

Therefore, three equilibrium equations can be established as below.

Force Equilibrium Equation

$$\sum P = (C_c + T_s) - P = -595.37 \text{ kip}$$

Moment Equilibrium Equation (x-axis)

$$\sum M_x = (M_{x,c} + M_{x,s}) - M_{ux} = -859.53 \text{ kip} - \text{ft}$$

Moment Equilibrium Equation (y-axis)

$$\sum M_y = (M_{y,c} + M_{y,s}) - M_{uy} = -4210.37 \text{ kip} - \text{ft}$$

The research team used the goal seek algorithm equipped in Excel to satisfy the equilibrium equations.

1st Goal Seek Cycle

Step	To satisfy	By changing	Updated variables	Equilibrium Equations
1	$\sum M_y = 0$	Extreme Compressive Fiber Strain (ε_c)	$y_n' = 0$ in. (Case II) $\varepsilon_c = -0.00042$ $\theta = 73.40°$	$\sum P = 747.55$ kip $\sum M_x = 50.83$ kip $-$ ft $\sum M_y = 0$ kip $-$ ft
2	$\sum P = 0$	Neutral Axis Depth (y_n')	$y_n' = -11.30$ in. (Case II) $\varepsilon_c = -0.00042$ $\theta = 73.40°$	$\sum P = 0$ kip $\sum M_x = 137.05$ kip $-$ ft $\sum M_y = -601.16$ kip $-$ ft
3	$\sum M_x = 0$	Neutral Axis Inclination (θ)	$y_n' = -11.30$ in. (Case II) $\varepsilon_c = -0.00042$ $\theta = 76.07°$	$\sum P = 44.80$ kip $\sum M_x = 0$ kip $-$ ft $\sum M_y = -395.41$ kip $-$ ft

2nd Goal Seek Cycle

Step	To satisfy	By changing	Updated variables	Equilibrium Equations
1	$\sum M_y = 0$	Extreme Compressive Fiber Strain (ε_c)	$y_n' = -11.30$ in. (Case II) $\varepsilon_c = -0.00045$ $\theta = 76.07°$	$\sum P = 126.48$ kip $\sum M_x = 88.17$ kip $-$ ft $\sum M_y = 0$ kip $-$ ft
2	$\sum P = 0$	Neutral Axis Depth (y_n')	$y_n' = -12.95$ in. (Case II) $\varepsilon_c = -0.00045$ $\theta = 76.07°$	$\sum P = 0$ kip $\sum M_x = 111.89$ kip $-$ ft $\sum M_y = -100.67$ kip $-$ ft
3	$\sum M_x = 0$	Neutral Axis Inclination (θ)	$y_n' = -12.95$ in. (Case II) $\varepsilon_c = -0.00045$ $\theta = 78.02°$	$\sum P = 36.25$ kip $\sum M_x = 0$ kip $-$ ft $\sum M_y = 74.31$ kip $-$ ft

3rd Goal Seek Cycle

Step	To satisfy	By changing	Updated variables	Equilibrium Equations
1	$\sum M_y = 0$	Extreme Compressive Fiber Strain (ε_c)	$y_n' = -12.95$ in. (Case II) $\varepsilon_c = -0.00045$ $\theta = 78.02°$	$\sum P = 22.30$ kip $\sum M_x = -15.18$ kip $-$ ft $\sum M_y = 0$ kip $-$ ft
2	$\sum P = 0$	Neutral Axis Depth (y_n')	$y_n' = -13.24$ in. (Case II) $\varepsilon_c = -0.00045$ $\theta = 78.02°$	$\sum P = 0$ kip $\sum M_x = -10.43$ kip $-$ ft $\sum M_y = -16.74$ kip $-$ ft
3	$\sum M_x = 0$	Neutral Axis Inclination (θ)	$y_n' = -13.24$ in. (Case II) $\varepsilon_c = -0.00045$ $\theta = 77.84°$	$\sum P = -3.38$ kip $\sum M_x = 0$ kip $-$ ft $\sum M_y = -33.18$ kip $-$ ft

After a few more cycles, three values satisfying the equilibrium conditions can be obtained as below:

$$y_n' = 13.28 \text{ in. (Case II)}$$

$$\varepsilon_c = -0.00045$$

$$\theta = 77.95°$$

Appendix B Derivation of 3D Strut-and-Tie Model Element Forces

Load Case VI: Axial Compression combined with Moderate Biaxial Flexure
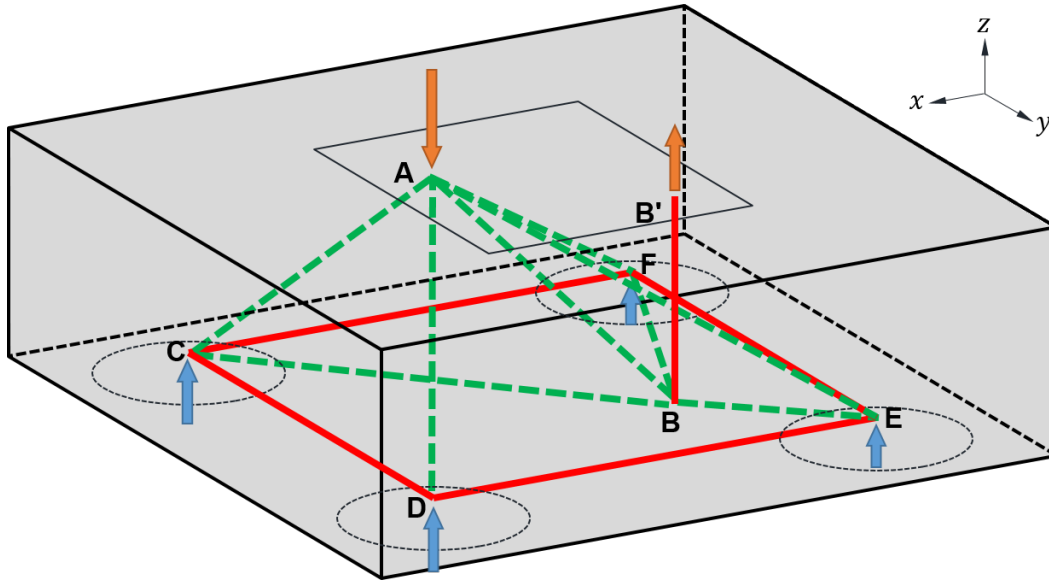
Figure B.1 3D strut-and-tie model (axonometric view): Load Case VI

From the sectional analysis,

Resultant Forces:

$$F_A = -1736.2 \text{ kip}; \quad F_B = 80.2 \text{ kip}$$

Reactions:

$$R_C = 657.3 \text{ kip}; \quad R_D = 520.2 \text{ kip}; \quad R_E = 170.7 \text{ kip}; \quad R_F = 307.8 \text{ kip}$$

Node	x-coordinate [in.]	y-coordinate [in.]	z-coordinate [in.]
A	23.70	-9.19	54.00
B	-36.08	16.53	5.41
C	63.00	-63.00	5.41
D	63.00	63.00	5.41
E	-63.00	63.00	5.41
F	-63.00	-63.00	5.41

Node D

Known Forces:

$$F_x = 0; \; F_y = 0; \; F_z = R_D = 520.2 \text{ kip}$$

Element	Length	Unit Vector		
		$\hat{\imath}$	$\hat{\jmath}$	$\hat{k}$
DA	95.5	-0.412	-0.756	0.509
DC	126.0	0	-1	0
DE	126.0	-1	0	0

$$\begin{bmatrix} \dfrac{\overrightarrow{DA}}{|\overrightarrow{DA}|} & \dfrac{\overrightarrow{DC}}{|\overrightarrow{DC}|} & \dfrac{\overrightarrow{DE}}{|\overrightarrow{DE}|} \end{bmatrix} \begin{bmatrix} F_{DA} \\ F_{DC} \\ F_{DE} \end{bmatrix} = \begin{bmatrix} -F_x \\ -F_y \\ -F_z \end{bmatrix}$$

$$\begin{bmatrix} F_{DA} \\ F_{DC} \\ F_{DE} \end{bmatrix} = \begin{bmatrix} \dfrac{\overrightarrow{DA}}{|\overrightarrow{DA}|} & \dfrac{\overrightarrow{DC}}{|\overrightarrow{DC}|} & \dfrac{\overrightarrow{DE}}{|\overrightarrow{DE}|} \end{bmatrix}^{-1} \begin{bmatrix} -F_x \\ -F_y \\ -F_z \end{bmatrix} = \begin{bmatrix} -0.412 & 0 & -1 \\ -0.756 & -1 & 0 \\ 0.509 & 0 & 0 \end{bmatrix}^{-1} \begin{bmatrix} 0 \\ 0 \\ -520.2 \end{bmatrix}$$

$$= \begin{bmatrix} -1022.2 \text{ kip (Strut)} \\ 772.9 \text{ kip (Tie)} \\ 420.7 \text{ kip (Tie)} \end{bmatrix}$$

Node C

Known Forces:

$$F_x = 0; \; F_y = F_{DC} = 772.9 \text{ kip}; \; F_z = R_C = 657.3 \text{ kip}$$

Element	Length	Unit Vector		
		$\hat{\imath}$	$\hat{\jmath}$	$\hat{k}$
CA	82.5	-0.477	0.652	0.589
CB	127.1	-0.780	0.626	0
CF	126.0	-1	0	0

$$\begin{bmatrix} \dfrac{\overrightarrow{CA}}{|\overrightarrow{CA}|} & \dfrac{\overrightarrow{CB}}{|\overrightarrow{CB}|} & \dfrac{\overrightarrow{CF}}{|\overrightarrow{CF}|} \end{bmatrix} \begin{bmatrix} F_{CA} \\ F_{CB} \\ F_{CF} \end{bmatrix} = \begin{bmatrix} -F_x \\ -F_y \\ -F_z \end{bmatrix}$$

$$\begin{bmatrix} F_{CA} \\ F_{CB} \\ F_{CF} \end{bmatrix} = \begin{bmatrix} \dfrac{\overrightarrow{CA}}{|\overrightarrow{CA}|} & \dfrac{\overrightarrow{CB}}{|\overrightarrow{CB}|} & \dfrac{\overrightarrow{CF}}{|\overrightarrow{CF}|} \end{bmatrix}^{-1} \begin{bmatrix} -F_x \\ -F_y \\ -F_z \end{bmatrix} = \begin{bmatrix} -0.477 & -0.780 & -1 \\ 0.652 & 0.626 & 0 \\ 0.589 & 0 & 0 \end{bmatrix}^{-1} \begin{bmatrix} 0 \\ -772.9 \\ -657.3 \end{bmatrix}$$

$$= \begin{bmatrix} -1115.6 \text{ kip (Strut)} \\ -71.9 \text{ kip (Strut)} \\ 587.7 \text{ kip (Tie)} \end{bmatrix}$$

This calculation result justifies the bottom mat configuration of the 3D strut-and-tie model for Load Case VI (Figure 5.3a). The y-force components of Struts AC and AD are 727.9 kip (=1115.6 × 0.652) and 772.9 kip (=1022.2 × 0.756), respectively. Therefore, an additional strut (Strut BC) with the y-force component of 45 kip (=71.9×0.626) is required to be connected to Node C to satisfy the equilibrium condition.

Node F

Known Forces:

$$F_x = F_{CF} = 587.7 \text{ kip}; \ F_y = 0; \ F_z = R_F = 307.8 \text{ kip}$$

Element	Length	Unit Vector		
		$\hat{\imath}$	$\hat{\jmath}$	$\hat{k}$
FA	113.0	0.767	0.476	0.430
FB	84.0	0.321	0.947	0
FE	126.0	0	1	0

$$\begin{bmatrix} \dfrac{\overrightarrow{FA}}{|\overrightarrow{FA}|} & \dfrac{\overrightarrow{FB}}{|\overrightarrow{FB}|} & \dfrac{\overrightarrow{FE}}{|\overrightarrow{FE}|} \end{bmatrix} \begin{bmatrix} F_{FA} \\ F_{FB} \\ F_{FE} \end{bmatrix} = \begin{bmatrix} -F_x \\ -F_y \\ -F_z \end{bmatrix}$$

$$\begin{bmatrix} F_{FA} \\ F_{FB} \\ F_{FE} \end{bmatrix} = \begin{bmatrix} \dfrac{\overrightarrow{FA}}{|\overrightarrow{FA}|} & \dfrac{\overrightarrow{FB}}{|\overrightarrow{FB}|} & \dfrac{\overrightarrow{FE}}{|\overrightarrow{FE}|} \end{bmatrix}^{-1} \begin{bmatrix} -F_x \\ -F_y \\ -F_z \end{bmatrix} = \begin{bmatrix} 0.767 & 0.321 & 0 \\ 0.476 & 0.947 & 1 \\ 0.430 & 0 & 0 \end{bmatrix}^{-1} \begin{bmatrix} -587.7 \\ 0 \\ -307.8 \end{bmatrix}$$

$$= \begin{bmatrix} -715.9 \text{ kip (Strut)} \\ -120.1 \text{ kip (Strut)} \\ 454.6 \text{ kip (Tie)} \end{bmatrix}$$

Node E

Known Forces:

$$F_x = F_{DE} = 420.7 \text{ kip}; \ F_y = -F_{FE} = -454.6 \text{ kip}; \ F_z = R_E = 170.7 \text{ kip}$$

Element	Length	Unit Vector		
		$\hat{\imath}$	$\hat{\jmath}$	$\hat{k}$
EA	122.8	0.706	-0.588	0.396
EB	53.7	0.501	-0.865	0

For the calculation, the *y*- and *z*-force components are only considered.

$$\left[\frac{\overrightarrow{EA}}{\left|\overrightarrow{EA}\right|} \ \ \frac{\overrightarrow{EB}}{\left|\overrightarrow{EB}\right|}\right]\begin{bmatrix}F_{EA}\\F_{EB}\end{bmatrix} = \begin{bmatrix}-F_y\\-F_z\end{bmatrix}$$

$$\begin{bmatrix}F_{EA}\\F_{EB}\end{bmatrix} = \left[\frac{\overrightarrow{EA}}{\left|\overrightarrow{EA}\right|} \ \ \frac{\overrightarrow{EB}}{\left|\overrightarrow{EB}\right|}\right]^{-1}\begin{bmatrix}-F_y\\-F_z\end{bmatrix} = \begin{bmatrix}0 & 2.528\\-1.156 & -1.717\end{bmatrix}^{-1}\begin{bmatrix}-F_y\\-F_z\end{bmatrix}$$

$$= \begin{bmatrix}-431.5 \text{ kip (Strut)}\\-232.3 \text{ kip (Strut)}\end{bmatrix}$$

Almost the same result can be obtained from the *x*- and *z*-force components.

$$\begin{bmatrix}F_{EA}\\F_{EB}\end{bmatrix} = \left[\frac{\overrightarrow{EA}}{\left|\overrightarrow{EA}\right|} \ \ \frac{\overrightarrow{EB}}{\left|\overrightarrow{EB}\right|}\right]^{-1}\begin{bmatrix}-F_x\\-F_z\end{bmatrix} = \begin{bmatrix}0 & 2.528\\-1.156 & -1.717\end{bmatrix}^{-1}\begin{bmatrix}-F_y\\-F_z\end{bmatrix}$$

$$= \begin{bmatrix}-431.5 \text{ kip (Strut)}\\-231.6 \text{ kip (Strut)}\end{bmatrix}$$

Node B

Known Forces:

$$F_z = F_{BB'} = 80.2 \text{ kip}$$

Element	Length	Unit Vector		
		$\hat{\imath}$	$\hat{\jmath}$	$\hat{k}$
BA	81.2	0.736	-0.317	0.598

$$F_{BA} = -\frac{80.2}{0.598} = -134.0 \text{ kip (Strut)}$$

Equilibrium Condition Check at Node B

Element	Force	x-force component [kip] (Unit vector)	y-force component [kip] (Unit vector)	z-force component [kip] (Unit vector)
BA	-134.0	-98.7 (0.736)	42.5 (-0.317)	-80.2 (0.598)
BC	-71.9	-56.0 (0.780)	45.0 (-0.626)	0 (0)
BE	-232.3	116.4 (-0.501)	-201.0 (0.865)	0 (0)
BF	-120.1	38.5 (-0.321)	113.7 (-0.947)	0 (0)
F_B	80.2	0 (0)	0 (0)	80.2 (1)
Sum		0.2	0.2	0

Node A

Equilibrium Condition Check at Node A

Element	Force	x-force component [kip] (Unit vector)	y-force component [kip] (Unit vector)	z-force component [kip] (Unit vector)
AB	-134.0	98.7 (-0.736)	-42.5 (0.317)	80.2 (-0.598)
AC	-1115.6	-531.6 (0.477)	727.9 (-0.653)	657.3 (-0.589)
AD	-1022.2	-420.8 (0.412)	-772.9 (0.756)	520.2 (-0.509)
AE	-431.5	304.6 (-0.706)	-253.6 (0.588)	170.7 (-0.396)
AF	-715.9	549.2 (-0.767)	340.9 (-0.476)	307.8 (-0.430)
F_A	-1736.2	0 (0)	0 (0)	-1736.2 (1)
Sum		0.1	-0.1	0

Load Case VII: Axial Compression combined with Large Biaxial Flexure
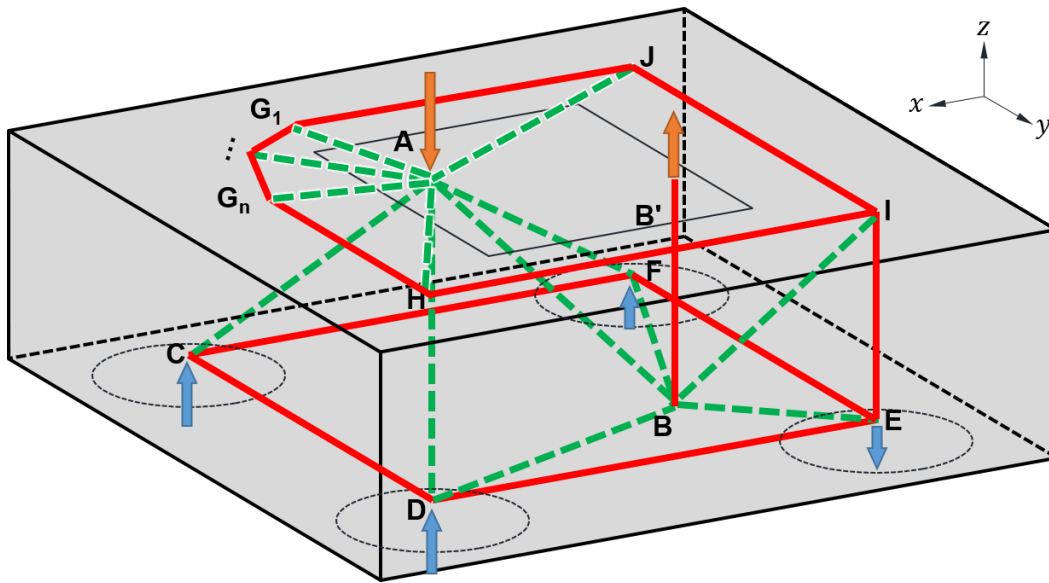
Figure B.2 3D strut-and-tie model (axonometric view): Load Case VII

From the sectional analysis,

Resultant Forces:

$$F_A = -1471.3 \text{ kip}; \quad F_B = 456.3 \text{ kip}$$

Reactions:

$$R_C = 571.4 \text{ kip}; \quad R_D = 462.4 \text{ kip}; \quad R_E = -63.9 \text{ kip}; \quad R_F = 45.1 \text{ kip}$$

Node	x-coordinate [in.]	y-coordinate [in.]	z-coordinate [in.]
A	34.08	-6.24	55.25
B	-35.42	9.98	5.41
C	63.00	-63.00	5.41
D	63.00	63.00	5.41
E	-63.00	63.00	5.41
F	-63.00	-63.00	5.41
H	63.00	63.00	55.25
I	-63.00	63.00	55.25
J	-63.00	-63.00	55.25

Node C

Known Forces:

$$F_x = 0; \ F_y = 0; \ F_z = R_C = 571.4 \text{ kip}$$

Element	Length	Unit Vector		
		$\hat{\imath}$	$\hat{\jmath}$	$\hat{k}$
CA	80.9	-0.358	0.702	0.616
CD	126.0	0	1	0
CF	126.0	-1	0	0

$$\left[\frac{\overrightarrow{CA}}{|\overrightarrow{CA}|} \ \ \frac{\overrightarrow{CD}}{|\overrightarrow{CD}|} \ \ \frac{\overrightarrow{CF}}{|\overrightarrow{CF}|} \right] \begin{bmatrix} F_{CA} \\ F_{CD} \\ F_{CF} \end{bmatrix} = \begin{bmatrix} -F_x \\ -F_y \\ -F_z \end{bmatrix}$$

$$\begin{bmatrix} F_{CA} \\ F_{CD} \\ F_{CF} \end{bmatrix} = \left[\frac{\overrightarrow{CA}}{|\overrightarrow{CA}|} \ \ \frac{\overrightarrow{CD}}{|\overrightarrow{CD}|} \ \ \frac{\overrightarrow{CF}}{|\overrightarrow{CF}|} \right]^{-1} \begin{bmatrix} -F_x \\ -F_y \\ -F_z \end{bmatrix} = \begin{bmatrix} -0.358 & 0 & -1 \\ 0.702 & 1 & 0 \\ 0.626 & 0 & 0 \end{bmatrix}^{-1} \begin{bmatrix} 0 \\ 0 \\ -571.4 \end{bmatrix}$$

$$= \begin{bmatrix} -927.3 \text{ kip (Strut)} \\ 650.8 \text{ kip (Tie)} \\ 331.5 \text{ kip (Tie)} \end{bmatrix}$$

Node D

Known Forces:

$$F_x = 0; \ F_y = -F_{CD} = -650.8 \text{ kip}; \ F_z = R_D = 462.4 \text{ kip}$$

Element	Length	Unit Vector		
		$\hat{\imath}$	$\hat{\jmath}$	$\hat{k}$
DA	90.1	-0.321	-0.769	0.553
DB	111.8	-0.880	-0.474	0
DE	126.0	-1	0	0

$$\left[\frac{\overrightarrow{DA}}{|\overrightarrow{DA}|} \ \ \frac{\overrightarrow{DB}}{|\overrightarrow{DB}|} \ \ \frac{\overrightarrow{DE}}{|\overrightarrow{DE}|} \right] \begin{bmatrix} F_{DA} \\ F_{DB} \\ F_{DE} \end{bmatrix} = \begin{bmatrix} -F_x \\ -F_y \\ -F_z \end{bmatrix}$$

$$\begin{bmatrix} F_{DA} \\ F_{DB} \\ F_{DE} \end{bmatrix} = \begin{bmatrix} \dfrac{\overrightarrow{DA}}{|\overrightarrow{DA}|} & \dfrac{\overrightarrow{DB}}{|\overrightarrow{DB}|} & \dfrac{\overrightarrow{DE}}{|\overrightarrow{DE}|} \end{bmatrix}^{-1} \begin{bmatrix} -F_x \\ -F_y \\ -F_z \end{bmatrix} = \begin{bmatrix} -0.321 & -0.880 & -1 \\ -0.769 & -0.474 & 0 \\ 0.553 & 0 & 0 \end{bmatrix}^{-1} \begin{bmatrix} 0 \\ 650.8 \\ -462.4 \end{bmatrix}$$

$$= \begin{bmatrix} -853.7 \text{ kip (Strut)} \\ -17.8 \text{ kip (Strut)} \\ 284.0 \text{ kip (Tie)} \end{bmatrix}$$

Node F

Known Forces:

$$F_x = F_{CF} = 331.5 \text{ kip}; \; F_y = 0; \; F_z = R_F = 45.1 \text{ kip}$$

Element	Length	Unit Vector		
		$\hat{\imath}$	$\hat{\jmath}$	$\hat{k}$
FA	123.0	0.789	0.461	0.405
FB	78.0	0.354	0.935	0
FE	126.0	0	1	0

$$\begin{bmatrix} \dfrac{\overrightarrow{FA}}{|\overrightarrow{FA}|} & \dfrac{\overrightarrow{FB}}{|\overrightarrow{FB}|} & \dfrac{\overrightarrow{FE}}{|\overrightarrow{FE}|} \end{bmatrix} \begin{bmatrix} F_{FA} \\ F_{FB} \\ F_{FE} \end{bmatrix} = \begin{bmatrix} -F_x \\ -F_y \\ -F_z \end{bmatrix}$$

$$\begin{bmatrix} F_{FA} \\ F_{FB} \\ F_{FE} \end{bmatrix} = \begin{bmatrix} \dfrac{\overrightarrow{FA}}{|\overrightarrow{FA}|} & \dfrac{\overrightarrow{FB}}{|\overrightarrow{FB}|} & \dfrac{\overrightarrow{FE}}{|\overrightarrow{FE}|} \end{bmatrix}^{-1} \begin{bmatrix} -F_x \\ -F_y \\ -F_z \end{bmatrix} = \begin{bmatrix} 0.789 & 0.3540 & 0 \\ 0.461 & 0.935 & 1 \\ 0.405 & 0 & 0 \end{bmatrix}^{-1} \begin{bmatrix} -331.5 \\ 0 \\ -45.1 \end{bmatrix}$$

$$= \begin{bmatrix} -111.3 \text{ kip (Strut)} \\ -689.2 \text{ kip (Strut)} \\ 696.1 \text{ kip (Tie)} \end{bmatrix}$$

Node E

Known Forces:

$$F_x = F_{DE} = 284.0 \text{ kip}; \ F_y = -F_{FE} = -696.1 \text{ kip}; \ F_y = R_F = 45.1 \text{ kip}$$

Based on the given strut-and-tie model configuration,

Element	Length	Unit Vector		
		$\hat{\imath}$	$\hat{\jmath}$	$\hat{k}$
EB	59.8	0.462	-0.887	0

$$F_{BE \ from \ F_{DE}} = \frac{-284.0}{0.462} = -615.4 \neq F_{BE \ from \ F_{FE}} = \frac{696.1}{-0.887} = -784.7 \text{ kip}$$

A new nodal position of Node E is determined to transfer the force discrepancy between Ties FE (696.1 kip) and DE (284.0 kip) to estimate the error built in the model. Therefore, the unit vector of Strut EB satisfying the equilibrium condition at Node E can be determined.

$$\hat{\imath} = \frac{F_{DE}}{\sqrt{F_{DE}^2 + F_{FE}^2}} = \frac{284.0}{\sqrt{284.0^2 + (-696.1)^2}} = 0.378$$

$$\hat{\jmath} = \frac{F_{FE}}{\sqrt{F_{DE}^2 + F_{FE}^2}} = \frac{-696.1}{\sqrt{284.0^2 + (-696.1)^2}} = -0.926$$
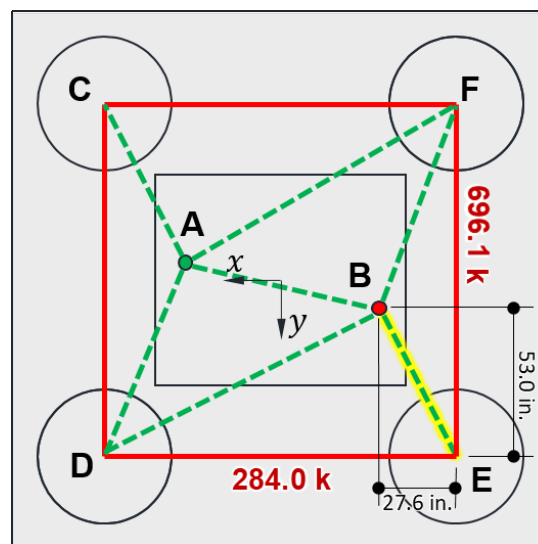

Figure B.3 Plan view of 3D strut-and-tie model: Load Case VII

Based on the determined unit vector, the new Node E can be positioned at 6-in. shifted over the x-axis from its original position, and its new *x*-coordinate can be computed as below.

$$x_E = -63 + \left(27.6 - \frac{53.0}{0.926}(0.378)\right) = -63 + (27.6 - 6.0) = -57.0 \text{ in.}$$

Hence, the error is estimated by comparing the y-axis applied moment computed from the shifted Node E ($M_{uy,new\ E}$) and that of the original value (M_{uy}).

$$M_{uy,new\ E} = \frac{(63.0)(571.4 + 462.4 - 45.1) + 57.0(63.9)}{12} = 5494.2 \text{ kip} - \text{ft}$$

$$\% \text{ Error} = \left|\frac{M_{uy} - M_{uy,new\ E}}{M_{uy}}\right| \times 100 = \left|\frac{5526.0 - 5494.2}{5526.0}\right| \times 100 = 0.58 \%$$

Therefore, the error is negligible, and Strut BE derived from the new unit vector is:

$$F_{BE\ from\ F_{DE}} = \frac{-284.0}{0.378} = F_{BE\ from\ F_{FE}} = \frac{696.1}{-0.926} = -751.8 \text{ kip}$$

It should be noted that the newly derived Strut BE and its unit vector are not exploited in nodal strength checks but for checking equilibrium conditions at Node B only.

Node I

Known Forces:

$$F_x = 0; \ F_y = 0; \ F_z = R_E = -63.9 \text{ kip}$$

Element	Length	Unit Vector		
		$\hat{\imath}$	$\hat{\jmath}$	$\hat{k}$
IB	77.8	0.354	-0.681	-0.641
IH	126.0	1	0	0
IJ	126.0	0	-1	0

$$\begin{bmatrix} \dfrac{\vec{IB}}{|\vec{IB}|} & \dfrac{\vec{IH}}{|\vec{IH}|} & \dfrac{\vec{IJ}}{|\vec{IJ}|} \end{bmatrix} \begin{bmatrix} F_{IB} \\ F_{IH} \\ F_{IJ} \end{bmatrix} = \begin{bmatrix} -F_x \\ -F_y \\ -F_z \end{bmatrix}$$

$$\begin{bmatrix} F_{IB} \\ F_{IH} \\ F_{IJ} \end{bmatrix} = \begin{bmatrix} \dfrac{\vec{IB}}{|\vec{IB}|} & \dfrac{\vec{IH}}{|\vec{IH}|} & \dfrac{\vec{IJ}}{|\vec{IJ}|} \end{bmatrix}^{-1} \begin{bmatrix} -F_x \\ -F_y \\ -F_z \end{bmatrix} = \begin{bmatrix} 0.354 & 1 & 0 \\ -0.681 & 0 & -1 \\ -0.641 & 0 & 0 \end{bmatrix}^{-1} \begin{bmatrix} 0 \\ 0 \\ 63.9 \end{bmatrix}$$

$$= \begin{bmatrix} -99.8 \text{ kip (Strut)} \\ 35.4 \text{ kip (Tie)} \\ 68.0 \text{ kip (Tie)} \end{bmatrix}$$

Node H

Known Forces:

$$F_x = -F_{IH} = -35.4 \text{ kip}; \ F_y = 0; \ F_z = 0$$

Element	Length	Unit Vector		
		$\hat{\imath}$	$\hat{\jmath}$	$\hat{k}$
HA	75.0	-0.385	-0.923	0
HG$_n$	N/A	0	-1	0

For the calculation, the *x*- and *y*-force components are only considered.

$$\begin{bmatrix} \dfrac{\vec{HA}}{|\vec{HA}|} & \dfrac{\vec{HG_n}}{|\vec{HG_n}|} \end{bmatrix} \begin{bmatrix} F_{HA} \\ F_{HG_n} \end{bmatrix} = \begin{bmatrix} -F_x \\ -F_y \end{bmatrix}$$

$$\begin{bmatrix} F_{HA} \\ F_{HG_n} \end{bmatrix} = \begin{bmatrix} \dfrac{\overrightarrow{HA}}{|\overrightarrow{HA}|} & \dfrac{\overrightarrow{HG_n}}{|\overrightarrow{HG_n}|} \end{bmatrix}^{-1} \begin{bmatrix} -F_x \\ -F_y \end{bmatrix} = \begin{bmatrix} -0.385 & 0 \\ -0.923 & -1 \end{bmatrix}^{-1} \begin{bmatrix} -F_x \\ -F_y \end{bmatrix}$$

$$= \begin{bmatrix} -91.9 \text{ kip (Strut)} \\ 84.8 \text{ kip (Tie)} \end{bmatrix}$$

Node J

Known Forces:

$$F_x = 0; \ F_y = F_{IJ} = 68.0 \text{ kip}; \ F_z = 0$$

Element	Length	Unit Vector		
		$\hat{\imath}$	$\hat{\jmath}$	$\hat{k}$
JA	112.5	0.863	0.505	0
JG$_1$	N/A	1	0	0

For the calculation, the *x*- and *y*-force components are only considered.

$$\begin{bmatrix} \dfrac{\overrightarrow{JA}}{|\overrightarrow{JA}|} & \dfrac{\overrightarrow{JG_1}}{|\overrightarrow{JG_1}|} \end{bmatrix} \begin{bmatrix} F_{JA} \\ F_{JG_1} \end{bmatrix} = \begin{bmatrix} -F_x \\ -F_y \end{bmatrix}$$

$$\begin{bmatrix} F_{JA} \\ F_{JG_1} \end{bmatrix} = \begin{bmatrix} \dfrac{\overrightarrow{JA}}{|\overrightarrow{JA}|} & \dfrac{\overrightarrow{JG_1}}{|\overrightarrow{JG_1}|} \end{bmatrix}^{-1} \begin{bmatrix} -F_x \\ -F_y \end{bmatrix} = \begin{bmatrix} 0.863 & 1 \\ 0.505 & 0 \end{bmatrix}^{-1} \begin{bmatrix} -F_x \\ -F_y \end{bmatrix}$$

$$= \begin{bmatrix} -134.7 \text{ kip (Strut)} \\ 116.3 \text{ kip (Tie)} \end{bmatrix}$$

$$\begin{bmatrix} \dfrac{\overrightarrow{IB}}{|\overrightarrow{IB}|} & \dfrac{\overrightarrow{IH}}{|\overrightarrow{IH}|} & \dfrac{\overrightarrow{IJ}}{|\overrightarrow{IJ}|} \end{bmatrix} \begin{bmatrix} F_{IB} \\ F_{IH} \\ F_{IJ} \end{bmatrix} = \begin{bmatrix} -F_x \\ -F_y \\ -F_z \end{bmatrix}$$

$$\begin{bmatrix} F_{IB} \\ F_{IH} \\ F_{IJ} \end{bmatrix} = \begin{bmatrix} \dfrac{\vec{IB}}{|\vec{IB}|} & \dfrac{\vec{IH}}{|\vec{IH}|} & \dfrac{\vec{IJ}}{|\vec{IJ}|} \end{bmatrix}^{-1} \begin{bmatrix} -F_x \\ -F_y \\ -F_z \end{bmatrix} = \begin{bmatrix} 0.354 & 1 & 0 \\ -0.681 & 0 & -1 \\ -0.641 & 0 & 0 \end{bmatrix}^{-1} \begin{bmatrix} 0 \\ 0 \\ 63.9 \end{bmatrix}$$

$$= \begin{bmatrix} -99.8 \text{ kip (Strut)} \\ 35.4 \text{ kip (Tie)} \\ 68.0 \text{ kip (Tie)} \end{bmatrix}$$

Node B

Known Forces:

$$F_z = F_B + R_E = 392.4 \text{ kip}$$

Element	Length	Unit Vector		
		$\hat{\imath}$	$\hat{\jmath}$	$\hat{k}$
BA	87.1	0.798	-0.186	0.573

$$F_{BA} = -\frac{392.4}{0.573} = -685.4 \text{ kip (Strut)}$$

Equilibrium Condition Check at Node B

Element	Force	x-force component [kip] (Unit vector)	y-force component [kip] (Unit vector)	z-force component [kip] (Unit vector)
BA	-685.4	-547.2 (0.798)	127.7 (-0.186)	-392.4 (0.573)
BD	-17.8	-15.7 (0.880)	-8.5 (0.474)	0 (0)
*BE	-751.8	284.0 (-0.378)	-696.1 (0.926)	0 (0)
BF	-689.2	243.6 (-0.354)	644.7 (-0.935)	0 (0)
BI	-99.8	35.4 (-0.354)	-68.0 (0.681)	-63.9 (0.640)
F_B	456.3	0 (0)	0 (0)	456.3 (1)
Sum		0.1	-0.1	0

*Newly derived Strut BE satisfying the equilibrium condition at Node E

Node A

Equilibrium Condition Check at Node A

Element	Force	x-force component [kip] (Unit vector)	y-force component [kip] (Unit vector)	z-force component [kip] (Unit vector)
AB	-685.4	547.2 (-0.798)	-127.7 (0.186)	392.4 (-0.573)
AC	-927.3	-331.5 (0.357)	650.8 (-0.702)	571.4 (-0.616)
AD	-835.7	-268.3 (0.321)	-642.3 (0.769)	462.4 (-0.553)
AF	-111.3	87.9 (-0.789)	51.4 (-0.461)	45.1 (-0.405)
AH	-91.9	-35.4 (0.385)	-84.8 (0.923)	0 (0)
FJ	-134.7	116.3 (-0.863)	68.0 (-0.505)	0 (0)
F_A	-1471.3	0 (0)	0 (0)	-1471.3 (1)
Sum		116.2	-84.6	0

Therefore, the force components of the resolved strut (Strut AG) of the widespread struts (Struts $AG_1, AG_2, ..., AG_n$) are determined to satisfy the equilibrium condition at Node A.

Element	Force	x-force component [kip] (Unit vector)	y-force component [kip] (Unit vector)	z-force component [kip] (Unit vector)
AG	-143.7	-116.2 (-0.808)	84.6 (0.589)	0 (0)

References

ACI Committee 318-19, (2019), *Building Code Requirements for Reinforced Concrete (ACI 318-19) and Commentary (318R-19)*, American Concrete Institute, Farmington Hills, MI.

AASHTO LRFD, (2020), *Bridge Design Specifications, 9th Edition*, American Association of State Highway and Transportation Officials, Washington, D.C.

Ballestrino, S. D., Marin, J. R., Diaz, E. G., and Peiretti, H. C., (2011), Example 1: Solving Structural Design Problems with Strut-and-Tie Models, *fib Bulletin 61: Design Examples for Strut-and-Tie Models*, Ed. Karl-Heinz Reineck, Lausanne: fib, pp. 1-30.

Williams, C., Deschenes, D., and Bayrak, O., (2012), *Strut-and-Tie Model Design Examples for Bridges*, Rep. FHWA/TX-12/5-5253-01-1. Center for Transportation Research, The University of Texas at Austin.

Yi, Y., Kim, H., Boehm, R. A., Webb, Z. D., Choi, J., Wang, H., Murcia-Delso, J., Hrynyk, T.D., and Bayrak, O. (2022), *3D Strut-and-Tie Modeling for Design of Drilled Shaft Footings*, Report No. FHWA/TX-21/0-6953-R1, Center for Transportation Research, The University of Texas at Austin.